공학박사학위논문

Parameterized reduced order models for nonlinear finite element systems based on stiffness evaluation method

비선형 유한 요소 해석을 위한

등가 강성 행렬 기법 기반의 파라메트릭 축소 모델

2016 년 8 월

서울대학교 대학원

기계항공공학부

김 의 영

Abstract

To solve material/geometric nonlinear structural systems, iterative evaluation of internal forces and tangent stiffness matrices is required. This increases the computation time for nonlinear static/dynamic analysis. Although various reduced-order modeling techniques have been proposed to effectively solve nonlinear structural analysis problems, problems arise in the reduction of the system matrices. Since most reduction methods only reduce the system matrix after the stiffness and mass matrix construction process, the construction itself proceeds in full domain. In most cases of nonlinear analysis, the construction of system matrix takes a large amount of computation time, comparable to the computation time of the solving process. Although this problem can be tackled with STiffness Evaluation Procedure (STEP), which uses polynomial formulations to describe nonlinear internal forces, the construction time of the reduced model increases rapidly with the cubic power of the system size.

In this paper, Stiffness Evaluation method based on Element Connectivity (SEEC) is proposed. The element connectivity of the finite element models is used to evaluate the nonlinear stiffness coefficients. The proposed method minimizes the effect of the system size when the computational model is constructed. In addition, the Reduced Order Modeling (ROM) technique using Proper Orthogonal Decomposition (POD) is applied to enhance the efficiency of the SEEC method, which is referred to as SEECROM. This enables effective analysis and design of large-scale problems. Moreover, SEECROM is

easily characterized by design parameters. The parameterization is readily achieved with element-wise nature of the proposed method. SEECROM is successfully demonstrated for structural dynamic analysis of geometrically nonlinear shell structures under the perturbation of external loads. SEECROM-Parameterization is also successfully demonstrated for static and dynamic analysis of hyperelastic materials that have material and geometric nonlinearities.

In the case of flexible multibody systems, nonlinearities are caused by the rigid motions of the structure rather than the deformation of the flexible parts. Since the approaches to the multibody dynamics are different from the structural dynamics, the reduction methods which have been developed for the structural analyses cannot be utilized in direct manner. However, this can be achieved with the aid of Absolute Nodal Coordinate Formulation (ANCF), which takes the analogous format to the governing finite element formulation of structural dynamics. SEECROM method is combined to ANCF to form an efficient reduced model of the flexible multibody system. A number of examples are provided for the verification of the proposed reduction method and its parameterization.

For the application to the optimization of nonlinear structures, it is vital that reduced order models be efficiently parameterized for the design parameters. SEECROM-Parameterization fits easily to the optimization problems concerning nonlinear systems. To show the validity of the proposed methodology, two sample optimization problems are subjected to a static structural system with a hyperelastic material and a multibody dynamic system.

Keywords

Structural dynamics; Geometric nonlinearities; Material nonlinearities; Finite elements; Reduced order models; Parameterization; Stiffness evaluation; Multibody dynamics; Structural optimization

Student Number: 2010-20662

TABLE OF CONTENTS

LIST OF TABLES

LIST OF FIGURES

1. INTRODUCTION

Different from linear analyses, which can be conducted in a single solution step, nonlinear analyses are usually solved by performing iterations of the linear analysis. Therefore, a nonlinear analysis takes more computational resources than a linear one. In cases of structural dynamic analysis or design problems, which contain nonlinearities, the iterative nonlinear analysis is again recursively solved at every iteration step. Therefore, many studies have been carried out to solve nonlinear analysis problems in reduced time and effort.

Reduced-order modeling techniques, which are well developed for linear systems, have also been adapted for nonlinear systems. However, in nonlinear analysis, the system matrices should be re-constructed as the structure deforms. The problem here is that the re-construction process is carried out in full domain even with a model reduction technique. Most reduction methods merely aim at shrinking the fully constructed matrix to a reduced one. While the computation time for the solution-solving process (i.e., inverse of tangent stiffness matrices) is reduced, the construction of the system matrices of the reduced one takes the same amount of time as that of the full analysis.

As a computationally efficient approach of nonlinear analysis, Muravyov and Rizzi proposed the STEP (STiffness Evaluation Procedure) method [1]. In this method, nonlinear internal forces are represented by a 3rd order polynomial formulation of displacements. Since the coefficients of each term of polynomial displacements, which are called stiffness, are evaluated to construct an internal force model, the method is

referred to as “stiffness evaluation.” If the representative model is accurate enough, the nonlinear internal force vector and the tangent stiffness matrix can be promptly computed as the structure deforms. In recent years, as extensions of the STEP method, nonintrusive structural dynamic reduced-order modeling approaches have been proposed [2]. They are also referred to as “indirect” since they do not require any internal information of the governing equations or the detailed formula for the system. This enables straightforward use of commercial codes such as NASTRAN, ABAQUS, and ANSYS. The nonintrusive approaches were validated in various applications, including prediction of fatigue life [3-4], nonlinear stochastic computations [5-6], and nonlinear post-buckling analyses [7]. A strategy that enables STEP applications to more complex structures was also proposed by Perez at al. [8] The nonlinear static response analysis of a nine-bay panel model with 86,000 degrees of freedom and 85 reduction modes was successfully conducted.

Still, further consideration should be given to the efficiency of the process of identifying the internal force model. Usually in the stiffness evaluation procedure, the coefficients of the polynomial displacements can be identified by a series of results of the full finite element simulations. The required number of computations increases with the cubic power of the system size. In the cases of large-scale problems, the identification of nonlinear stiffness coefficients of these stiffness evaluation methods is computationally prohibited even with the reduced-order modeling techniques. In most cases, the computational efficiency is mainly based on the size of the problems.

In structural optimization problems, the issue outlined above becomes worse as it is necessary to update the design variables in every iteration. If a nonlinear dynamic system is concerned, for instance, the time marching simulation of the system should be

performed in each iteration of the optimization process. A step of time integration simulation includes a number of nonlinear structural analyses, which again includes a set of linear analyses. In this case, therefore, a parameterization technique, which reconstructs the system as a function of design parameters, is useful. However, not many research activities have been conducted on the parameterization of stiffness evaluation procedure. Although there is an integrated method that combines stiffness evaluation with reduced-order modeling and a parameterization technique [9], it does not directly use the strength of the stiffness evaluation method for the parameterization.

The main goal of this paper is to develop a method that extends the application of the stiffness evaluation procedure to large-scale analyses and design problems. To this end, in this work, Stiffness Evaluation method based on the Element Connectivity (SEEC) is presented. The element connectivity of the finite element models is used to evaluate the stiffness coefficients. In finite element methods, the internal force at a specific degree of freedom is related to the displacements at the corresponding degrees of freedom within the connected elements. Therefore, in the proposed methods, the stiffness coefficients are evaluated within the connected elements. Then the required number of full finite element computations for the evaluation of the stiffness coefficients is mainly determined by the characteristics of the element rather than by the problem size. Moreover, to enhance the efficiency, Reduced Order Modeling (ROM) using Proper Orthogonal Decomposition (POD) is applied to the proposed method. This process is referred to as SEECROM. Different from the conventional approaches with reduced-order modeling, the reduction is carried out after the stiffness evaluation. One more advantage of the proposed method is the easy utilization of parameterization. Due to the element-wise nature of the

identification process of stiffness coefficients, SEECROM models are easily constructed with variation of design parameters.

The present study was conducted to propose an efficient nonlinear model reduction method by enhancing the stiffness evaluation methods. The two main targets of this paper can be briefly described as follows: 1) For large-scale problems, the proposal of a stiffness evaluation method that has less dependency on the system size 2) For design problems, effective parameterization of the proposed stiffness evaluation method.

The proposal of SEECROM and its parameterization is followed by two other applications. The first application is the reduced order modeling of multibody dynamics. Most analyses of flexible multibody dynamics are based on Floating Frame of Reference Formulation (FFRF). It imposes the local coordinates for each flexible part, which enables the use of linear stiffness matrices. In the formulations of FFRF, however, inertia parts are introduced and the mass matrix becomes nonlinear. Therefore, the utilization of the reduction methods that have been developed based on the structural analyses cannot be directly achieved. The alternative approach is Absolute Nodal Coordinate Formulation (ANCF), which uses global absolute coordinates and slopes. This leads to a constant mass matrix and nonlinear stiffness matrix which is analogous to the system matrices of nonlinear static structural analysis. Since the additional inertia terms are also vanished due to the use of absolute nodal coordinates, the equation of motion with ANCF forms in a similar way in nonlinear static structural system. This enables the utilization of ROM methods developed for the static nonlinear structural analysis. SEECROM and its parameterization technique is combined to ANCF for the reduced modeling of multibody dynamics. Various examples which include free-falling pendulum, slider crank and four-

bar mechanism are successfully demonstrated.

In addition, the parameterized SEECROM can be easily applied to the structural optimization of nonlinear system. If nonlinearities are present in the system, the optimization process inherits the problem of the previous nonlinear reduction methods. This has been the obstacle to the study of the optimization concerning nonlinear systems. The iterations within the optimization process tends to deflate the efficiency of reduced order models while inflate the error rate. Thus the accuracy and the efficiency of the reduced model become crucial factors. The parameterization of the nonlinear model is another important factor for the application of reduced order models to the optimization procedure. If SEECROM-Parameterization is conducted with the proper sampling strategy, it can provide the desired reduced order model which meets the requirements. Two cases of optimization problems are subjected to a structural nonlinear system and a multibody dynamic system to validate the proposed method.

This paper is organized as follows. Sect. 2 introduces the conventional stiffness evaluation method of nonlinear structural analysis. In Sect. 3, the new stiffness evaluation method is derived based on the finite element connectivity. Its extension to the reduced-order modeling and parameterization are presented in Sect. 4 and Sect. 5, respectively. Test examples and results are included in each of these sections. The other two applications of the proposed method are presented in Sect. 6 and Sect. 7. The application to multibody dynamics is covered in Sect. 6 and the extension to the structural optimization is presented in Sect. 7. The conclusions are given in Sect. 8.

2. STIFFNESS EVALUATION

2.1. Stiffness evaluation methods

The equations of motion of an arbitrary structural system can be written as

$$M_{ij}\ddot{u}_j + C_{ij}\dot{u}_j + \Gamma_i(\mathbf{u}) = F_i \ , \quad i, j = 1, ..., N. \tag{2.1}$$

where M_{ij} and C_{ij} are the mass and the linear proportional damping matrices, respectively, $\mathbf{u}$ is the displacement vector, and F_i is the external force vector. The total number of degrees of freedom of the system is equal to N. If material or geometric nonlinearities are considered, the internal force $\Gamma_i(\mathbf{u})$ is modified from its linear composition. It becomes nonlinear in the displacement term $\mathbf{u}$; as the structure deforms, the values of the internal force change. Therefore, to solve the system with nonlinearities, an iterative evaluation of deformed states is required. Newton's method is commonly used to solve the structural nonlinearities. Eq. (2.2) represents the iterative process with the tangent stiffness matrix $K_{ij}^t(\mathbf{u}_0)$ and the internal force $\Gamma_i(\mathbf{u}_0)$ with the displacement $\mathbf{u}_0$. The equation is solved for Δu_j, and then the next iteration step is generated by Eq. (2.3) with the updated displacement $\mathbf{u}$. The tangent stiffness matrix can be computed from the $\mathbf{u}$-derivative of the internal force as shown in Eq. (2.4). Eq. (2.2)-(2.4) are repeated until the equilibrium of the system is obtained.

$$M_{ij}\ddot{u}_j + C_{ij}\dot{u}_j + K_{ij}^t(\mathbf{u}_0)\Delta u_j + \Gamma_i(\mathbf{u}_0) = F_i \tag{2.2}$$

where $\Delta\mathbf{u} = \mathbf{u} - \mathbf{u}_0$ (2.3)

$$K_{ij}^{t}(\mathbf{u}_0) = \left.\frac{\partial \Gamma_i}{\partial u_j}\right|_{\mathbf{u}=\mathbf{u}_0} \tag{2.4}$$

Since the iterative nature makes the solution process of the full nonlinear system inefficient, many studies have been carried out to solve the nonlinear analysis in reduced time and effort. Various reduced-order modeling techniques have also been proposed to enhance the efficiency of solving these nonlinearities. However, most reduction methods aim at shrinking the fully constructed matrix to a reduced one. The construction of the internal force and the tangent stiffness are still conducted in full domain, which is still a large-sized problem since the construction of the system matrices takes a large portion of the total computation time of nonlinear analyses. Moreover, the equilibrium of the system can easily be destabilized if a reduction technique tries to shrink the construction process of the internal force.

A stiffness evaluation technique is one possible solution to tackle this efficiency problem. It uses polynomial formulations to describe nonlinear internal forces. The internal force is expressed by 3rd order polynomial terms in displacement $\mathbf{u}$, which is shown in Eq. (2.5). The validity of the use of the 3rd degree polynomial functions is discussed in Appendix A.

$$M_{ij}\ddot{u}_j + C_{ij}\dot{u}_j + K_{ij}^{(1)}u_j + K_{ijk}^{(2)}u_j u_k + K_{ijkl}^{(3)}u_j u_k u_l = F_i\ , \quad i,j,k,l = 1,...,N \tag{2.5}$$

where $K_{ij}^{(1)}, K_{ijk}^{(2)}, K_{ijkl}^{(3)}$ are the nonlinear stiffness coefficients.

In this paper, the polynomial terms of the internal force are expressed in compact form and represented with tildes as below.

$$M_{ij}\ddot{u}_j + C_{ij}\dot{u}_j + \tilde{\Gamma}_i(\mathbf{u}) = F_i \tag{2.6}$$

$$\text{where} \quad \tilde{\Gamma}_i(\mathbf{u}) = \tilde{K}_{ijkl} u_j u_k u_l \tag{2.7}$$

The iterative form is shown as,

$$M_{ij}\ddot{u}_j + C_{ij}\dot{u}_j + \tilde{K}^t_{ij}(\mathbf{u}_0)\Delta u_j + \tilde{\Gamma}_i(\mathbf{u}_0) = F_i \tag{2.8}$$

$$\text{where} \quad \tilde{K}^t_{ij}(\mathbf{u}_0) = \left.\frac{\partial \tilde{\Gamma}_i(\mathbf{u})}{\partial u_j}\right|_{\mathbf{u}=\mathbf{u}_0} \tag{2.9}$$

Here we shortened the expression by including 1 as a value of the displacement $\mathbf{u}$, which enables $u_j u_k u_l$ to indicate u_j as well as $u_j u_k$ ($u_j(1)(1)$ and $u_j u_k(1)$, respectively). The stiffness coefficient $\tilde{K}_{ijkl}$ is basically a collection of the coefficients for all possible combinations of displacements.

Once the stiffness coefficient $\tilde{K}_{ijkl}$ is evaluated, the iterative computations of the i^{th} component of the nonlinear internal force $\tilde{\Gamma}_i(\mathbf{u})$ can be conducted efficiently. Let $u_j u_k u_l$ is rearranged as the vector function of $u^c(\mathbf{u})$, then the internal force can be represented as in the form of linear multiplications. See Eq. (2.10).

$$\tilde{\Gamma}_i(\mathbf{u}) = \tilde{K}^c_{ij} u^c_j(\mathbf{u}), \quad j = 1, ..., p \tag{2.10}$$

where p is the total number of the combinations. The subscript c represents the rearrangement by the vector alignment of the combinations. While the internal force $\Gamma_i(\mathbf{u})$ in its original form requires a process of reconstruction (integration, assembly, etc.) as the structure deforms, the internal force $\tilde{\Gamma}_i(\mathbf{u})$ in the stiffness evaluation method

does not require any reconstruction process. Since the stiffness coefficient in the stiffness evaluation method is constant against deformation, the nonlinear internal force is computed in a linear manner without the re-identification process.

Still, the efficiency is insufficient in most cases of the stiffness evaluation. In the evaluation process of the stiffness coefficients $\tilde{K}_{ijkl}$, the required number of full finite element nonlinear analyses is equal to the number of unknown stiffness coefficients to be evaluated. Therefore, the construction time for a polynomial model of the internal force increases with the cubic power of the total number of degrees of freedom.

There are basically two approaches to the identification of the stiffness coefficients. It depends on the sampling of the displacements and the corresponding internal forces. One approach imposes a series of load cases on the finite element model and obtains the induced responses. The other approach prescribes a set of displacements to evaluate the stiffness coefficients. Regardless of the approaches chosen, however, the number of stiffness coefficients to be identified remains equal.

Let the number of full degrees of freedom be N; then the number of nonlinear stiffness coefficients to be evaluated is ${}_{N+1}\mathbf{H}_3 - 1$. This can be expressed as $\frac{1}{6}(N+3)(N+2)(N+1)-1$. For example, if N =100, the number of required nonlinear computations is 176,850. If N =1,000, the number increases to 167,668,500.

2.2. Stiffness evaluation methods with reduced order modeling

Combined with the model order reduction method, the efficiency of the stiffness

evaluation method can be enhanced. Instead of using the original coordinates in full domain, the reduced coordinates are used to identify the nonlinear stiffness coefficients. Then, the number of nonlinear stiffness coefficients to be evaluated becomes ${}_{m+1}\mathbf{H}_3 - 1$ with a reduced number of degrees of freedom m. It increases with the cubic power of the size of the reduced system. However, the reduction rate is determined by the characteristics of the full model. Therefore, even with the reduced-order modeling, the stiffness evaluation method is strongly dependent on the size and the complexity of the full model.

There is an alternative approach to reducing the computational effort from $O(N^3)$ to $O(N^2)$ [8]. It uses a tangent stiffness matrix in the process of stiffness coefficient identification to improve the efficiency of the construction of the internal force model. Nonlinear static response analysis of a nine-bay panel model with 86,000 degrees of freedom and 85 reduction modes was successfully conducted with this approach. Still, the computational efficiency is mostly determined by the size and the complexity of the full finite element problems. In this work, a stiffness evaluation method that has less relation to the number of total elements or degrees of freedom is proposed.

3. STIFFNESS EVALUATION BASED ON ELEMENT CONNECTIVITY

In the conventional stiffness evaluation methods, the computational effort for solving full finite element nonlinear analysis problems increases proportionally to the 3rd power of the number of total degrees of freedom. This is the main factor that prevents the method from being applied to larger and more complex problems. In this section, we propose a new stiffness evaluation method that reduces the dependency of computational efficiency on the full model size/complexity.

3.1. Determination of displacements combination

In general, a linear internal force Γ_i and its stiffness matrix K_{ij} are composed as shown below.

$$\begin{bmatrix} \Gamma_1 \\ \Gamma_2 \\ \vdots \\ \vdots \\ \Gamma_N \end{bmatrix} = \begin{bmatrix} K_{11} & K_{12} & \cdots & \cdots & K_{1N} \\ K_{21} & K_{22} & & & \\ \vdots & & \ddots & & \\ \vdots & & & \ddots & \\ K_{N1} & & & & K_{NN} \end{bmatrix} \begin{bmatrix} u_1 \\ u_2 \\ \vdots \\ \vdots \\ u_N \end{bmatrix} \tag{3.1}$$

If the stiffness matrix is constructed properly, a large portion of the elements on the off-diagonal sides of the matrix will have zero values as in Eq. (3.2). The zero value of K_{ij} means that Γ_i does not have a dependency on u_j.

$$\begin{bmatrix} \Gamma_1 \\ \Gamma_2 \\ \vdots \\ \vdots \\ \Gamma_N \end{bmatrix} = \begin{bmatrix} K_{11} & K_{12} & \dots & 0 & 0 \\ K_{21} & K_{22} & \dots & 0 & 0 \\ \vdots & \vdots & \ddots & & 0 \\ 0 & 0 & & \ddots & \vdots \\ 0 & 0 & 0 & \dots & K_{NN} \end{bmatrix} \begin{bmatrix} u_1 \\ u_2 \\ \vdots \\ \vdots \\ u_N \end{bmatrix} \tag{3.2}$$

This is simply shown with four linear elements in Fig. 3.1. The linear force value Γ_i is only affected by the displacements that belong to the adjacent elements.

Because of the nature of finite element methods, the dependencies are bounded by the element connectivity in nonlinear cases as well. The nonlinear stiffness coefficients in stiffness evaluation methods also have similar characteristics. The nonlinear internal force $\tilde{\Gamma}_i(\mathbf{u})$ of the i^{th} degree of freedom is determined by $\tilde{K}_{ijkl} u_j u_k u_l$, where $\tilde{K}_{ijkl}$ has non-zero values if the internal force $\tilde{\Gamma}_i(\mathbf{u})$ has a dependency on $u_j u_k u_l$. It is shown already that the nonlinear relation can be expressed in a linear manner with Eq. (2.10). With the rearranged format, the internal force vector in stiffness evaluation can be written as

$$\begin{bmatrix} \tilde{\Gamma}_1 \\ \tilde{\Gamma}_2 \\ \vdots \\ \vdots \\ \tilde{\Gamma}_N \end{bmatrix} = \begin{bmatrix} \tilde{K}^c_{11} & \tilde{K}^c_{12} & \dots & 0 & 0 \\ \tilde{K}^c_{21} & \tilde{K}^c_{22} & \dots & 0 & 0 \\ \vdots & \vdots & \ddots & & 0 \\ 0 & 0 & & \ddots & \vdots \\ 0 & 0 & 0 & \dots & \tilde{K}^c_{Np} \end{bmatrix} \begin{bmatrix} u^c_1 \\ u^c_2 \\ \vdots \\ \vdots \\ u^c_p \end{bmatrix} \tag{3.3}$$

where N is the size of the full domain and p is the total number of displacement combinations.

The method we propose here is based on the characteristics of the finite elements described above. As for the computation of the internal force $\tilde{\Gamma}_i$ on the i^{th} degree of

freedom, the adjacent elements around the i^{th} node are selected. Then the 3-combinations of displacements from these selected elements are computed element by element. Then, $\tilde{\Gamma}_i$ is expressed as the sum of these element-wise polynomial terms. This operation is denoted in Eq. (3.4).

$$\tilde{\Gamma}_i(\mathbf{u}) = \tilde{K}_{ijkl}\sum_{n=1}^{AE}\left[u_j u_k u_l\right]_n = \tilde{K}_{ij}\sum_{n=1}^{AE}\left[u_j^c(\mathbf{u})\right]_n \tag{3.4}$$

where AE indicates the number of adjacent elements.

Fig. 3.2 illustrates the nonlinear internal force at the specific degree of freedom q. To compute the internal force value, the combination terms are composed only within the adjacent elements around the point q. See Eq. (3.5).

$$\tilde{\Gamma}_q = \tilde{K}_{qj}\ \left[u_j^c\right]_{E6} + \left[u_j^c\right]_{E7} + \left[u_j^c\right]_{E10} + \left[u_j^c\right]_{E11} \tag{3.5}$$

Then, the length p of the polynomial displacement vector $u_i^c(\mathbf{u})$, which is the number of unknown nonlinear stiffness coefficients, is greatly reduced since all the coefficients that belong to the outside of the adjacent elements have zero values. The number of nonlinear stiffness coefficients to be evaluated per degree of freedom of internal forces becomes $4({}_{e+1}\mathbf{H}_3 - 1) - \gamma = \frac{2(e+3)(e+2)(e+1)}{3} - 4 - \gamma$, where e is the number of degrees of freedom in one element and γ is the number of shared combinations within adjacent elements. For example, if the element has 4 nodes per element and 2 degrees of freedom per node, the number of unknown coefficients per internal force becomes 529 (γ =127) regardless of the problem size. Whether the total number of degrees of freedom is 100 or 10,000, the number of unknowns per internal

force remains 529 in this case. Therefore, the difference in the number of unknowns between the conventional stiffness evaluation and the proposed method grows as the problem size increases.

The relations between the number of unknowns and the total degrees of freedom are summarized in Table 3.1. It should be noted that the size of the reduced system is largely determined by the characteristics of the problem, such as the size or the complexity of the problem, which again determine the total number of unknowns. In contrast, with the SEEC method, the number of unknowns increases linearly with the problem size. These are illustrated in Fig. 3.3. with a fixed reduction rate of 1% and the element described in the previous paragraph.

With the proposed approach, therefore, the composition of displacement combinations and nonlinear stiffness coefficients is mainly determined by the element connectivity of the chosen finite element. The total size of the problem only linearly influences the total number of unknowns. Furthermore, the identification of stiffness coefficient matrix is independently obtained from a specific internal force DOF by DOF. Thus the stiffness evaluation process can be easily parallelized. Since the element connectivity is effectively used in the proposed method, this new stiffness method is named as Stiffness Evaluation based on Element Connectivity (SEEC).

3.2. Evaluation of stiffness coefficients

3.2.1. Sampling

It is pointed out that with the SEEC approach, the number of the unknown coefficients for the stiffness evaluation is mainly determined by the type of the finite element with the linear dependency on the problem size. In addition, the number of required sampling sets is entirely determined by the element characteristics. The sampling set that is composed of displacements and the corresponding internal forces are required for the identification of the stiffness coefficients. In the conventional method, the number of sampling sets is equal to the number of unknown coefficients. On the other hand, in the SEEC approach, the number of sampling sets is determined by the unknown coefficients per internal force without the linear dependency on N. Since the evaluation process per internal force is conducted independently, the same solution sets can be applied for the each computation per internal force. Hence the number of the sampling sets is entirely determined by the element type.

In the case of a four-node shell element with 5 degrees of freedom per node, there are 20 degrees of freedom in an element. If the number of adjacent elements is 4, the number of combinations for an internal force equals to $4({}_{20+1}\mathbf{H}_3 - 1) - \gamma$. With the consideration of shared combination number γ, this becomes 5,995, which determines the number of sampling sets required in the sampling process. It is notable that the number does not change with the size or the complexity of the problem.

The sampling procedure is listed below.

1) Compose the displacement combinations for each degree of freedom of nonlinear internal force. They are automatically computed by the type of the element and the mesh chosen for the problem.
2) Determine the training problem(s). The training problem whose solution sufficiently

includes the span of the target responses should be set up in advance. Then, determine the number of iteration steps according to the number of the required solution sets, which is determined by the number of displacement combinations per internal force.

3) Solve the training problems and save the sampling sets of [displacements-internal forces]. These sampling sets are used for the evaluation of the nonlinear stiffness coefficients in Sect. 3.2.2. They are also used for the construction of the reduced model in Sect. 4. In this paper, proper orthogonal modes extracted from the sampled data are applied in reduced-order modeling.

If the training problem is the nonlinear structural dynamic analysis, the sampling sets are stored from the each time step or with selected iteration steps in each time step. The strength of this procedure using training problems is that one can easily include the effective sampling points by intuition.

3.2.2. Minimum norm Least Squares

If s number of sampling sets are saved in the sampling procedure, the nonlinear internal force on i^{th} degree of freedom can be expressed as below.

$$\begin{bmatrix} \Gamma_{i1} & \Gamma_{i2} & \cdots & \Gamma_{is} \end{bmatrix}_{sampling} = \begin{bmatrix} \tilde{K}_{i1} & \tilde{K}_{i2} & \cdots & \tilde{K}_{ip} \end{bmatrix} \begin{bmatrix} u_{11}^c & u_{12}^c & \cdots & u_{1s}^c \\ u_{21}^c & u_{22}^c & \cdots & u_{2s}^c \\ \vdots & \vdots & \ddots & \vdots \\ u_{p1}^c & u_{p2}^c & \cdots & u_{ps}^c \end{bmatrix}_{sampling} \tag{3.6}$$

where p is the number of displacement combinations and s is the number of the

stored sampling sets from the sampling process.

The data sets from the sampling are indicated by $sampling$ in lower case. From the sampling procedure, displacements and their corresponding internal forces are saved. The internal force matrix $\Gamma_{sampling}$ is directly stored from the sampling process. The displacement combination matrix $\left[u^c\right]_{sampling}$ is formed as follows. The set of combinations obtained from the adjacent elements are rearranged into a $p\times 1$ vector as in Eq. (3.3). Then, the sampled displacements are employed to create a $p\times s$ displacement combination matrix.

Using the Least Squares method, the nonlinear stiffness coefficients $\tilde{K}$ in Eq. (3.6) can be determined even if s is not equal to p. The process is illustrated below. First, as shown in Eq. (3.7), Eq. (3.6) can be reorganized into the form of $Ax=b$.

$$\underbrace{\begin{bmatrix} u_{11}^c & u_{12}^c & \cdots & u_{1p}^c \\ u_{21}^c & u_{22}^c & \cdots & u_{2p}^c \\ \vdots & \vdots & \ddots & \vdots \\ u_{s1}^c & u_{s2}^c & \cdots & u_{sp}^c \end{bmatrix}}_{sampling} \begin{bmatrix} \tilde{K}_{i1} \\ \tilde{K}_{i2} \\ \vdots \\ \tilde{K}_{ip} \end{bmatrix} = \underbrace{\begin{bmatrix} \Gamma_{i1} \\ \Gamma_{i2} \\ \vdots \\ \Gamma_{is} \end{bmatrix}}_{sampling} \tag{3.7}$$

where $$A=\underbrace{\begin{bmatrix} u_{11}^c & u_{12}^c & \cdots & u_{1p}^c \\ u_{21}^c & u_{22}^c & \cdots & u_{2p}^c \\ \vdots & \vdots & \ddots & \vdots \\ u_{s1}^c & u_{s2}^c & \cdots & u_{sp}^c \end{bmatrix}}_{sampling}, \quad x=\begin{bmatrix} \tilde{K}_{i1} \\ \tilde{K}_{i2} \\ \vdots \\ \tilde{K}_{ip} \end{bmatrix}, \quad b=\underbrace{\begin{bmatrix} \Gamma_{i1} \\ \Gamma_{i2} \\ \vdots \\ \Gamma_{is} \end{bmatrix}}_{sampling} \tag{3.8}$$

Eq. (3.7) can be solved differently by using the characteristics of A. The sampling process and the problem itself affect the composition of A matrix. A is not necessarily a square matrix, while the size of the matrix is determined by [the number of

sampled sampling sets s] × [the size of the polynomial displacement vector p]. Even if it is square, the rank is not guaranteed to be full. One of the methods of obtaining the solution when the matrix has rank deficiency is the minimum norm Least Squares, which is represented in Eq. (3.9). This method yields a unique solution of Eq. (3.7) with the rectangular and rank-deficient matrix A.

$$\min_x \|b - Ax\|_2 \quad , \quad \min_x \|x\|_2 \tag{3.9}$$

The minimum norm Least Square solution can be obtained by QR factorization with column pivoting. It yields sparse solutions, which means that the solution has zero elements. A solution where the elements have as few non-zeros as possible is obtained. The solution x with k nonzero elements is obtained by QR factorization with column pivoting where k is the rank of A as in Eq. (3.10).

$$\text{rank}(A) = k \ < \ \min(s, p) \tag{3.10}$$

The process of QR factorization with column pivoting is illustrated below.

By QR factorization, the $s \times p$ matrix A is expressed as,

$$A = Q\begin{pmatrix} R \\ 0 \end{pmatrix} \tag{3.11}$$

where R is a $p \times p$ upper triangular matrix and Q is an $s \times s$ orthogonal square matrix, which have the characteristics as shown in Eq. (3.12) and Eq. (3.13), respectively.

$$\|x\|_2 = \|Qx\|_2 \tag{3.12}$$

$$Q^T Q = I \tag{3.13}$$

In the method of QR factorization with column pivoting, the column permutation matrix

E is multiplied to Eq. (3.11). E is composed such that the diagonal elements of R have magnitude in descending order.

$$A = Q\begin{pmatrix} R \\ 0 \end{pmatrix} E^T \tag{3.14}$$

Eq. (3.14) represents the column pivoting method where R becomes the matrix in Eq. (3.15). If k is the effective rank of A, R_{11} is a $k \times k$ upper triangular matrix.

$$R = \begin{pmatrix} R_{11} & R_{12} \\ 0 & 0 \end{pmatrix} \tag{3.15}$$

The solution χ in Eq. (3.8) is obtained from Eq. (3.16)-(3.18)

$$Q^T A x = Q^T b \tag{3.16}$$

$$x = E\begin{pmatrix} R_{11}^{-1}\hat{c} \\ 0 \end{pmatrix} \tag{3.17}$$

$$c = Q^T b \tag{3.18}$$

where $\hat{c}$ is the first k elements of c.

The i^{th} row of the nonlinear stiffness coefficients matrix $\tilde{K}_{ij}$ in Eq. (3.19) is constructed from the solution χ above. To construct the stiffness coefficients completely, χ should be solved by the number of total degrees of freedom. However, since the number of displacement combinations p is relatively small and parallel computations are easily applied as the computation works independently, the construction process can be achieved efficiently. For further understanding of QR factorization for minimum norm Least Square solutions, see references [10,11].

$$\tilde{\Gamma}_i = \tilde{K}_{ij} u_j^c(\mathbf{u}) \tag{3.19}$$

$$\begin{bmatrix} \tilde{\Gamma}_1 \\ \tilde{\Gamma}_2 \\ \vdots \\ \vdots \\ \tilde{\Gamma}_N \end{bmatrix} = \begin{bmatrix} \tilde{K}_{11} & \tilde{K}_{12} & \cdots & \cdots & \tilde{K}_{1p} \\ \tilde{K}_{21} & \tilde{K}_{22} & & & \\ \vdots & & \ddots & & \\ \vdots & & & \ddots & \\ \tilde{K}_{N1} & & & & \tilde{K}_{Np} \end{bmatrix} \begin{bmatrix} u_1^c \\ u_2^c \\ \vdots \\ \vdots \\ u_p^c \end{bmatrix} \tag{3.20}$$

Once the stiffness coefficients matrix $\tilde{K}_{ij}$ is established, the nonlinear internal forces at deformed states are obtained as follows. First, the displacement combination vector $u^c(\mathbf{u})$ is computed from the current displacements. Then, the stiffness coefficient matrix is multiplied with the combination vector, which simply yields the nonlinear internal forces. These are shown in Eqs. (3.19)-(3.20).

3.3. Computation of tangent stiffness

The internal force composed of the stiffness coefficients is differentiated to yield the tangent stiffness. The differentiation is iteratively repeated in every time step, which guides the system to a force equilibrium state. Although Finite Difference Method (FDM) is easily applied to compute tangent stiffness [12], it requires a great deal of computational resources. The computational efficiency can be enhanced if the tangent stiffness is directly provided by analytical differentiation of internal forces.

The tangent stiffness can be analytically derived with the stiffness evaluation method as in Eq. (3.21). Since the internal force is composed as the sum of the 3rd order displacement combinations, the tangent stiffness matrix is obtained by simple

differentiations in terms of its displacement as given below.

$$\tilde{K}_{iq}^{t}(\mathbf{u}_0) = \left.\frac{\partial \tilde{\Gamma}_i(\mathbf{u})}{\partial u_q}\right|_{\mathbf{u}=\mathbf{u}_0} = \tilde{K}_{ijkl}\left(\delta_{jq}u_k u_l + \delta_{kq}u_l u_j + \delta_{lq}u_j u_k\right)\Big|_{u=u_0} \tag{3.21}$$

where δ_{ij} is Kronecker delta in Eq. (3.22)

$$\delta_{ij} = \begin{cases} 0 & \text{if } i \neq j, \\ 1 & \text{if } i = j. \end{cases} \tag{3.22}$$

The equations above for the computation of tangent stiffness can be used within the proposed method. Although the computation efficiency of Eq. (3.21) itself is not improved compared with FDM, the addition of the analytical approach maintains the accuracy and the stability of the system.

Table 3.1

Relation between the number of unknowns and problem size

	CONVENTIONAL METHOD		PROPOSED METHOD
	Full	With ROM	SEEC
PER INTERNAL FORCE	$\frac{1}{6}(N^3+6N^2+11N)$	$\frac{1}{6}(m^3+6m^2+11m)$	$\frac{1}{6}(e^3+6e^2+11e)-\gamma$
ENTIRE DOMAIN	$\frac{1}{6}(N^4+6N^3+11N^2)$	$\frac{1}{6}(m^4+6m^3+11m^2)$	$N\{\frac{1}{6}(e^3+6e^2+11e)-\gamma\}$

N : Total number of degrees of freedom
m : Number of degrees of freedom in reduced system
e : Number of degrees of freedom in one element
γ : Number of shared combinations within adjacent elements

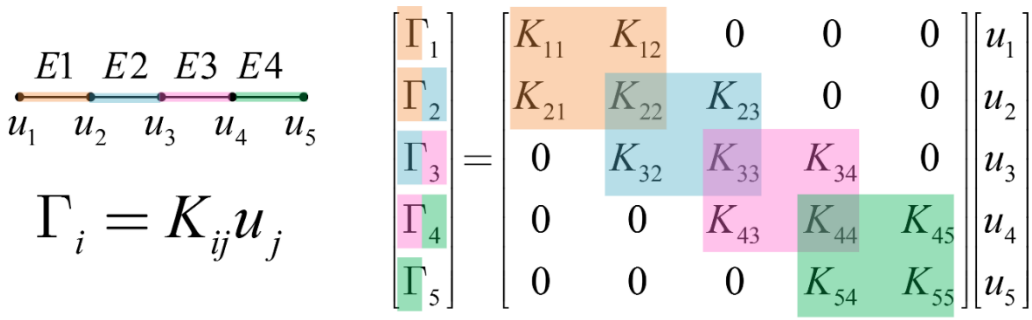

Figure 3.1. Relation between force values and element connectivity

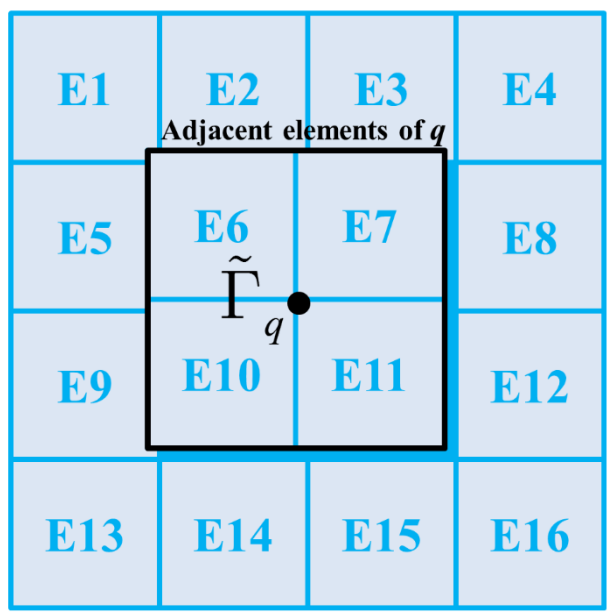

Figure 3.2. Element-wise construction of nonlinear internal force

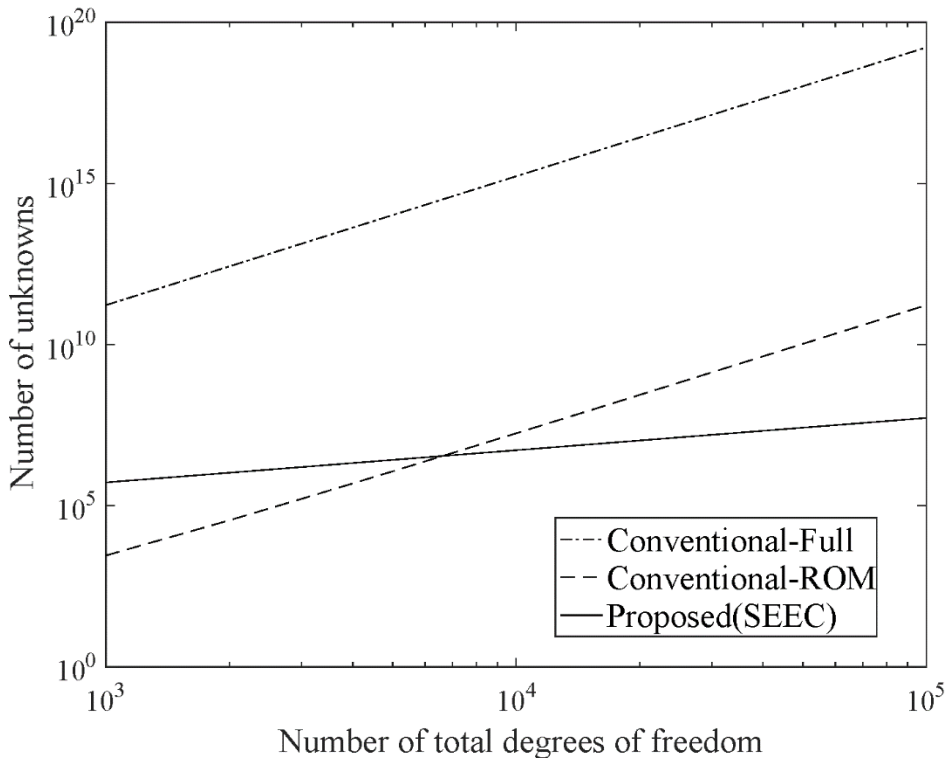

Figure 3.3. Relation between number of unknowns and problem size

4. REDUCED ORDER MODELING USING SEEC

In this section, ROM is combined with the SEEC method to improve the computation efficiency of the SEEC method. It is applied to reduce the computation time of Eq. (3.19) and Eq. (3.20); the reduced modeling here is not related to the stiffness evaluation procedure given in Sect. 3.2. Instead, it applies to the use of the internal force model constructed in the previous section. The combined method is referred to as SEECROM.

One of the critical differences between SEECROM and the other ROM-based stiffness evaluation approaches is related to the application sequence of the ROM. The conventional approaches apply ROM before the evaluation of the stiffness coefficients. This makes the computation of internal force to take place on the reduced coordinates, and results in a loss in accuracy. On the other hand, SEECROM applies ROM after the evaluation of the stiffness coefficients. Since the stiffness evaluation is performed on the full original coordinates, the accuracy can be guaranteed. It is important in the reduced-order modeling of nonlinear structural dynamics that the reduction is conducted while keeping the equilibrium of the governing equation. If the equilibrium is maintained based on the reduced coordinates, the stability as well as the accuracy of the system continues to deteriorate as the analysis is repeated. SEECROM resolves this issue by performing ROM after SEEC. While the preceding SEEC method guarantees accuracy with sufficient efficiency (the former by the full coordinate computation and the latter by the element connectivity), the following ROM enhances the efficiency further without degradation of accuracy.

4.1. Proper orthogonal decomposition

In this paper, POD is used as a reduction method. It is known that the POD method yields the best representation of given data sets. The proper orthogonal modes obtained from the POD process are the orthogonal bases for forming the reduced coordinates. The reduction modes are extracted from the displacement data sets stored in Sect.3.2.1. If the number of degrees of freedom exceeds the number of sampling sets, the method of snapshots [13,14] can be used. The procedure of POD reduction using the snapshot method is briefly given below. For a more detailed explanation, check references [15,16].

Eq. (33) represents the snapshots matrix from the displacements of sampling data.

$$U = \begin{bmatrix} u_1^{(1)} - \bar{u}_1 & u_1^{(2)} - \bar{u}_1 & \cdots & u_1^{(s)} - \bar{u}_1 \\ u_2^{(1)} - \bar{u}_2 & u_2^{(2)} - \bar{u}_2 & \cdots & u_2^{(s)} - \bar{u}_2 \\ \vdots & \vdots & \vdots & \vdots \\ u_N^{(1)} - \bar{u}_N & u_N^{(2)} - \bar{u}_N & \cdots & u_N^{(s)} - \bar{u}_N \end{bmatrix} \tag{4.1}$$

where N, S and $\bar{u}$ represent the number of total degrees of freedom, number of sampling sets, and average value of sampled displacements u, respectively. The POD modes ϕ can be obtained from the eigenmodes $\hat{U}$ in Eq. (4.2) to form the POD representation of the displacements u^{POD} in Eq. (4.3). Then, a number of dominant POD modes are selected for the reduction of the system according to the targeted reduction rate.

$$\hat{U} = U \cdot U^T \tag{4.2}$$

$$u_i^{POD} = \phi_{ij} r_j + \bar{u}_i, \quad j = 1, \ldots, m \tag{4.3}$$

where r is the generalized coordinates for the reduced model and m is the number of

selected reduction modes.

4.2. Proper orthogonal decomposition with SEEC

If $\mathbf{u}$ is substituted by u^{POD}, Eq. (2.6) and Eq. (2.8) can be expressed in the reduced form, respectively, as

$$\phi_{li} M_{lk} \phi_{kj} \ddot{r}_j + \phi_{li} C_{lk} \phi_{kj} \dot{r}_j + \phi_{ki} \tilde{\Gamma}_k(\mathbf{u}) = \phi_{ki} F_k . \tag{4.4}$$

$$\phi_{li} M_{lk} \phi_{kj} \ddot{r}_j + \phi_{li} C_{lk} \phi_{kj} \dot{r}_j + \phi_{li} \tilde{K}^t_{lk}(\mathbf{u}_0) \phi_{kj} \Delta r_j + \phi_{ki} \tilde{\Gamma}_k(\mathbf{u}_0) = \phi_{ki} F_k \tag{4.5}$$

Note that the internal force $\tilde{\Gamma}_i(\mathbf{u})$ is computed from the full coordinate $\mathbf{u}$.

Furthermore, the computation of the tangent stiffness $\tilde{K}^t$ in Eq. (4.5) is accelerated with the reduced-order modeling. Let the internal force be represented with the reduction modes as shown in Eq. (4.6). This can be differentiated by r to construct the reduced tangent stiffness matrix. See Eq. (4.7).

$$\phi_{ki} \tilde{\Gamma}_k(\mathbf{u}) = \phi_{ki} \tilde{K}_{kjql} \phi_{jv} \phi_{qw} \phi_{lz} r_v r_w r_z \tag{4.6}$$

$$\begin{aligned} \phi_{li} \tilde{K}^t_{lk}(\mathbf{u}_0) \phi_{kj} &= \phi_{li} \left. \frac{\partial \tilde{\Gamma}_l(\mathbf{u})}{\partial r_k} \right|_{\mathbf{u}=\mathbf{u}_0} \phi_{kj} \\ &= \phi_{li} \tilde{K}_{ljqz} \left(\phi_{jk} u_q u_z + \phi_{qk} u_z u_j + \phi_{zk} u_j u_q \right) \Big|_{u=u_0} \phi_{kj} \end{aligned} \tag{4.7}$$

If the reduced form of stiffness coefficients $\phi^T \tilde{K}$ are saved in advance and used for the repeated computations in nonlinear analysis, the efficiency is further improved since the reduced tangent stiffness matrix is directly obtained.

4.3. Application of SEECROM

A few sets of structural dynamic analyses of geometric nonlinear elements were performed for the validation of SEECROM. Previously, it was addressed that the efficiency of SEEC is determined by the complexity of the element itself, rather than by the size of the problem. The shell element used here, which has 54 degrees of freedom per element, is sufficient to verify the effectiveness of the proposed method.

For the demonstration of the proposed method, an offline-online methodology was applied. In the offline stage, the stiffness evaluation models are constructed. As presented in Sect. 3, after the determination of the combinations, the stiffness coefficients are evaluated with the sampling process. With these stiffness coefficients and POD of sampled displacements, the nonlinear internal force model is constructed based on the reduced coordinates. In the online stage, the internal force model constructed in the offline stage is solved. The approximate solutions of internal forces are obtained by various displacement inputs. The efficiency and the accuracy of SEECROM are compared by the results in the online stage.

The nonlinear shell element used in the example had 9 nodes per element and 6 degrees of freedom per node, which yielded 54 degrees of freedom per element. Fig. 4.1 shows the configurations of the example. The uniform thickness of the shell was 0.01 m. With fixed ends, the shell was subjected to out-of-plane dynamic loads at the middle of the other ends. The structural dynamic analysis was performed under the perturbation of the external dynamic loads. The dynamic load was composed of two design parameters μ_1 and μ_2 as shown in Fig. 4.2. In the offline stage, sampling loads were imposed to obtain

solution sets and perform POD. Sampling loads of 100 N, 500 N, and 1,000 N, as denoted with the dotted lines in Fig. 4.2, were imposed. The shell had an elastic modulus of 5 GPa and a density of 5,000 kg/m3. A Newmark method was applied for nonlinear transient analysis.

For the verification of the accuracy of SEECROM, a set of nonlinear transient analyses were performed for the 9 different sets of design parameters. The properties of the design parameters and the results of full order and SEECROM analysis are shown in Fig. 4.3. Eight elements (total number of degrees of freedom = 270) were used for both models, and 27 POD modes were used for SEECROM. In the graphs of Fig. 4.3, it can be seen that the response results from the two approaches overlap regardless of the variation in design variables, which proves the accuracy of SEECROM.

For the verification of the efficiency of SEECROM method, the nonlinear transient analysis was repeated as the number of elements was increased by 8/32/72. (The total number of degrees of freedom was increased as 270/918/1950.) The computation time and the displacement response were compared between the SEECROM method and the POD-only reduction method. In this example, the reduced models were constructed with 32 POD modes in both methods. It should be noted that the required number of sampling sets was fixed regardless of the number of elements used. Two load cases (CASE 1 & CASE 2) were created for the verification, which are drawn with solid lines whereas the sampling loads for the training analyses are drawn with dotted lines in Fig. 4.4 and Fig. 4.5.

The snapshots displayed in Fig. 4.6 and Fig. 4.7 are the responses of full-order nonlinear transient analyses under the load cases of CASE 1 and CASE 2, respectively. The

responses of reduced analyses are compared in Fig. 4.8 and Fig. 4.9. The results from SEECROM are denoted with red solid lines, and the POD results are drawn with blue dotted lines. The black dotted lines show the responses under the sampling loads for reference.

Excellent agreement between the two reduction methods is obtained for the two load cases. The accuracy of SEECROM is guaranteed regardless of whether the obtained response and the sampled responses have a similar tendency (CASE 2) or not (CASE 1).

The computation times for SEECROM and POD-only reduction methods are compared for CASE 1 and CASE 2 in Fig. 4.10 and Fig. 4.11. The "time rate" represents the computation time of the POD method divided by the computation time of the SEECROM method. The SEECROM method is approximately 15 times faster than the POD reduction method in CASE 1 and 17 times faster in CASE 2. It should be noted that the rate is maintained regardless of the size of the system.

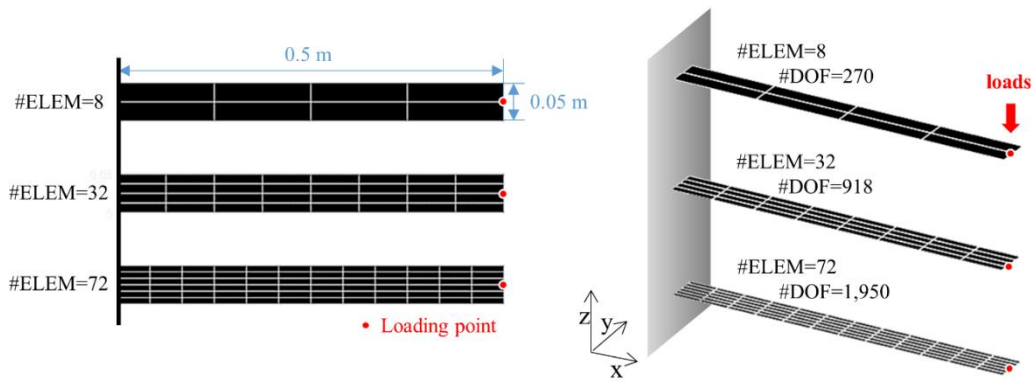

Figure 4.1. Configuration of shell element

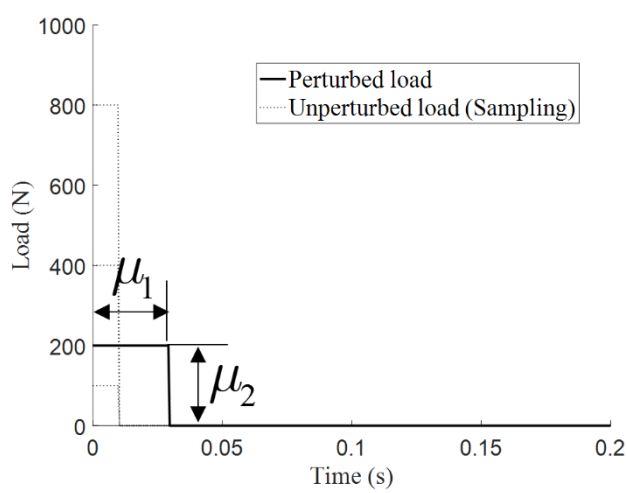

Figure 4.2. External loads for shell example

Sampling

	μ_1	μ_2
1	0.01	100
2	0.01	400
3	0.01	800

Perturbation of design variables

	μ_1	μ_2
1	0.005	100
2	0.005	200
3	0.005	400

	μ_1	μ_2
4	0.01	100
5	0.01	200
6	0.01	400

	μ_1	μ_2
7	0.02	100
8	0.02	200
9	0.02	400

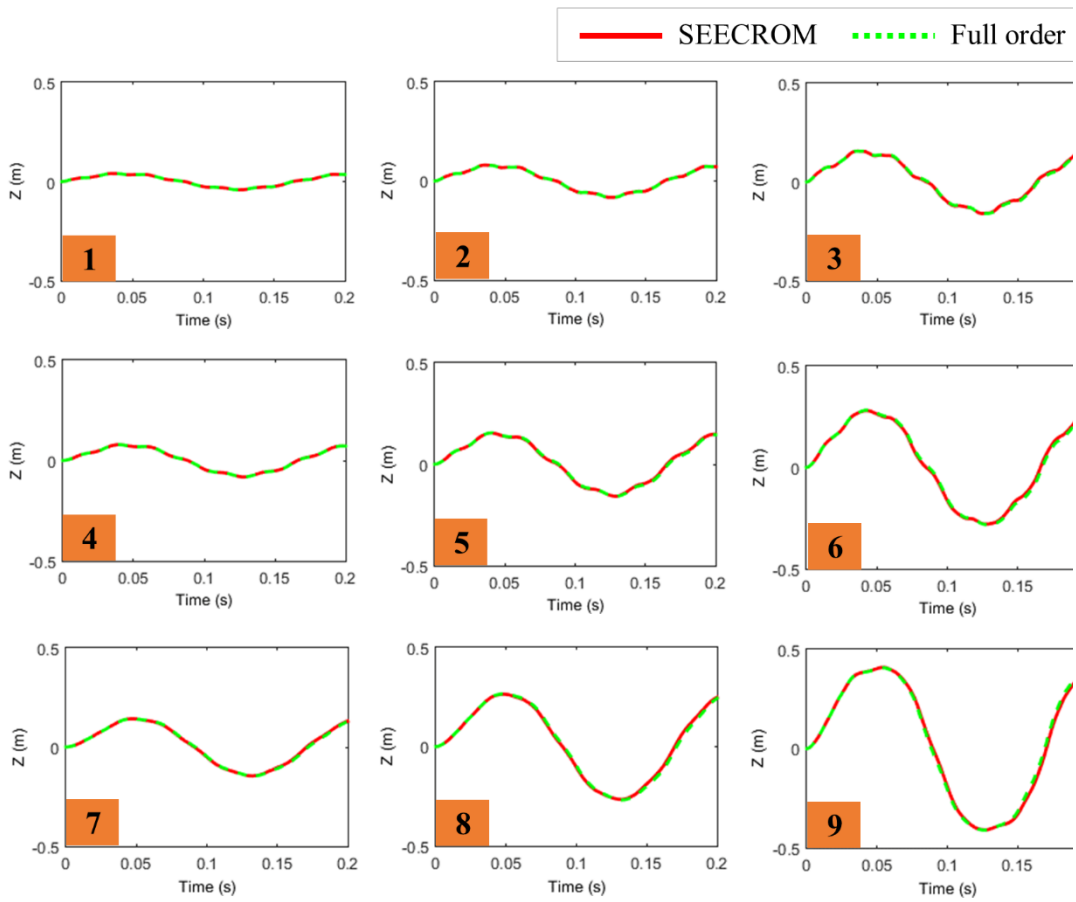

Figure 4.3. Responses under perturbation of external loads

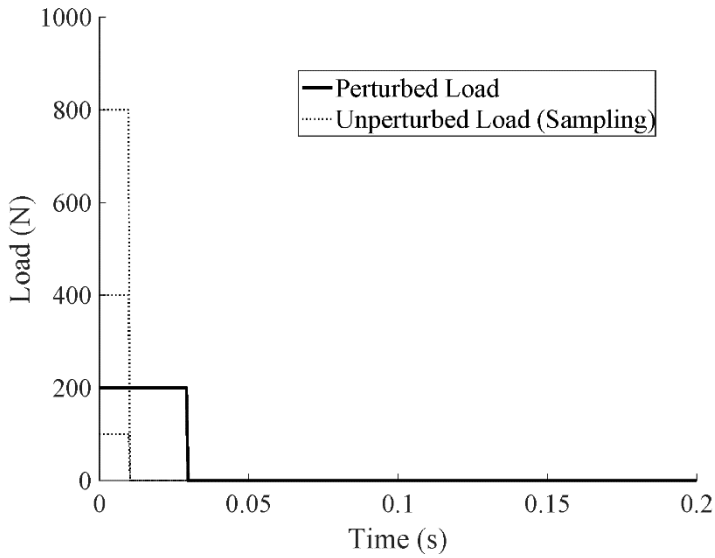

Figure 4.4. Load configurations: CASE 1

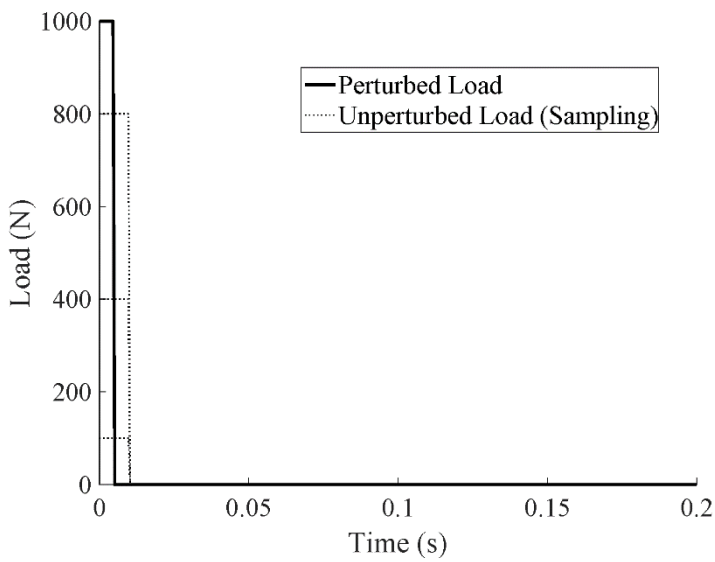

Figure 4.5. Load configurations: CASE 2

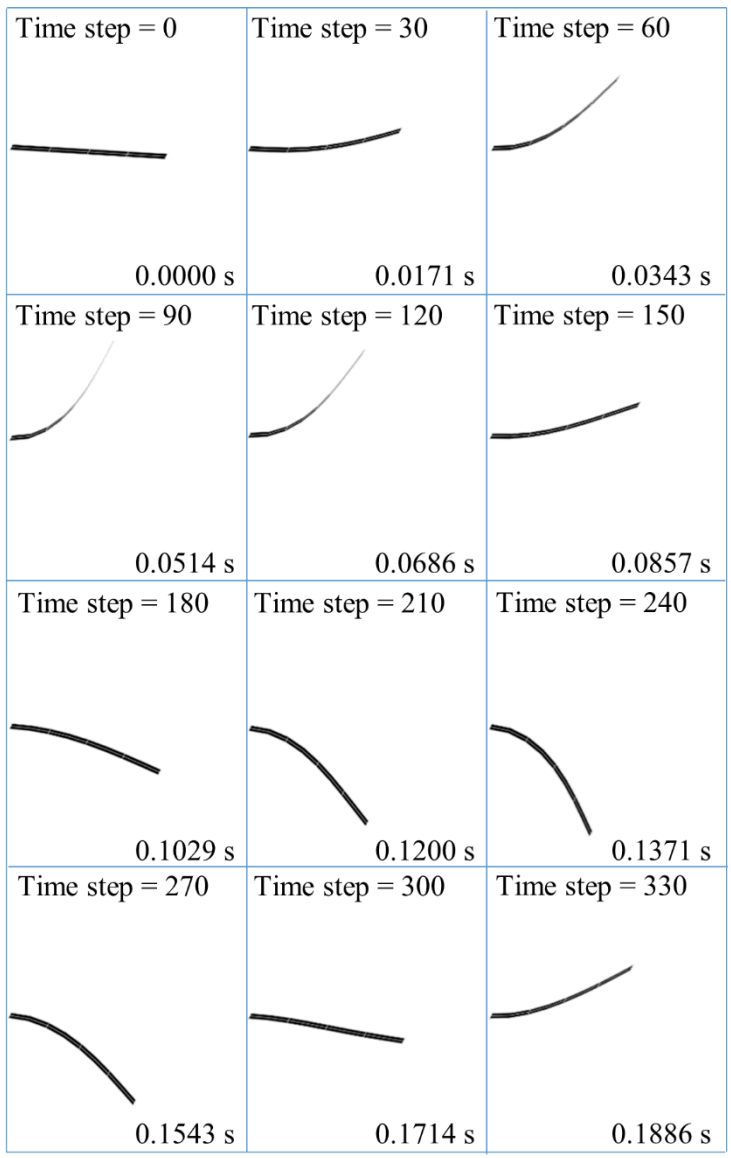

Figure 4.6. Time response of shell: CASE 1

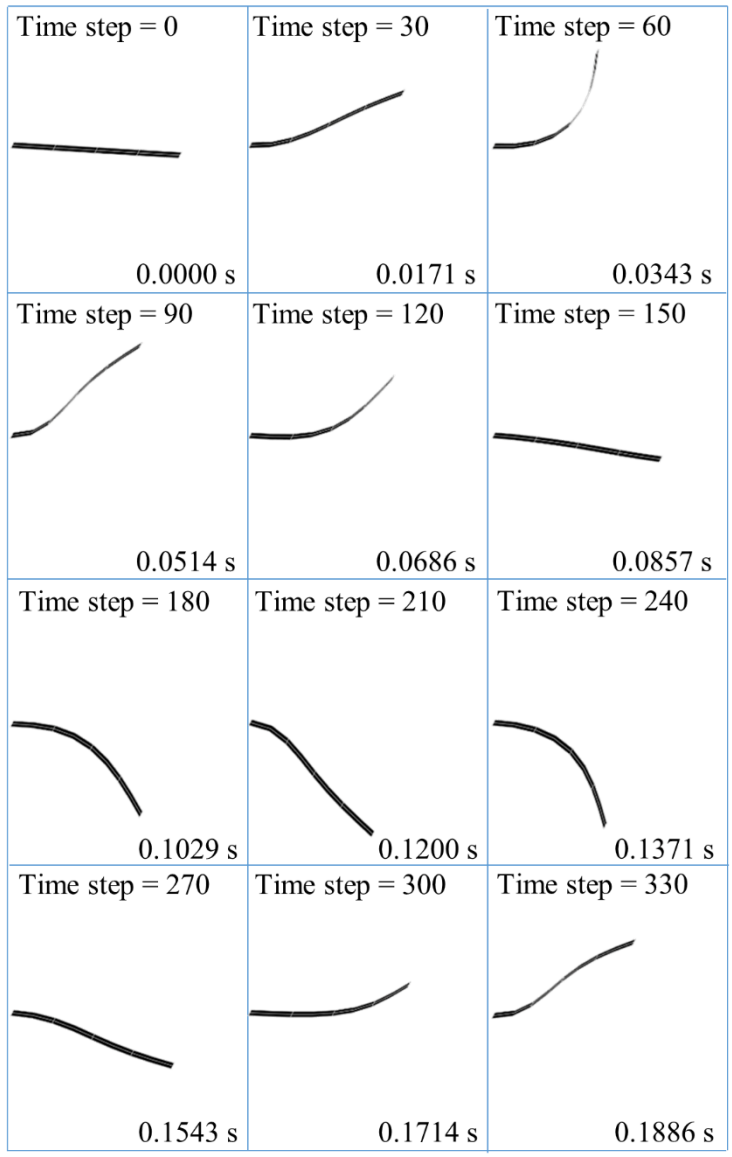

Figure 4.7. Time response of shell: CASE 2

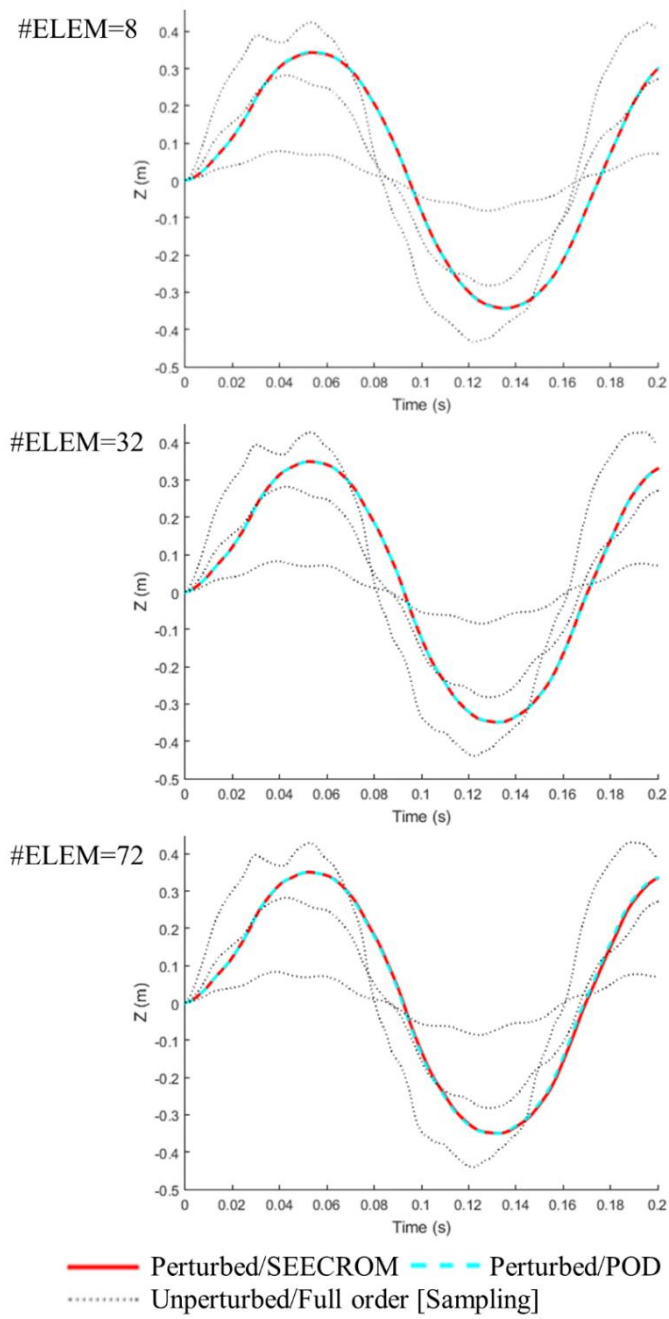

Figure 4.8. Time response under design variable perturbation: CASE 1

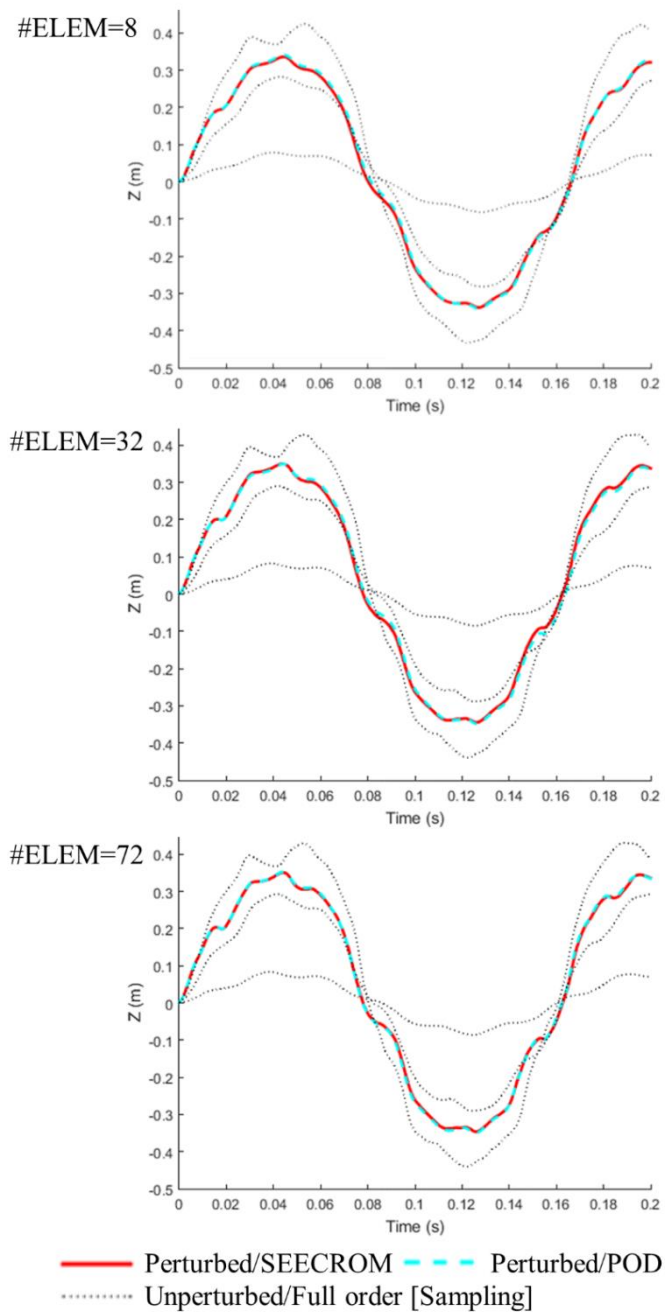

Figure 4.9. Time response under design variable perturbation: CASE 2

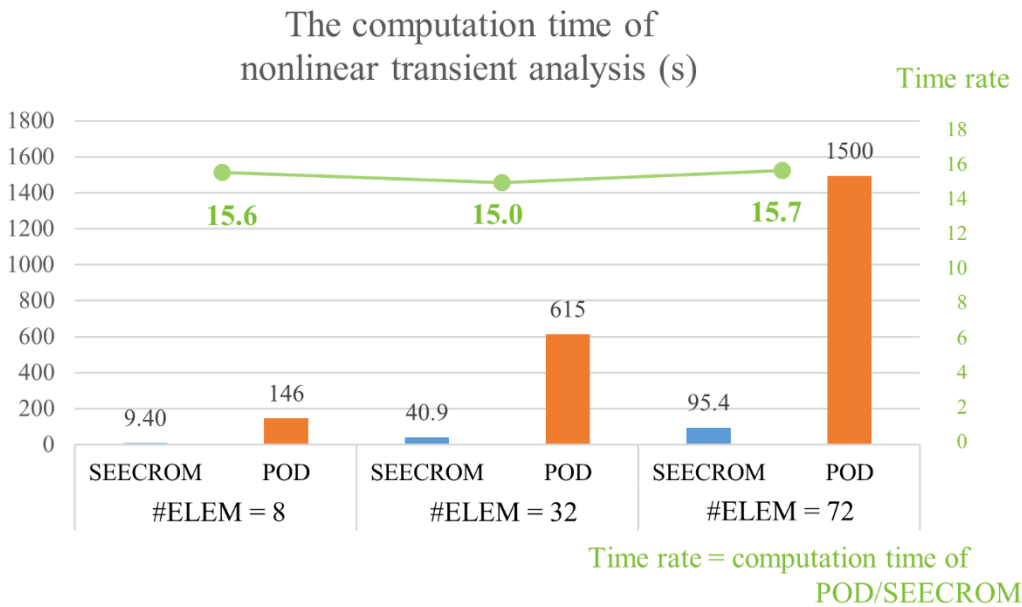

Figure 4.10. Computation time comparison by number of elements: CASE 1

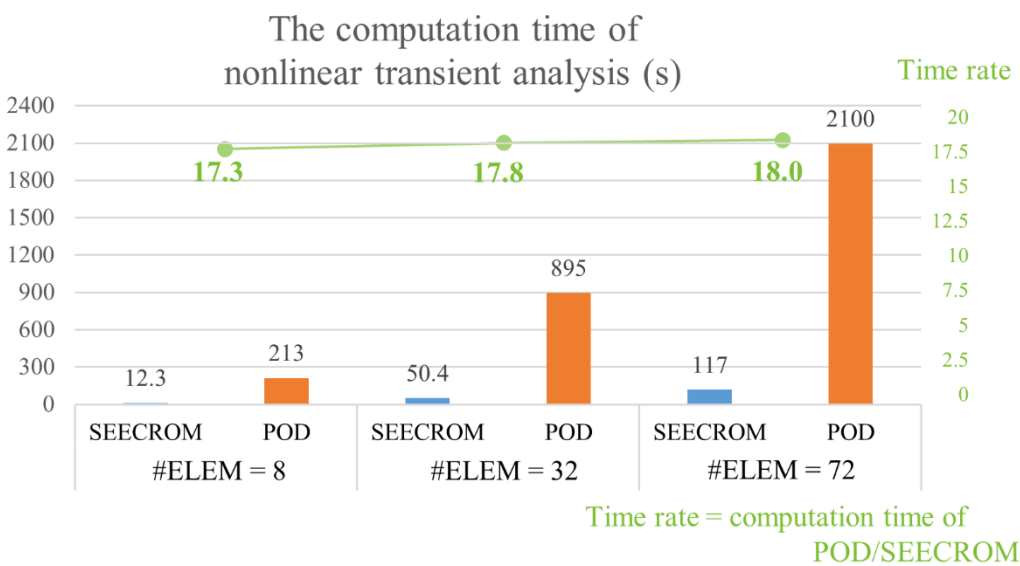

Figure 4.11. Computation time comparison by number of elements: CASE 2

5. PARAMETERIZATION BASED ON SEECROM

In the process of parametric studies or design optimizations, the system is continuously solved under different values of input parameters. If the relation between the parameters and the system matrices is complex, the whole process becomes quite inefficient since the system matrices should be reconstructed whenever the parameters change. The process of parameterization makes the system be characterized by input parameter variations. The system is decomposed into the parameter-related terms and the parameter-non-related terms. Thus, the aim of this section is the parameterization of SEECROM model. The nonlinear internal force model composed of SEECROM will be further characterized by the design parameters.

5.1. Parameterization strategy of SEECROM

The parameterization technique should be adjusted to fit the purpose. As for the parameter studies or design optimizations, the element-wise-imposed parameters are the most common cases. In these cases, the values of parameters are imposed element by element, which is a huge advantage for the parameterization of SEECROM. Furthermore, the displacement combinations are also determined element by element with the SEEC approach.

Fig. 5.1 shows the identical element composition to the element composition shown in Fig. 3.2. The addition to the Fig. 3.2 is the parameter variations; the design parameter λ is distributed in an element-wise manner. Then, Eq. (3.4) and Eq. (3.5) are simply

adjusted to have the design parameters. Eq. (5.1) below shows that the nonlinear internal force takes λ as an input parameters. The design parameters are multiplied with the displacement combinations for each element and summed up for the whole elements. For instance, Eq. (5.2) shows that the internal force at the specific degree of freedom q in Fig. 5.1 is determined with the design parameters and the displacement combinations within the adjacent elements.

$$\tilde{\Gamma}_i(\lambda,\mathbf{u}) = \tilde{K}_{ijkl}\sum_{n=1}^{AE}\lambda_n\left[u_j u_k u_l\right]_n = \tilde{K}_{ij}\sum_{n=1}^{AE}\lambda_n\left[u_j^c(\mathbf{u})\right]_n \tag{5.1}$$

$$\tilde{\Gamma}_q = \tilde{K}_{qj}\ \ \lambda_1\left[u_j^c\right]_{E6} + \lambda_1\left[u_j^c\right]_{E7} + \lambda_2\left[u_j^c\right]_{E10} + \lambda_3\left[u_j^c\right]_{E11} \tag{5.2}$$

For clarification, the displacement combinations can be altered to include the design parameters as in Eq. (5.3). Let the displacements be the original input parameters of the nonlinear internal force model in SEEC method, then the relation below is considered as the inclusion of the new input parameters for the approximate model.

$$\hat{u}_j^c(\lambda,\mathbf{u}) = \lambda\left[u_j^c(\mathbf{u})\right] \tag{5.3}$$

Then, the equations for the SEEC internal force model with the parameterization are simplified as follows:

$$\tilde{\Gamma}_i(\lambda,\mathbf{u}) = \tilde{K}_{ij}\sum_{n=1}^{AE}\left[\hat{u}_j^c(\lambda,\mathbf{u})\right]_n \tag{5.4}$$

$$\tilde{\Gamma}_q = \tilde{K}_{qj}\ \ \left[\hat{u}_j^c\right]_{E6} + \left[\hat{u}_j^c\right]_{E7} + \left[\hat{u}_j^c\right]_{E10} + \left[\hat{u}_j^c\right]_{E11} \tag{5.5}$$

The sampling strategy with the parameterization is also not quite different from the non-parameterized SEEC. When determining the training problems, one needs to check for the range of the input parameters to be used for the online stage and to include the

response results from the boundary values of the input parameters. Eq. (5.6) shows the sampling sets with the parameterization and the stiffness coefficients $\tilde{K}$ to be identified.

$$\begin{matrix}\Gamma_{i1} & \Gamma_{i2} & \dots & \Gamma_{is}\end{matrix}_{sampling} = \begin{bmatrix}\tilde{K}_{i1} & \tilde{K}_{i2} & \dots & \tilde{K}_{ip}\end{bmatrix} \begin{bmatrix}\hat{u}^c_{11} & \hat{u}^c_{12} & \dots & \hat{u}^c_{1s} \\ \hat{u}^c_{21} & \hat{u}^c_{22} & \dots & \hat{u}^c_{2s} \\ \vdots & \vdots & \ddots & \vdots \\ \hat{u}^c_{p1} & \hat{u}^c_{p2} & \dots & \hat{u}^c_{ps}\end{bmatrix}_{sampling} \tag{5.6}$$

where p is the number of displacement combinations and s is the number of the sampling sets.

The process of the identification of the stiffness coefficients is essentially identical to the non-parameterized approach. As below, the sampling sets are reorganized into the form of $Ax = b$ to be solved with the minimum norm Least Square.

$$\underset{sampling}{\begin{bmatrix}\hat{u}^c_{11} & \hat{u}^c_{12} & \dots & \hat{u}^c_{1p} \\ \hat{u}^c_{21} & \hat{u}^c_{22} & \dots & \hat{u}^c_{2p} \\ \vdots & \vdots & \ddots & \vdots \\ \hat{u}^c_{s1} & \hat{u}^c_{s2} & \dots & \hat{u}^c_{sp}\end{bmatrix}} \begin{bmatrix}\tilde{K}_{i1} \\ \tilde{K}_{i2} \\ \vdots \\ \tilde{K}_{ip}\end{bmatrix} = \underset{sampling}{\begin{bmatrix}\Gamma_{i1} \\ \Gamma_{i2} \\ \vdots \\ \Gamma_{is}\end{bmatrix}} \tag{5.7}$$

$$\text{where } A = \underset{sampling}{\begin{bmatrix}\hat{u}^c_{11} & \hat{u}^c_{12} & \dots & \hat{u}^c_{1p} \\ \hat{u}^c_{21} & \hat{u}^c_{22} & \dots & \hat{u}^c_{2p} \\ \vdots & \vdots & \ddots & \vdots \\ \hat{u}^c_{s1} & \hat{u}^c_{s2} & \dots & \hat{u}^c_{sp}\end{bmatrix}}, \quad x = \begin{bmatrix}\tilde{K}_{i1} \\ \tilde{K}_{i2} \\ \vdots \\ \tilde{K}_{ip}\end{bmatrix}, \quad b = \underset{sampling}{\begin{bmatrix}\Gamma_{i1} \\ \Gamma_{i2} \\ \vdots \\ \Gamma_{is}\end{bmatrix}} \tag{5.8}$$

Therefore, the nonlinear internal force model with the parameterization is given by

$$\tilde{\Gamma}_i(\lambda, \mathbf{u}) = \tilde{K}_{ij} \hat{u}^c_j(\lambda, \mathbf{u}) \tag{5.9}$$

$$\begin{bmatrix} \tilde{\Gamma}_1 \\ \tilde{\Gamma}_2 \\ \vdots \\ \vdots \\ \tilde{\Gamma}_N \end{bmatrix} = \begin{bmatrix} \tilde{K}_{11} & \tilde{K}_{12} & \cdots & \cdots & \tilde{K}_{1p} \\ \tilde{K}_{21} & \tilde{K}_{22} & & & \\ \vdots & & \ddots & & \\ \vdots & & & \ddots & \\ \tilde{K}_{N1} & & & & \tilde{K}_{Np} \end{bmatrix} \begin{bmatrix} \hat{u}_1^c \\ \hat{u}_2^c \\ \vdots \\ \vdots \\ \hat{u}_p^c \end{bmatrix} \tag{5.10}$$

Since the reduced-order modeling and the computation of the tangent stiffness are strongly dependent on the displacements rather than other input parameters, the SEECROM-Parameterization is completed with the previously described ROM procedures. The complete form of the nonlinear internal force with SEECROM-Parameterization is given in Eq. (5.11) – Eq. (5.13).

$$\tilde{\Gamma}_i^R(\lambda, \mathbf{u}) = \tilde{K}_{ij}^R \hat{u}_j^c(\lambda, \mathbf{u}) \tag{5.11}$$

$$\tilde{\Gamma}_i^R(\lambda, \mathbf{u}) = \phi_{ki} \tilde{\Gamma}_k(\lambda, \mathbf{u}), \quad \tilde{K}_{ij}^R = \phi_{ki} \tilde{K}_{kj} \tag{5.12}$$

$$\begin{bmatrix} \tilde{\Gamma}_1^R \\ \tilde{\Gamma}_2^R \\ \vdots \\ \vdots \\ \tilde{\Gamma}_m^R \end{bmatrix} = \begin{bmatrix} \tilde{K}_{11}^R & \tilde{K}_{12}^R & \cdots & \cdots & \tilde{K}_{1p}^R \\ \tilde{K}_{21}^R & \tilde{K}_{22}^R & & & \\ \vdots & & \ddots & & \\ \vdots & & & \ddots & \\ \tilde{K}_{m1}^R & & & & \tilde{K}_{mp}^R \end{bmatrix} \begin{bmatrix} \hat{u}_1^c \\ \hat{u}_2^c \\ \vdots \\ \vdots \\ \hat{u}_p^c \end{bmatrix} \tag{5.13}$$

5.2. Application of SEECROM-Parameterization

The static and the structural nonlinear analyses of plane elements with a hyperelastic material are demonstrated to verify the accuracy and the efficiency of the proposed SEECROM-Parameterization method. The element has 4 nodes per element and 2 degrees of freedom per node, which yields 8 degrees of freedom per element. The

hyperelastic material is modeled as Neo-Hookean with a shear modulus of μ =1.5 MPa and bulk modulus of κ =1.0 GPa.

As shown in Fig. 5.2, a 0.02×0.02 m square plane with radius of R=0.002 m is bounded on one side and the external load is imposed on the other side. A total of 2,451 elements are uniformly constructed with 50 mesh each along the plane edge. The total number of the degrees of freedom is 5,568.

5.2.1. Static analysis of Neo-Hookean hyperelastic material

For the verification of the SEECROM-parameterization method with the hyperelastic example, a static case is demonstrated first. The selected design parameters included the thickness of the elements as well as the magnitude of the external load. Since the external loads and the internal force are not directly related to each other in construction, the SEECROM-Parameterization only concerns the thickness of the elements as the input parameters for the parameterization. Fig. 5.3 shows the composition of the input parameters. The whole domain was divided into 4 sections, and a different value of element thickness was imposed on each section.

In the sampling stage, training analyses were conducted for the various sampling values of loads and element thicknesses. The magnitude of the sampling load was fixed as 30 N while the sampling thicknesses of 4 sections were chosen from 3 different values (0.001 m / 0.002 m / 0.003 m). The response results of SEECROM-Parameterization were compared with the full analysis results. Additionally, for the verification of efficiency, reduced analysis with POD was conducted for reference. The reference method only uses

POD for reduced-order modeling. It does not use stiffness evaluation or a parameterization technique. The reduction rate for both reduction methods was 1 %. The number of reduced degrees of freedom was 51, and the number of total degrees of freedom was 5,568.

The design parameters were randomly perturbed for the static analysis in the online stage. An arbitrary chosen set of design parameters is given in Table 5.1. The deformation of the structure under the random perturbation is illustrated in Fig. 5.4. The light blue faces indicate the results of full analysis, while the dark blue edges indicate the deformation from the SEECROM-Parameterization. It can be seen that the two results are identical. Fig. 5.5 contains the computation time for the online stage. SEECROM-Parameterization and POD-only reduction is performed against the full-order analysis. Compared to the full analysis, POD analysis is 1.58 times faster whereas SEECROM-Parameterization is 23.1 times faster.

5.2.2. Dynamic analysis of Neo-Hookean hyperelastic material

The structural dynamic analysis of hyperelastic material is demonstrated in this section. As in the previous example, the load magnitude and the element thickness were selected as the design parameters. The SEECROM-Parameterization model was constructed with two input parameters of element thickness. Fig. 5.6 shows the division of the two design sections for the input parameters. The dynamic load uniformly imposed on the right side of the plane was composed as the multiplication of the load magnitude and the load profile shown in Fig. 5.7. For the training analyses in the sampling stage, the sampled

load magnitude was set to 30 N and the thicknesses of 2 sections were chosen from 3 sample values (0.001 m / 0.002 m / 0.003 m). The number of reduced degrees of freedom was 102, which is 2% of the full model.

For the transient analysis in the online stage, the design parameters were randomly perturbed as given in Table 5.2. The dynamic response of the structure under the random perturbation is illustrated in Fig. 5.8. The displayed snapshots indicate that the accuracy of SEECROM-Parameterization is maintained over the analysis time. The middle point on the right side of the plane was selected, and the displacement in the x-direction is plotted in Fig. 5.9. The figure shows that the responses from SEECROM-Parameterization and POD reduction agree well with the full-order response.

The computation time for the online stage is shown in Fig. 5.10. SEECROM-Parameterization and POD reduction were conducted against the full-order analysis. POD reduction was 1.51 times faster than the full analysis, whereas SEECROM-Parameterization was 23.8 times faster.

Table 5.1

Randomly perturbed design parameters for static case

Load magnitude	Element thickness			
	$\lambda 1$	$\lambda 2$	$\lambda 3$	$\lambda 4$
29.94 N	0.0012 m	0.0019 m	0.0012 m	0.0029 m

Table 5.2

Randomly perturbed design parameters for dynamic case

Load magnitude	Element thickness	
	$\lambda 1$	$\lambda 2$
28.94 N	0.0017 m	0.0014 m

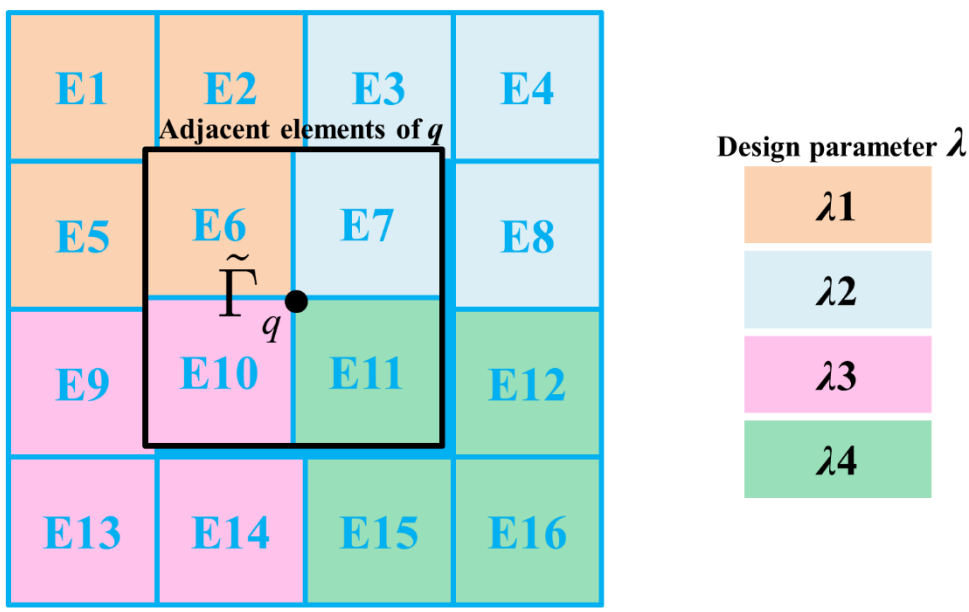

Figure 5.1. Element-wise construction of nonlinear internal force and its parameterization

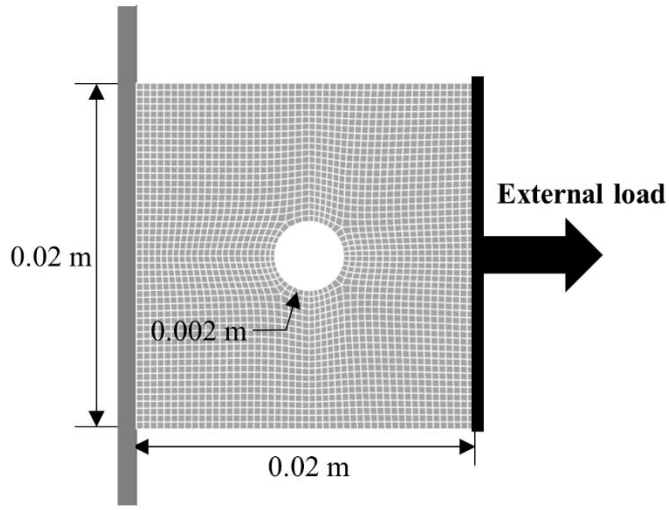

Figure 5.2. Analysis conditions for square plane for SEECROM-Parameterization

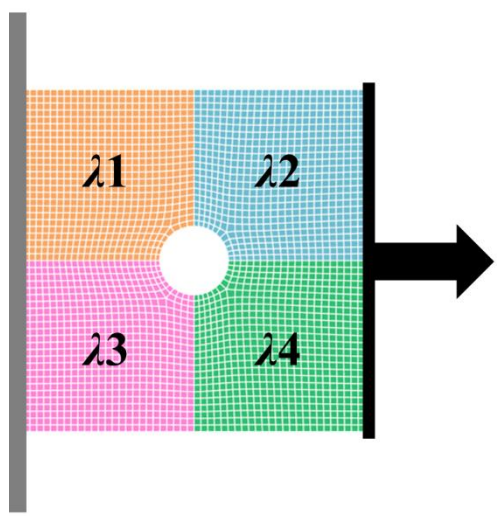

Figure 5.3. Input parameters for static analysis

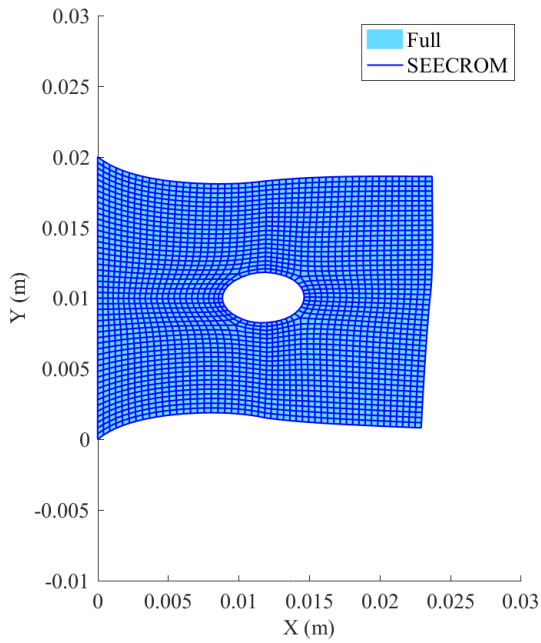

Figure 5.4. Static response under random perturbation of input parameters

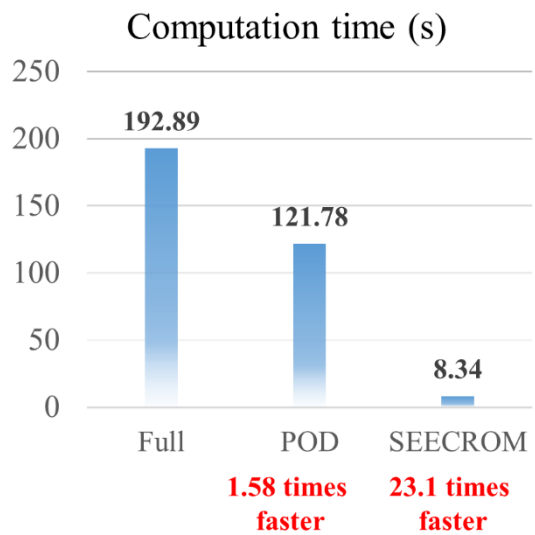

Figure 5.5. Computation time for online stage of static analysis under random perturbation of input parameters

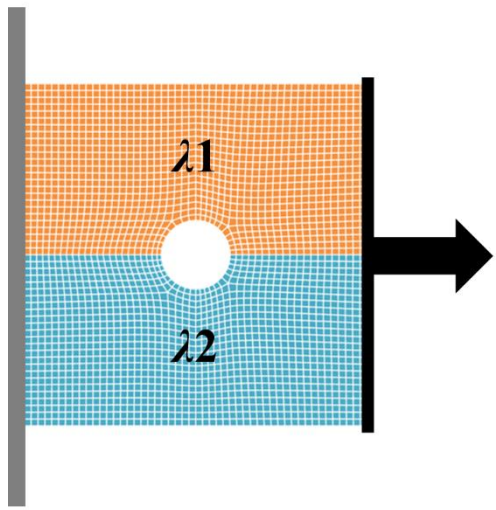

Figure 5.6. Input parameters for dynamic analysis

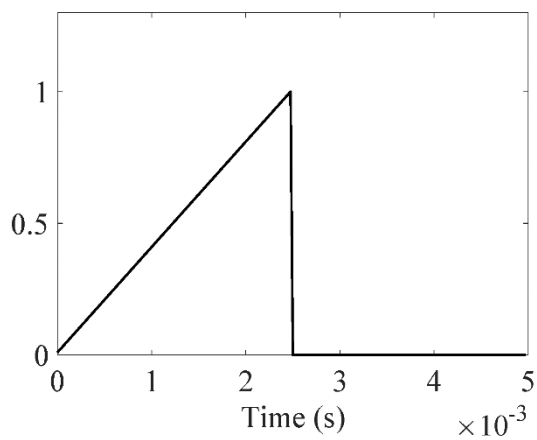

Figure 5.7. Amplitude of external dynamic loads

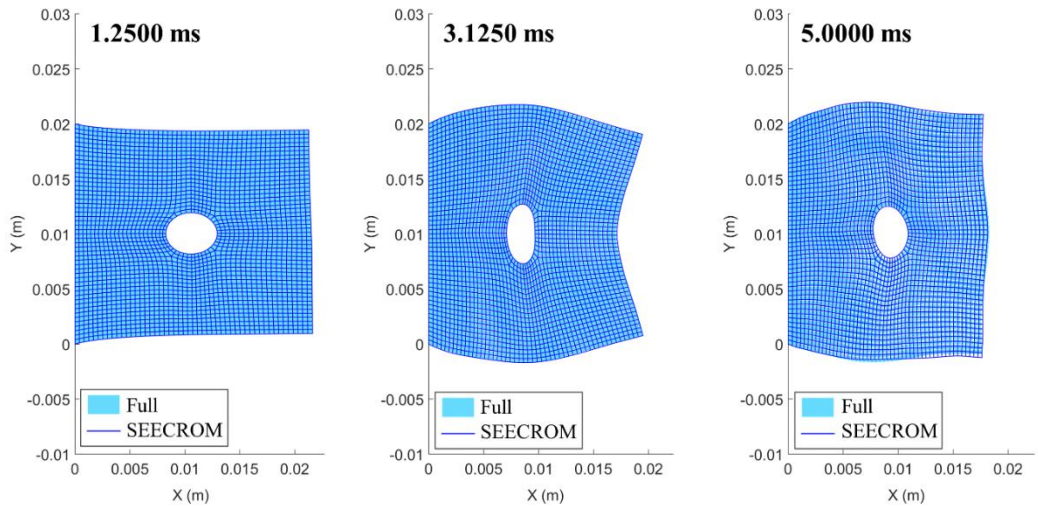

Figure 5.8. Dynamic response under random perturbation of input parameters: snapshots

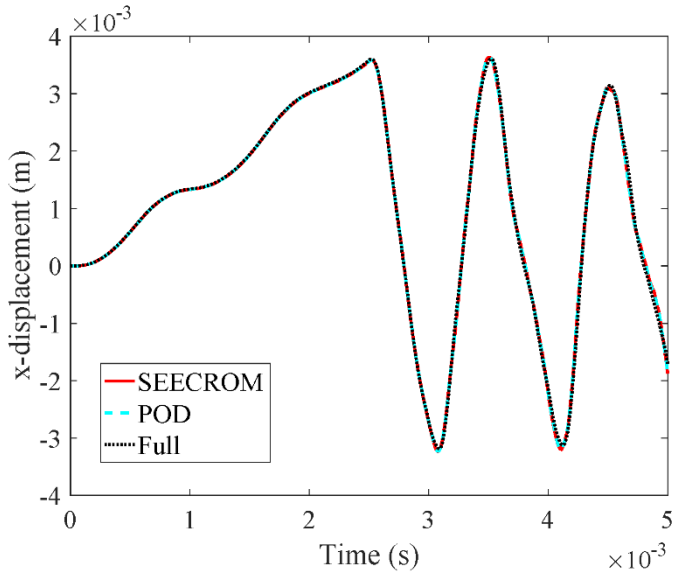

Figure 5.9. Dynamic response under random perturbation of input parameters: time response of selected point

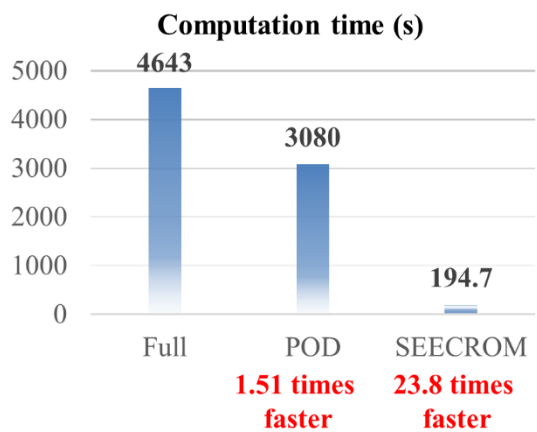

Figure 5.10. Computation time for online stage of dynamic analysis under random perturbation of input parameters

6. APPLICATON TO MULTIBODY DYNAMICS

6.1. Motivation

Recent years have witnessed growing interest in the efficient analysis of flexible multibody dynamics. For instance, control problems of flexible robot arm systems require real-time simulations of flexible multibody dynamics. To solve these systems with high accuracy, structural analysis of the flexible parts should be performed with a sufficient number of elements, which decreases the efficiency of the entire analysis. To meet the requirement of real-time simulation, a method that can increase the efficiency of large-system analysis is essential. Another example arises in the aircraft industries. For the development of aircraft with low emissions and high fuel efficiency, the design of high-aspect-ratio wings is crucial, which leads to large deformation of the structure. Therefore, aerodynamic analysis should be performed with the consideration of nonlinearities caused by the large deformation. Since this requires repetition of nonlinear structural analysis for each time step of dynamic analysis, high efficiency of the nonlinear analysis must be guaranteed. Therefore, an efficient analysis technique that considers the nonlinearities in rigid body motion as well as flexible deformation is highly demanded in the field of flexible multibody dynamics.

To enhance the efficiency of multibody dynamic simulations, the technique of reduced-order modeling (ROM) has been used widely. Still, the utilization of ROM in flexible multibody analysis problems has not been fully studied. The difficulty in the utilization of

ROM comes from the limitations of the ROM technique itself: although ROM has been well developed for linear systems, its adaption to use with nonlinear systems is still in its beginning stages. Whether nonlinearities arise from rigid body motion or the flexibility of structures, the system matrices should be re-constructed as the state of the system changes. The problem is that the re-construction of system matrices should be performed in the full domain before the reduction process begins. Since most reduction methods only shrink the computation time for the solution process after the reduction process, the time of the repeated construction process takes nearly the same amount as that of a full analysis.

The stiffness evaluation procedure (STEP) method, proposed by Muravyov and Rizzi [1] is one of the computationally efficient approaches of nonlinear analysis. It represents nonlinear internal forces by a third-order polynomial formulation of displacements. If the representative model is constructed with sufficient accuracy, the system matrices can be computed immediately as the nonlinear system is updated. However, the identification of the representative internal force model itself takes time. Since the coefficients of the polynomial displacements are identified by a series of responses from the finite element simulations in the full domain, the required number of simulations should be kept small. This creates a limitation on the application of the STEP method as the number of full simulations increases with the cubic power of the system size. It can be stated that the application of this approach to large-scale problems is computationally prohibitive.

In this section, the application of the STEP method is extended to multibody dynamic analyses. To this end, new stiffness evaluation methods developed for large-scale analyses are proposed in the previous sections. They are referred to as SEEC and SEECROM: the stiffness evaluation method based on element connectivity and its

reduced-order modeling, respectively. In the proposed methods, the stiffness coefficients are evaluated within the connected elements. This makes the number of required simulations determined by the characteristics of the element itself rather than by the problem size. Moreover, proper orthogonal decomposition (POD), which is a ROM method, is utilized to enhance the efficiency of the proposed method. System matrices are constructed by stiffness evaluations based on element connectivity information, which is followed by the reduction of system matrices by the POD method. In this way, the proposed method keeps the accuracy of the representative model and increases the efficiency of the reduced model.

SEEC and SEECROM were originally developed for analysis of nonlinear structural dynamics systems, where the mass matrix is composed of constants while the internal force vector and the stiffness matrix are nonlinear in the deformation of the structure. The nonlinear values should be updated repeatedly as the displacements change. Thus, the proposed methods construct efficient representative models for internal forces and stiffness matrices.

However, the composition of the system matrices in flexible multibody analysis is different from the structural analysis. In the floating frame of reference formulation (FFRF), which is the most widely used technique in the analysis of flexible multibody dynamics, the stiffness matrix is composed of constants while the mass matrix has nonlinearities. Not only should the mass matrix be updated repeatedly at every iteration, but the terms in relations with the inertia forces should also be computed recursively. Therefore, the proposed methods, which are developed to construct nonlinear internal force models, cannot be applied directly to this formulation of multibody dynamics.

Fortunately, there is an alternative approach for multibody dynamics that uses different coordinate systems from FFRF. This approach, referred to as absolute nodal coordinate formulation (ANCF), uses absolute coordinates and slopes. This leads to a constant mass matrix and a nonlinear stiffness matrix, which are analogous to the system matrices of nonlinear structural dynamics. Since the additional inertia terms also vanish due to the use of absolute nodal coordinates, the equation of motion with ANCF is formed in a similar way to nonlinear structural dynamics systems. This enables the direct utilization of ROM methods that have been developed for nonlinear structural analysis.

ANCF approaches were originally proposed by Shabana and co-authors [17–20]. The ANCF is designed particularly for large deformation analysis in multibody applications. It describes the absolute values of the displacements and finite slopes in a global coordinate system, which leads to stable solutions of the integration process under large rotations and deformations. However, in most cases, the multibody dynamic analysis with ANCF takes a large amount of time. The inefficiency comes from two main factors: 1) the complexity in the composition of nonlinear internal forces of ANCF elements and 2) the iterative calculations used to update the state of the system. Moreover, the computation time rises as the number of ANCF elements increases.

Various studies have been made to raise the efficiency of the ANCF approaches. ANCF elements were simplified in various ways with appropriate assumptions according to the characteristics of specific problems [19]. Mode-based reduced-order modeling, including the Craig–Bampton method, was applied to ANCF approaches [21–23]. Still, further consideration should be made with regard to the enhancement of efficiency while preserving the nonlinear nature of the ANCF approaches. Ways to reduce the time needed

for the re-construction of the system matrices should be devised, as well.

In this section, SEECROM is applied to ANCF beam elements. The proposed methods can be successfully applied to ANCF to yield efficient solution responses in flexible multibody dynamics. The previous reduction methods for ANCF-multibody dynamics have the same limitations as the reduction methods for nonlinear structural analysis: they only reduce the computation time for the solution process, and not the construction time for system matrices. Since the stiffness matrices in ANCF should be updated at every iteration, if the construction time for the system matrix is not reduced, there is a definite limit on the efficiency gain. Contrary to previous ROM methods, SEECROM handles the construction of the system matrices, fully enhancing the efficiency of flexible multibody dynamics. The applications of SEECROM to ANCF beam elements are demonstrated for various numerical examples such as a free-falling pendulum, a slider-crank mechanism, and a four-bar mechanism.

6.2. ANCF formulation

The most preferred and widely used approach in multibody dynamics is the floating frame of reference formulation (FFRF), which uses a mixed set of absolute and local reference coordinates. Although the use of mixed coordinates allows the stiffness matrix to take a simple form, as in linear static structural analyses for small-deformation problems, it also creates inertial forces and the nonlinear mass matrix. On the other hand, the absolute nodal coordinate formulation (ANCF) uses only absolute global coordinates. This simplifies the mass matrix and makes the inertia forces disappear. Instead, the

stiffness matrix takes a nonlinear form, which is analogous to the formulation of nonlinear structural dynamics. The composition of the nodal coordinates and the construction of the equation of motion and its system matrices in the case of ANCF beam elements are addressed below [20].

In the ANCF elements, displacements and displacement gradients are used as nodal coordinates. These absolute coordinates are defined in terms of the element shape function and the vector of nodal coordinates as below:

$$\mathbf{r} = \mathbf{Se} \tag{6.1}$$

where $\mathbf{r}$ is the global position vector of an arbitrary point on the neutral axis of the beam element, $\mathbf{S}$ is a global shape function, and $\mathbf{e}$ is the vector of nodal coordinates, which includes global displacements and gradients. The configurations of ANCF beam elements are shown in Fig. 6.1.

In Fig. 6.1, x is the length of an arbitrary point from the node, and l is the length of an undeformed beam element. X_1 and X_2 are global coordinates, and the vector of nodal coordinates $\mathbf{e}$ is given by

$$\underset{(8\times1)}{\mathbf{e}} = \left[\underbrace{e_1 \quad e_2}_{position} \quad \underbrace{e_3 \quad e_4}_{gradient} \quad \underbrace{e_5 \quad e_6}_{position} \quad \underbrace{e_7 \quad e_8}_{gradient} \right]^{\mathrm{T}} \tag{6.2}$$

$$\begin{aligned} e_1 &= r_1\big|_{x=0} & e_2 &= r_2\big|_{x=0} & e_3 &= \frac{\delta r_1}{\delta x}\bigg|_{x=0} & e_4 &= \frac{\delta r_2}{\delta x}\bigg|_{x=0} \\ e_5 &= r_1\big|_{x=l} & e_6 &= r_2\big|_{x=l} & e_7 &= \frac{\delta r_1}{\delta x}\bigg|_{x=l} & e_8 &= \frac{\delta r_2}{\delta x}\bigg|_{x=l} \end{aligned} \tag{6.3}$$

Then, the position vector $\mathbf{r}$ is described with the global shape function below:

$$\underset{(2\times 8)}{\mathbf{S}} = \begin{bmatrix} 1-3(\xi)^2+2(\xi)^3 & 0 & l\left(\xi-2(\xi)^2+(\xi)^3\right) & 0 \\ 0 & 1-3(\xi)^2+2(\xi)^3 & 0 & l\left(\xi-2(\xi)^2+(\xi)^3\right) \end{bmatrix} \tag{6.4}$$

$$\begin{bmatrix} 3(\xi)^2-2(\xi)^3 & 0 & l\left((\xi)^3-(\xi)^2\right) & 0 \\ 0 & 3(\xi)^2-2(\xi)^3 & 0 & l\left((\xi)^3-(\xi)^2\right) \end{bmatrix}$$

where $\xi = \frac{x}{l}$.

Now, with the global position vector $\mathbf{r}$, after some simple algebraic manipulations , the kinetic energy T of the beam is expressed as

$$T = \frac{1}{2}\int_V \rho \dot{\mathbf{r}}^{\mathrm{T}} \dot{\mathbf{r}} dV = \frac{1}{2}\dot{\mathbf{e}}^{\mathrm{T}}\left(\int_V \rho \mathbf{S}^T \mathbf{S} dV\right)\dot{\mathbf{e}} = \frac{1}{2}\dot{\mathbf{e}}^{\mathrm{T}}\mathbf{M}\dot{\mathbf{e}} \tag{6.5}$$

where V is volume, ρ is mass density, and $\mathbf{M}$ is the element mass matrix, which is constant. While the ANCF leads to a simple expression for the mass matrix, it results in a relatively complex expression for the stiffness matrix. The element stiffness matrix $\mathbf{K}$ can be derived from the strain energy U, which is given by

$$U = \frac{1}{2}\int_0^l \left(Ea\left(\frac{\partial u_l}{\partial x}\right)^2 + EI\left(\frac{\partial^2 u_t}{\partial x^2}\right)^2 \right) dx = \frac{1}{2}\mathbf{e}^{\mathrm{T}}\mathbf{K}\mathbf{e} \tag{6.6}$$

where E is the modulus of elasticity, a is the cross-sectional area, I is the second moment of area of the beam element, u_l are the longitudinal displacements, and u_t are the transverse displacements.

Since the element coordinates $\mathbf{e}$ only contain the absolute values of positions and gradients, it can be seen that the stiffness matrix for the ANCF beam element becomes a highly nonlinear function. Various methods have been proposed to reduce the

inefficiency due to this nonlinearity. In this paper, one of the simple methods proposed by Berzeri and Shabana [19] is utilized; it is assumed that the longitudinal deformation is small and the strain is constant within an element. Even with the simplest model, however, a significant amount of time is required to perform the time-marching simulation of multibody dynamics. Moreover, the computation time increases rapidly with the number of elements.

In the next section, the method for enhancing the efficiency of the ANCF model is presented. The reduction method developed for nonlinear structural dynamics is applied to the ANCF model based on the fact that their governing equations have analogous formulations. Although a simplified ANCF beam element is used in the numerical examples in this paper, the proposed method is readily applicable regardless of the formulation.

6.3. Reduced-order modeling of ANCF model with SEECROM

6.3.1. Application of SEECROM to ANCF beam elements

As addressed in the previous section, an ANCF beam element is composed of two nodes, and the each node contains four degrees of freedom, which include the global displacements X and Y as well as their corresponding global slopes. In total, eight degrees of freedom complete one element, as shown in Eq. (6.2). It is proposed that the SEECROM model is constructed in element-wise manner with the third-order polynomial displacement combination within each element. Since there are eight degrees of freedom

in an element and the number of adjacent elements is two, the number of displacement combinations for an internal force is equal to $2(_{8+1}\mathbf{H}_3 - 1) - \gamma$. With the consideration of shared combination γ, this number becomes 294. This determines the number of sampling sets to obtain in the sampling process.

Overall, there is no notable difference in the process of SEECROM model construction between ANCF analyses and structural analyses. The construction sequence follows the procedure described in Sect. 3 and Sect. 4.

6.3.2. Application of SEECROM

In this section, the proposed SEECROM method is applied to multibody dynamics to solve various examples that include a free-falling pendulum, a slider-crank mechanism, and a four-bar mechanism. These are successfully demonstrated with ANCF beam elements. The constraints for joints are imposed with Lagrange multiplier methods, and a Newmark method combined with a Newton-Raphson formulation is applied for the time integration scheme.

6.3.2.1. Double pendulum

The multibody dynamics analysis of a free-falling pendulum is performed based on ANCF. The pendulum has a pin joint in the middle, as shown in Fig. 6.2. The first body with a grey color has an elastic modulus of 80 MPa and an area of 900 mm2. For the red-colored second body, these quantities are 1 MPa and 900 mm2, respectively. The dynamic analysis was performed under the gravity force in the –y direction over a total

time of T=1.3 s. The sampling parameter is the mass of each body; the initial masses of the bodies were given as 1.216 kg and 0.982 kg, respectively. For the sampling process, training dynamic analyses were performed with a perturbed sampling mass. Fig. 6.3 shows the perturbed position of the end point of the pendulum during the sampling process. The perturbation rate varied as 0.5 / 1.0 / 1.5. Under the perturbation of the mass of the bodies, solution sets composed of the displacements and the corresponding internal forces were collected. According to the characteristics of the ANCF beam elements, the sufficient number of solution sets was computed as 294. These solution sets were used for the evaluation of the stiffness coefficients and the extraction of POD modes, which completed the SEECROM model of the given ANCF beam example. Then, with the SEECROM model, dynamic analyses were performed under a randomly imposed set of masses. The responses were compared to the POD-based reduced analyses and the full analyses. The reference analysis for reduction uses only POD based on the snapshot method.

With 80 elements for each body and a reduction rate of 4 %, the total and reduced number of degrees of freedom were 628 and 25, respectively. The multibody dynamic analyses were performed under the two different cases with randomly chosen mass sets of [1.057 kg, 0.6 kg] for CASE 1 and [1.121 kg, 1.390 kg] for CASE 2. The first and second values in the brackets indicate the masses of the first and second bodies, respectively.

The response results from the multibody dynamic analysis under the two cases of randomly perturbed mass are plotted in Figs. 6.4 to 6.7. The even-numbered figures represent the motion of the pendulum for every 15 time steps. The pendulum is drawn with darker lines over time while the initial position is denoted with a pink line. The odd-

numbered figures show the position of the end point over time for different methods including SEECROM, POD reduction, and full analysis. It can be seen that the three methods have the same responses under the randomly perturbed mass variables, which verifies the accuracy of the SEECROM model.

The efficiency can be verified with the results drawn in Figs. 6.8 and 6.9. The computation times of dynamic analysis under SEECROM and POD reduction are compared for CASE 1 and CASE 2 in Figs. 6.8 and 6.9, respectively. In CASE 1, it can be seen that the SEECROM method is approximately 167 times faster than full analysis, while the POD reduction method is 20.63 times faster. In CASE 2, SEECROM and POD methods are 210.7 and 18.83 times faster than full analysis, respectively.

For the verification of the efficiency of the SEECROM method under various system sizes, the process was repeated as the number of elements was increased by 20, 40, 80, and 160. (The total number of degrees of freedom was increased by 88, 168, 328, and 648.) Identical numbers of elements for each pendulum were imposed, and the reduced models were constructed with 26 POD modes for all cases. In Fig. 6.10, two specific time rates are depicted over the increasing numbers of elements. The first time rate refers to the computation time of the full analysis over the POD reduction method, and the second time rate refers to the computation time of the full analysis over the SEECROM method. They indicate the relative efficiency of POD and SEECROM method compared to the full analysis. It can be seen that the gap between two rates is widened as the number of elements increases. Although the POD reduction method becomes enhanced with the number of elements, the efficiency of the SEECROM method is magnified with the growth of system size.

6.3.2.2. Slider-crank mechanism

The multibody dynamic analysis of the slider-crank mechanism shown in Fig. 6.11 was performed with ANCF elements. SEECROM was applied, and results were compared to POD reduction and full system analysis. The crankshaft and the connecting rod were composed of 40 and 60 ANCF beam elements, respectively. The two bodies had identical areas of 78.54 mm2 and densities of 2,770 kg/m3. The Young's modulus of the crankshaft was 100 MPa while that of the connecting rod was 5 MPa. The moment M applied at the crank is expressed as

$$M = \begin{cases} \lambda \times 0.01(1 - e^{\frac{-t}{0.167}}) & t \leq 0.7 \\ 0 & t > 0.7 \end{cases} \tag{6.7}$$

where λ is the sampling parameter, which varied as 0.25 / 0.5 / 0.75 / 1 in the sampling process.

The dynamic analysis was performed under the randomly selected parameter λ=0.861. Fig. 6.12 shows the motion of the slider-crank under the perturbed moment, which is drawn with darker lines over time while the initial position is denoted with a pink line. Fig. 6.13 shows the position of the end point that slides along the x-axis. It can be seen that the results of SEECROM, POD, and full analysis match perfectly. The efficiency of the SEECROM method can be verified by Fig. 6.14: SEECROM analysis was 157.6 times faster than full system analysis, while the POD reduction method was 16.4 times faster than full analysis.

6.3.2.3. Four-bar mechanism

The multibody dynamic analysis of the four-bar mechanism shown in Fig. 6.15 was performed with ANCF elements. The dynamic response obtained using the SEECROM method was compared to POD reduction and full system analysis. The crankshaft, the coupler, and the follower were composed of 20, 50, and 40 ANCF beam elements, respectively. The material properties of each body are listed in Table 6.1. The moment applied at the crank is expressed as

$$M = \begin{cases} \lambda \times 10 \sin(3\pi t) & t \leq 0.2778 \\ \lambda \times 465.9 e^{-16.32t} & t > 0.2778 \end{cases} \tag{6.8}$$

where λ is the sampling parameter, which varied by 0.25 / 0.5 / 0.75 / 1 in the training analyses of the sampling process.

Dynamics analysis was performed with a randomly perturbed moment M with the selected parameter λ =0.935. The dynamic response of the structure under the perturbation is illustrated in Fig. 6.16. The displayed snapshots indicate the high degree of accuracy of the SEECROM method over the analysis time. The response of the full model drawn as the light blue line matched well with the dark blue line denoting the response of the SEECROM model. The change of the position of the joint between the coupler and the follower is shown in Fig. 6.17. The results of the three analyses match perfectly. The efficiency of the SEECROM method is verified by Fig. 6.18; while the SEECROM analysis was faster than the full system analysis by 63.1 times, the POD reduction method was 7.22 times faster than the full analysis.

6.4. Parameterization of ANCF model with SEECROM

6.4.1. Parameterization strategy of SEECROM

The procedure of parameterization for ANCF model basically follows the strategy introduced in Sect. 5.1. The internal force model using SEEC method has the element-wisely collected terms of 3rd order input displacements as the input variables. If design parameters are imposed in element wise manner, the internal force model can be constructed with the parameters which are combined with the 3rd order displacements combination to make the 4th order input variables. See Fig. 5.1 and Eq. (5.3)-(5.5) for more detail.

If the design parameter λ has a linear relation with the internal force such as Young's modulus in ANCF beam elements, the inclusion of the new input parameters λ is completed with the simple linear multiplication as expressed in Eq. (5.3). If the design parameter λ has a nonlinear relation with the internal force, the inclusion of the parameter should be carefully chosen under the consideration of the relation between the parameter and the internal forces. For example, let's assume that diameters d in ANCF beam elements are chosen as design parameters. While the relation between the diameters and the internal forces is nonlinear, the internal force in ANCF beam is affected proportionally by the area of the beam and the second moment of the area, which are represented by d^2 and d^4, respectively. Thus, for the parameterization of the diameters d in the ANCF beam elements, d^2 and d^4 should be separately included as the new input parameters instead of d itself.

6.4.2. Application of SEECROM-Parameterization

In this section, the parameterization of ANCF beam model is conducted based on SEECROM method to solve multibody dynamics under the changes of parameters. Various numerical examples which include free-falling pendulum, slider-crank and four-bar mechanism are demonstrated. The multiple point constraints for joints in the examples are imposed with Lagrange multiplier.

6.4.2.1. Double pendulum

The dynamic analysis of the pendulums with a pin joint in the middle shown in Fig. 6.19 was solved with SEECROM and its parameterization technique. The first pendulum with grey color are consist of 40 elements and has an area of 900 mm^2 with 1.216 kg of mass. For the red colored second pendulum, it has 40 elements and an area of 900 mm^2 with 0.982 kg of mass. The dynamic analysis was performed under the gravity force in –y direction over the total time T=1.3s. The design parameters for the parameterization are the Young's modulus E of each pendulum, which are indicated in the Fig. 6.19 with λ_1 and λ_2.

In the sampling stage, the design parameters are directly chosen as the sampling parameters. The training analyses were conducted as the parameters are changed by 1MPa / 10MPa / 100MPa. The response results of SEECROM were compared to the results from the full analysis and the POD reduction method under the randomly selected parameter values, $[\lambda_1^*, \lambda_2^*]$ = [70.9 MPa, 4.15 MPa]. The first and the second values in

the bracket equal to the Young's modulus of the first pendulum and the second pendulum, respectively. The total number of degrees of freedom is 328 and the reduction rate is 15 %.

The deformation of the structure under the random perturbation λ^* is illustrated in Fig. 6.20. It is drawn with more dark lines over time T=1.3s while the initial position is indicated with pink line. The position of the end point of the second pendulum is shown in Fig. 6.21. The results of two reduction method are well matched with the full system analysis. The computation time of the three methods are shown in Fig. 6.22. SEECROM analysis is faster than the full system analysis by 43.2 times and POD reduction method is 5.62 times faster than the full analysis.

6.4.2.2. Slider-crank mechanism

The slider crank is shown in Fig. 6.23 with the element-wisely imposed design parameters λ_1 and λ_2. The crankshaft and the connecting rod are composed with 40 and 60 ANCF beam elements, respectively. Two bodies have the identical area of 78.54 mm^2 and the density of 2770 kg/m^3. The moment M applied at the crank is expressed as

$$M = \begin{cases} 0.01(1-e^{\frac{-t}{0.167}}) & t \le 0.7 \\ 0 & t > 0.7 \end{cases} \tag{6.9}$$

The multibody dynamic analysis of the slider crank was performed based on ANCF. Young's modulus of each body is selected as the input parameters for the parameterization of the SEECROM-representation of the given ANCF model.

In the offline stage, the training analyses were conducted as the design parameters are

changed by 1 MPa / 10 MPa / 100 MPa. The response from the SEECROM method is compared to the POD reduction and the full system analysis under the randomly perturbed parameter values, [λ_1^*, λ_2^*] = [8.51 MPa, 6.34 MPa]. The total number of degrees of freedom is equal to 408 and the reduction rate is 15 % with the 61 reduction modes.

The dynamic response of the structure under the random perturbation λ^* is illustrated in Fig. 6.24, which is drawn with more dark lines over time T=1.6s with the initial position depicted in pink line. The position of the end point of the connecting rod that slides along the x-axis is shown in Fig. 6.25. The figure shows that the responses from SEECROM method and POD reduction method agree well with the full-order response. The computation time for the online stage is shown in Fig. 6.26. POD reduction was 11.56 times faster than the full analysis, whereas SEECROM-Parameterization was 123.1 times faster.

6.4.2.3. Four-bar mechanism

An example of four-bar mechanism is shown in Fig. 6.27 with the design parameters λ_1, λ_2 and λ_3, which are imposed for the crankshaft, the coupler and the follower, respectively. The multibody dynamic analysis of the example was performed with the ANCF beam elements under the moment M employed at the crank. The moment is expressed as

$$M = \begin{cases} \sin(3\pi t) & t \leq 0.2778 \\ 465.9e^{-16.32t} & t > 0.2778 \end{cases} \tag{6.10}$$

The material properties of each body are identical to the values listed in Table 6.1 except

the Young's modulus of each body, which is selected as the input parameters for the parameterization of the SEECROM model of the example.

A set of training analyses were conducted in the offline stage as the design parameters are changed by 10 MPa / 50 MPa / 100 MPa. Under the randomly perturbed parameter values of [λ_1^* , λ_2^* , λ_3^*] = [35.1 MPa, 59.2 MPa, 96.2 MPa], the dynamic response of the SEECROM is compared to the POD reduction and the full system analysis. The total number of degrees of freedom is 452 whereas the number of reduction modes is 54 with the reduction rate of 12 %.

The snapshots displayed on Fig. 6.28 are the responses of full order and SEECROM analyses under the perturbed parameter λ^*. The results from SEECROM are denoted with dark blue lines and the full order results are drawn with light blue lines. It can be seen that the excellent matching between the two methods is obtained. Moreover, the joint link between the coupler and the follower is selected as the observation point. The time response of the point in Y-direction is drawn in Fig. 6.29. It can be seen that the two reduction methods have the same results with the full system dynamic analysis. The efficiency of the proposed method can be verified from Fig. 6.30. Whereas the computation time of POD reduction was 8.46 times faster than the full analysis, the analysis using SEECROM method was 66.2 times faster.

Table 6.1

Material properties of four-bar mechanism

	Crankshaft	Coupler	Follower
Number of elements	20	50	40
length (m)	0.2	0.9	0.52
Density (kg/m^3)	2709	1402	4003
A (mm^2)	1257	1960	7068
E (MPa)	1,000	5	500

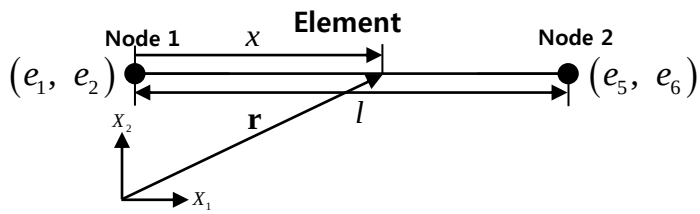

(a)

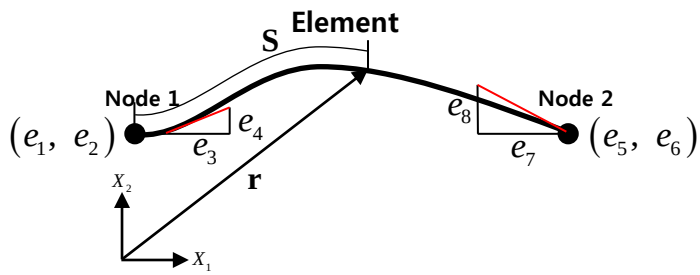

(b)

Figure 6.1. (a) Undeformed and (b) deformed configurations of ANCF elements

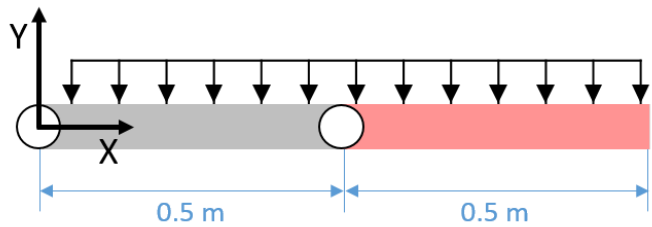

Figure 6.2. Configuration of the double pendulum with a pin joint in the middle

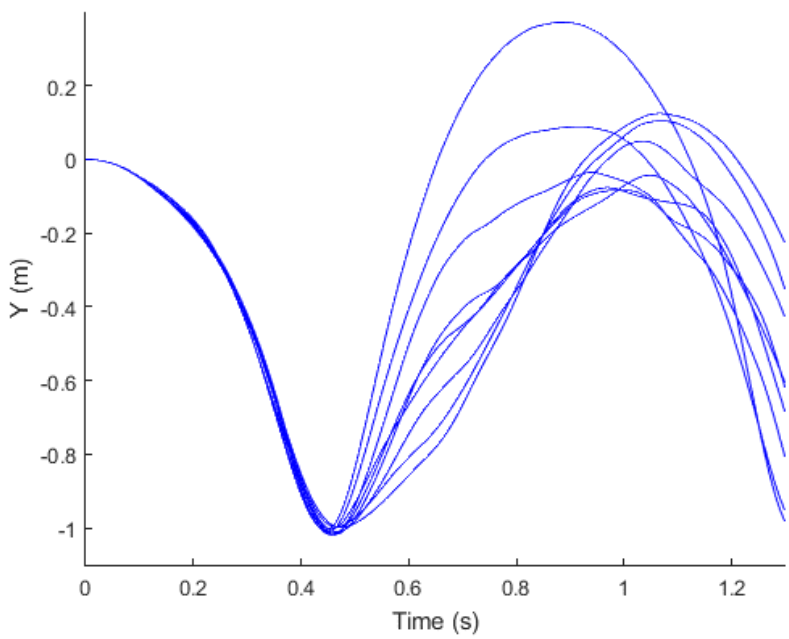

Figure 6.3. Traces of the dynamic analysis in the sampling process

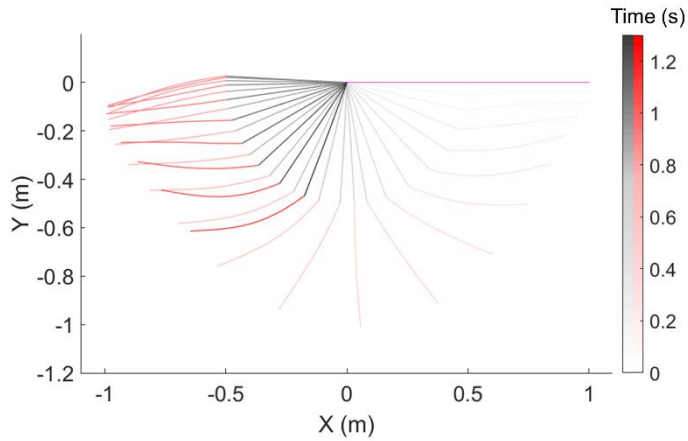

Figure 6.4. Deformation of the double pendulum under multibody dynamic analysis:

CASE 1

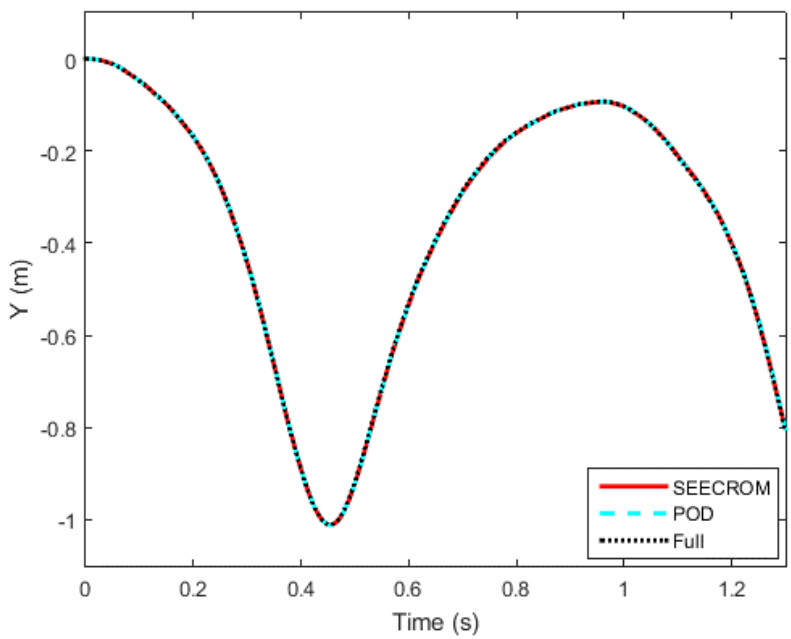

Figure 6.5. Transverse position of the end point of the double pendulum:

CASE 1

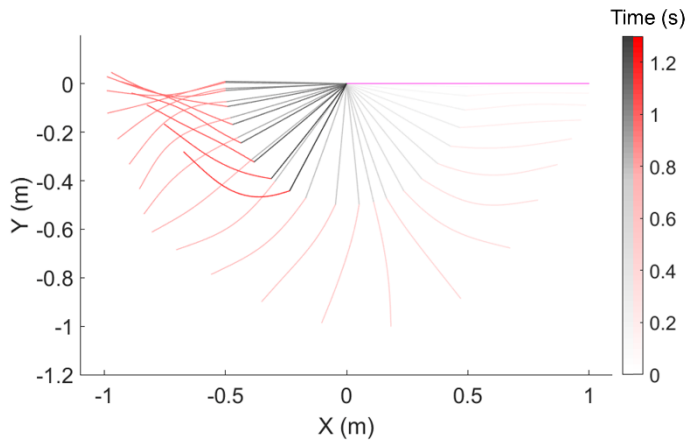

Figure 6.6. Deformation of the double pendulum under multibody dynamic analysis:

CASE 2

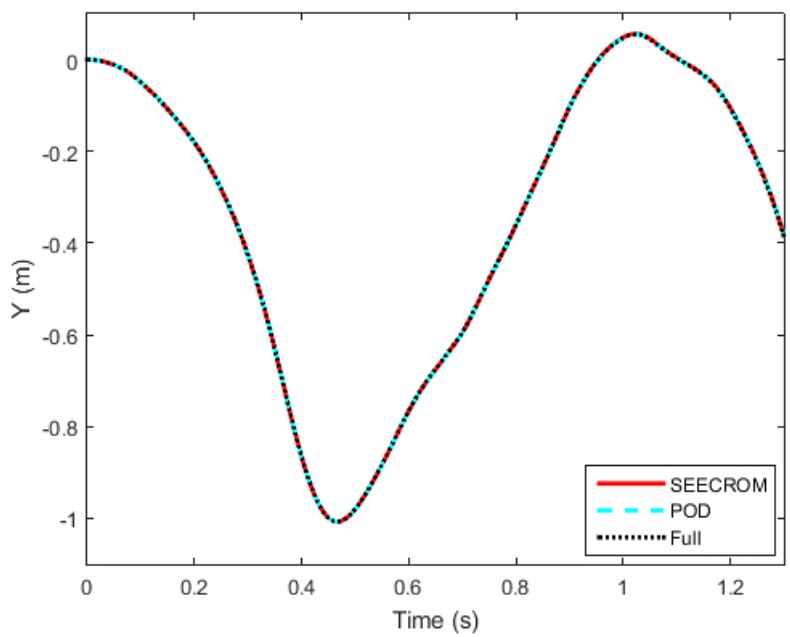

Figure 6.7. Transverse position of the end point of the double pendulum:

CASE 2

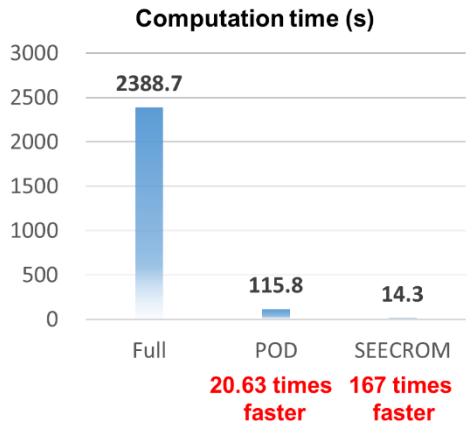

Figure 6.8. Computation time for the double pendulum:

CASE 1

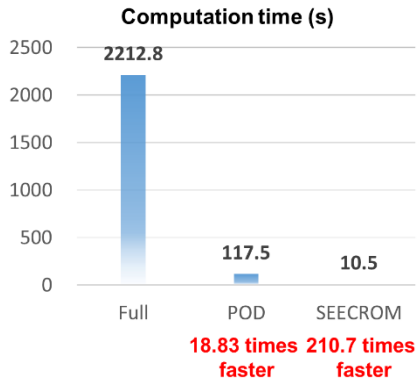

Figure 6.9. Computation time for the double pendulum:

CASE 2

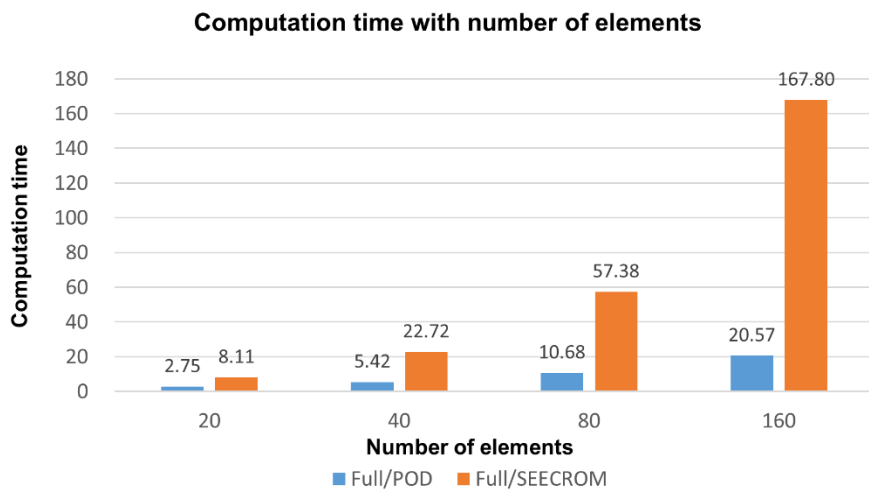

Figure 6.10. Computation time with the number of elements

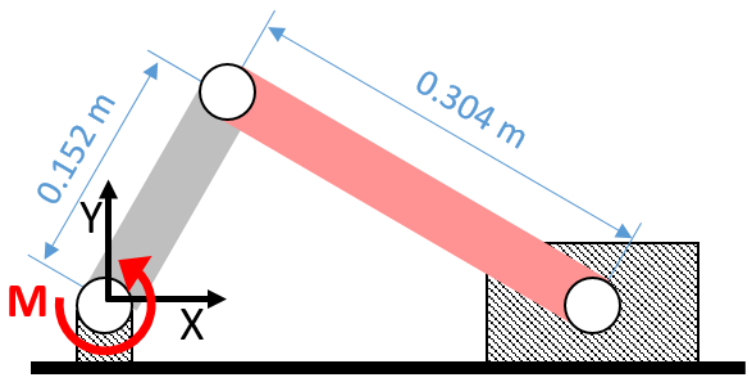

Figure 6.11. Configuration of slider-crank mechanism

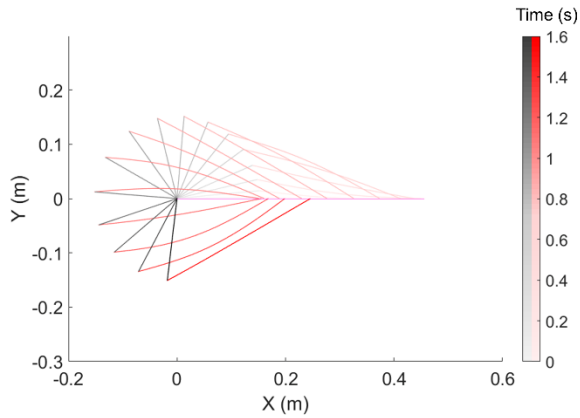

Figure 6.12. Deformation of the slider-crank mechanism with time (T=1.6s)

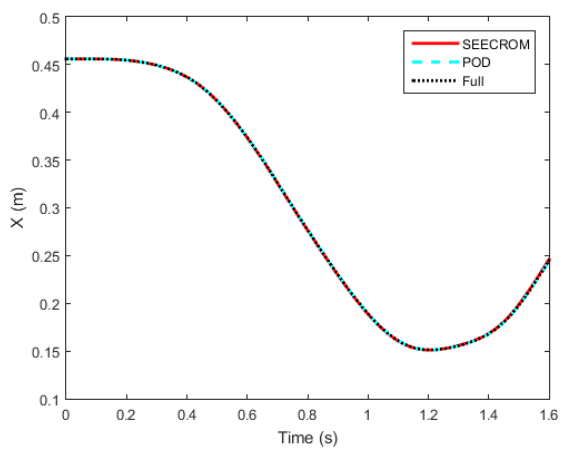

Figure 6.13. X-position of the end of the connecting rod with time

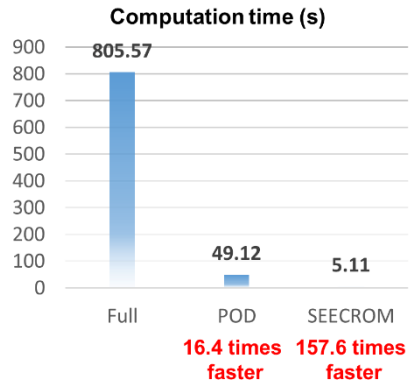

Figure 6.14. Computation time for the slider-crank mechanism

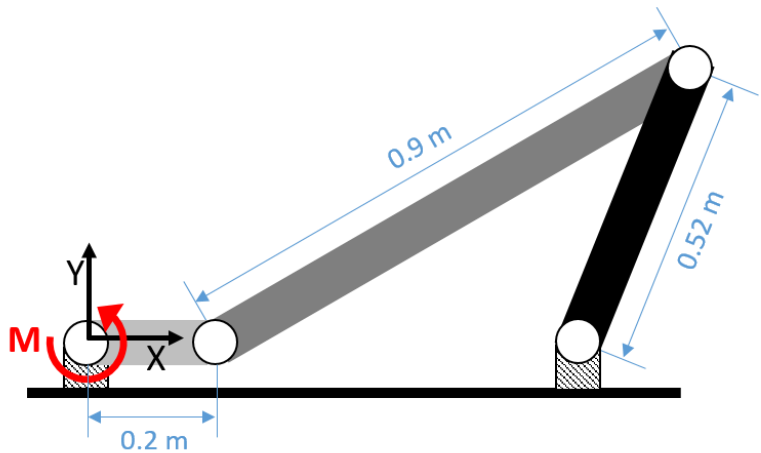

Figure 6.15. Configuration of the four-bar mechanism

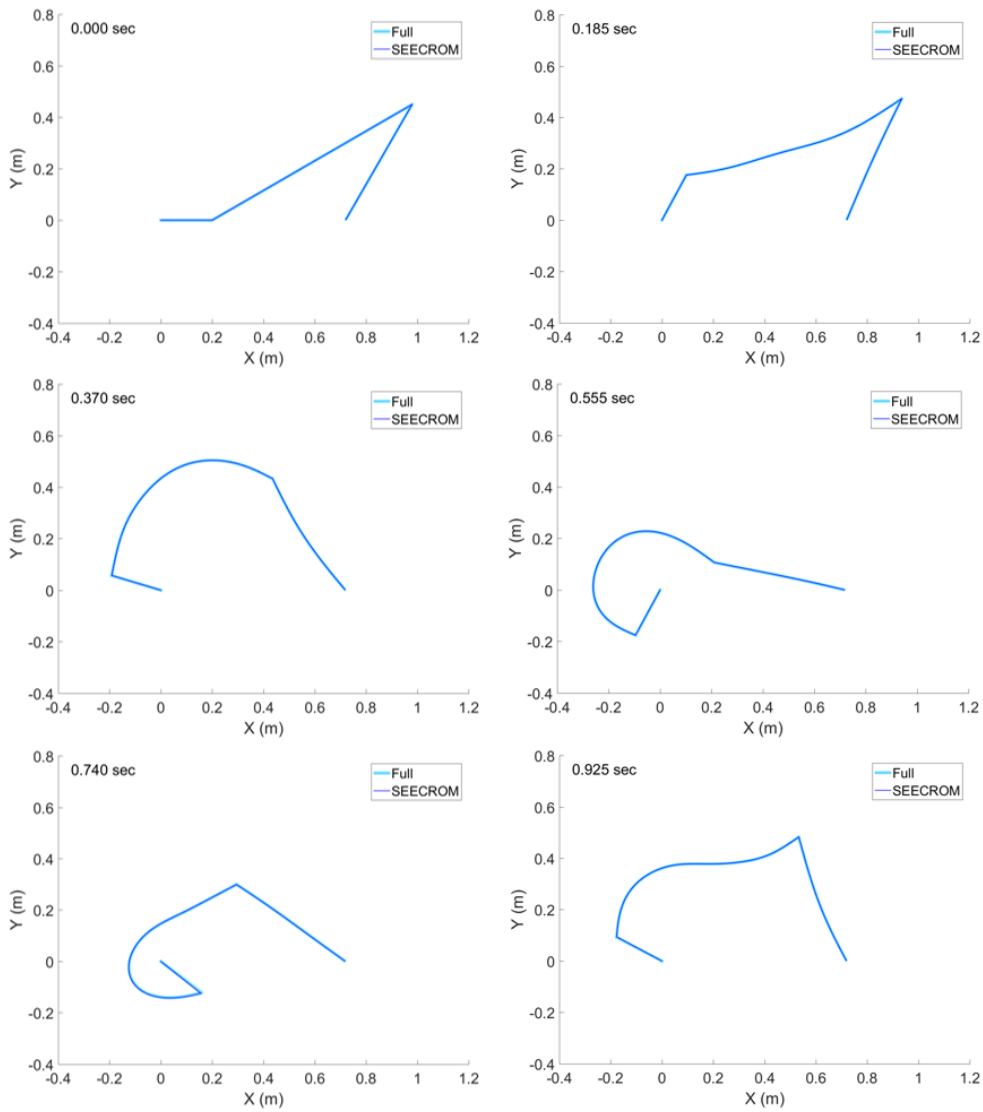

Figure 6.16. Deformation of the four-bar mechanism with time (T=1.1s)

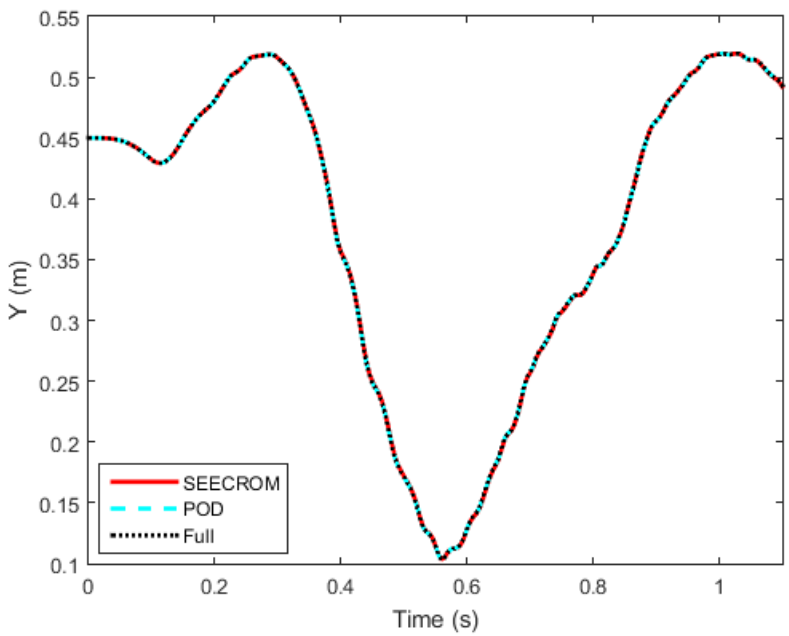

Figure 6.17. Y-position of the joint between the coupler and the follower

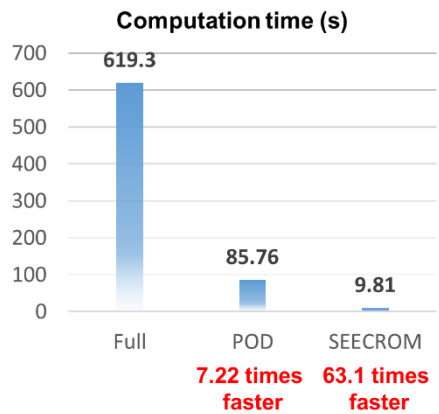

Figure 6.18. Computation time of the four-bar mechanism

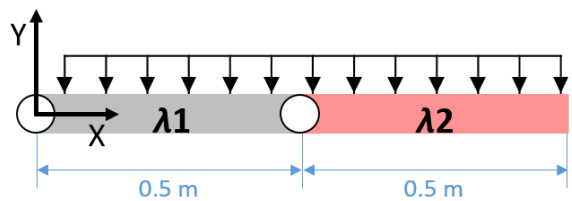

Figure 6.19. Configuration of the double pendulum with design parameters

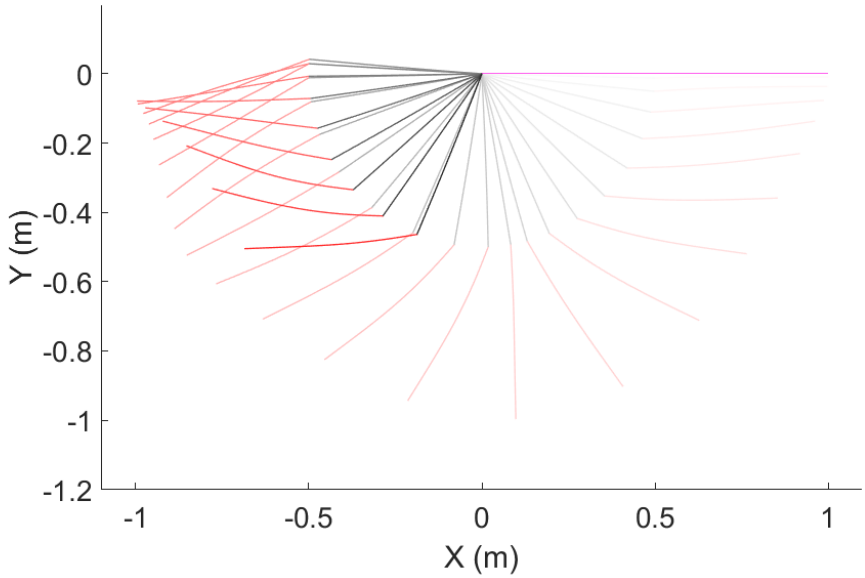

Figure 6.20. Deformation of the double pendulum under dynamic analysis

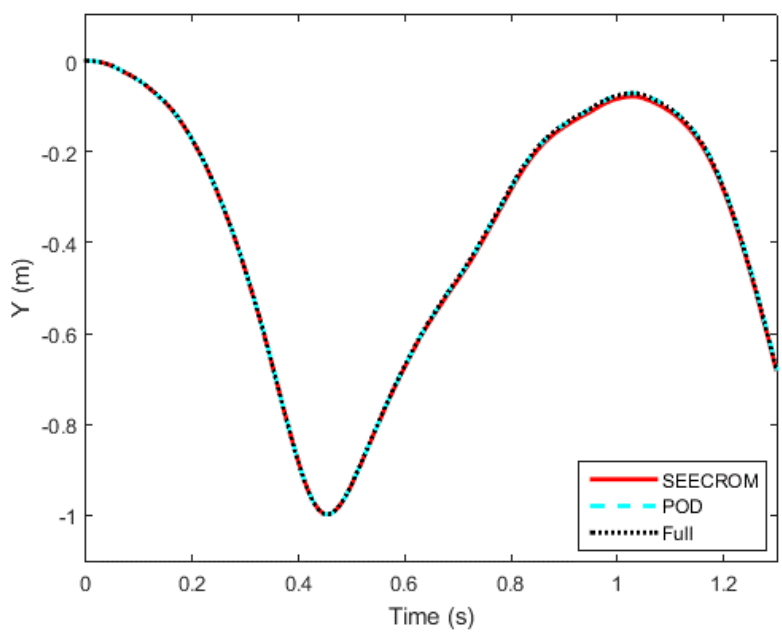

Figure 6.21. Transverse position of the end point of the double pendulum

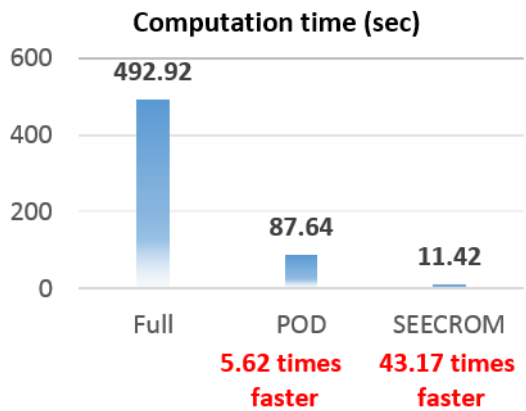

Figure 6.22. Computation time for the double pendulum with parameterization

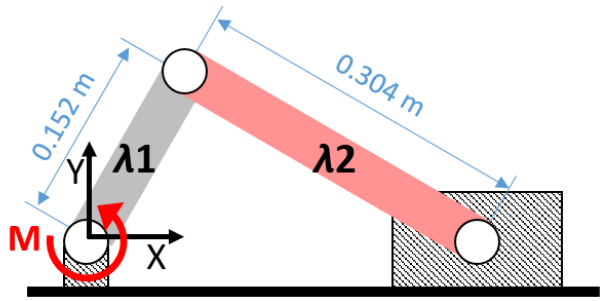

Figure 6.23. Configuration of the slider-crank mechanism with design parameters

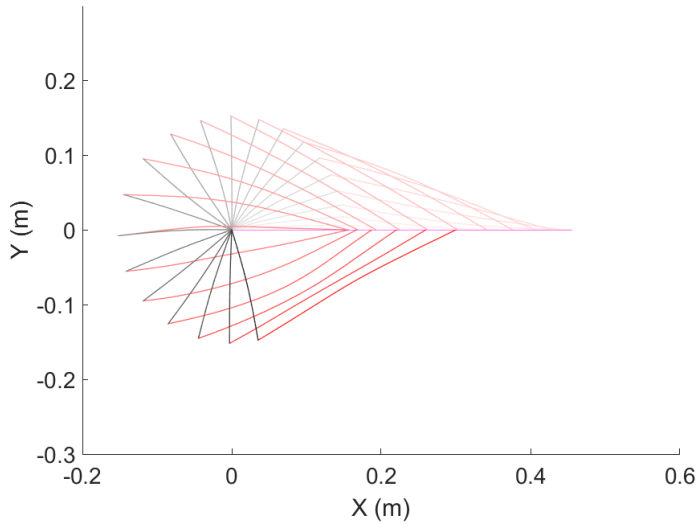

Figure 6.24. Deformation of the slider-crank mechanism with time (T=1.6s)

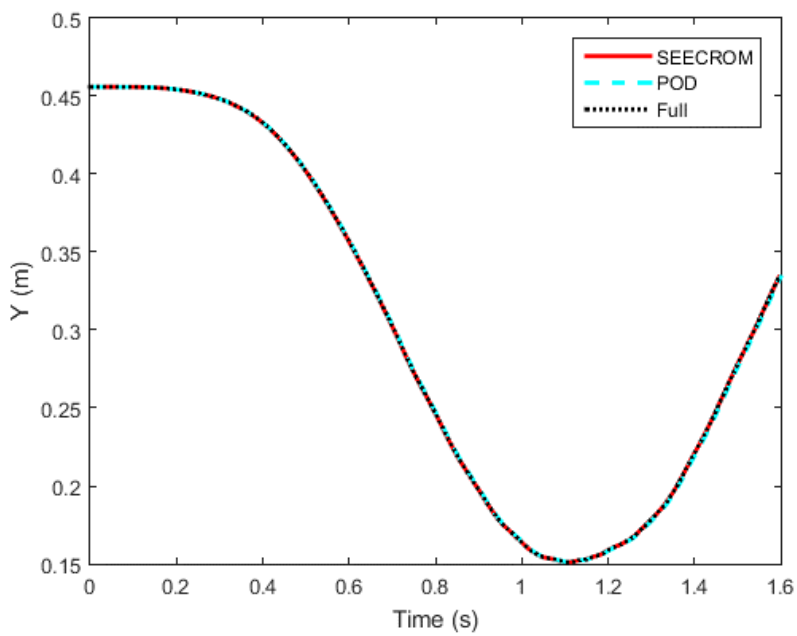

Figure 6.25. X-position of the end of the connecting rod with time

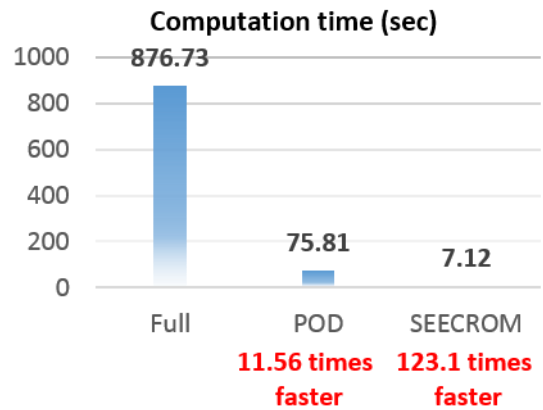

Figure 6.26. Computation time for the slider-crank mechanism with parameterization

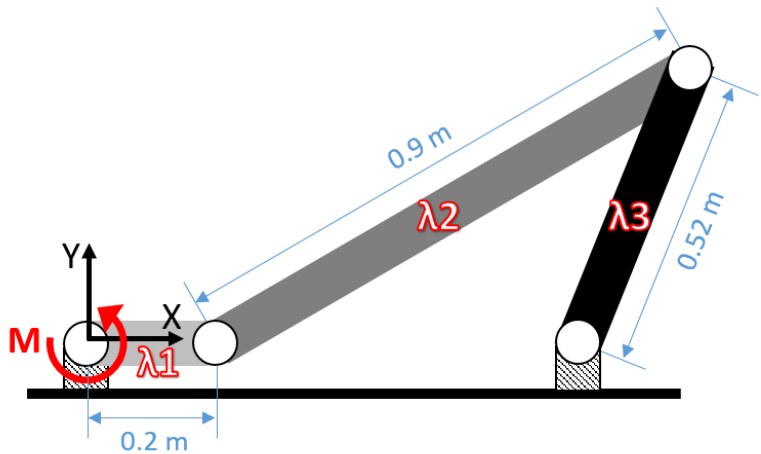

Figure 6.27. Configuration of the four-bar mechanism with design parameters

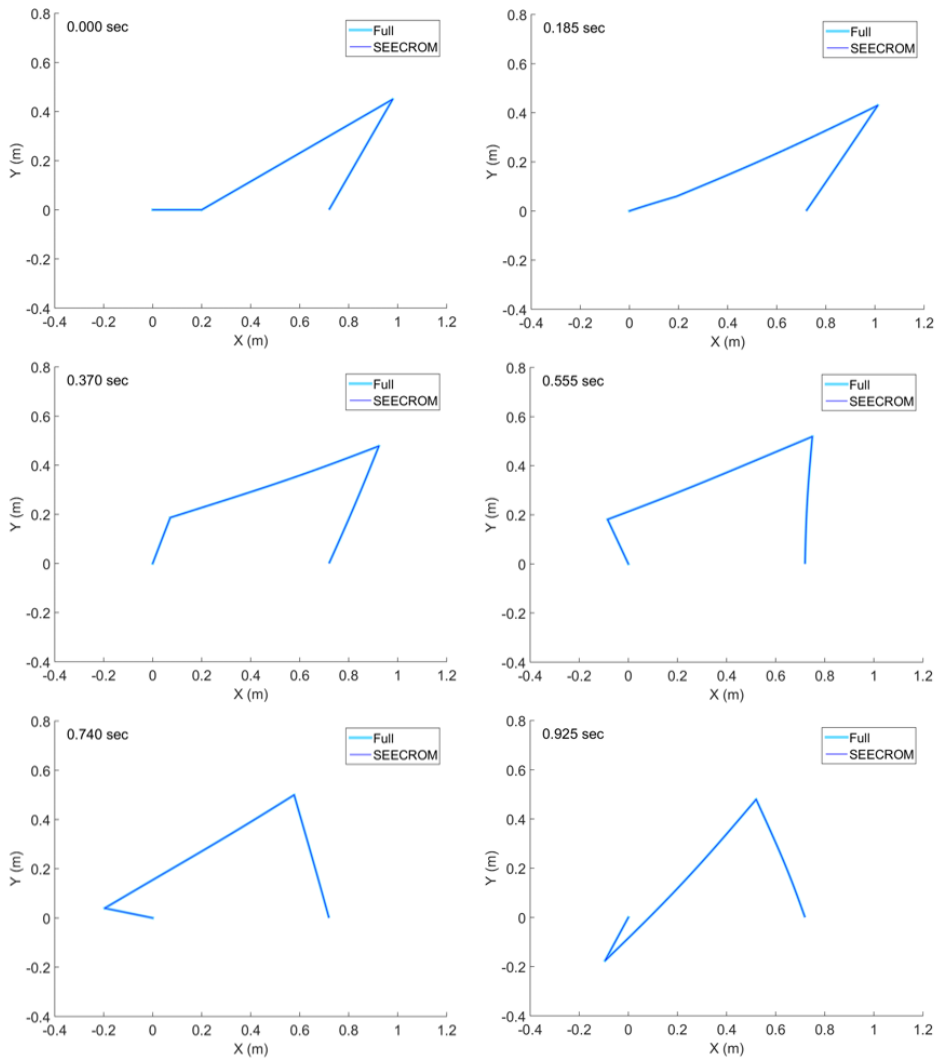

Figure 6.28. Deformation of the four-bar mechanism with time (T=1.1s)

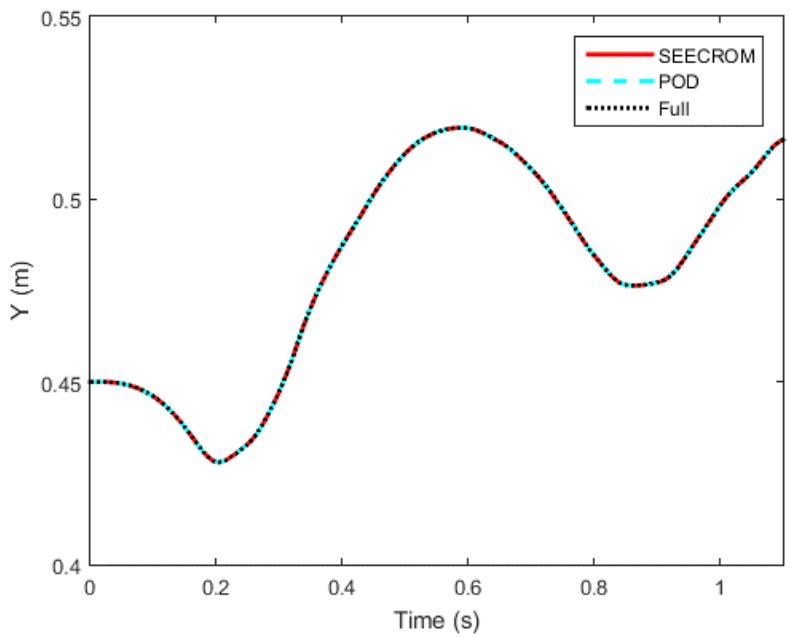

Figure 6.29. Y-position of the joint between the coupler and the follower

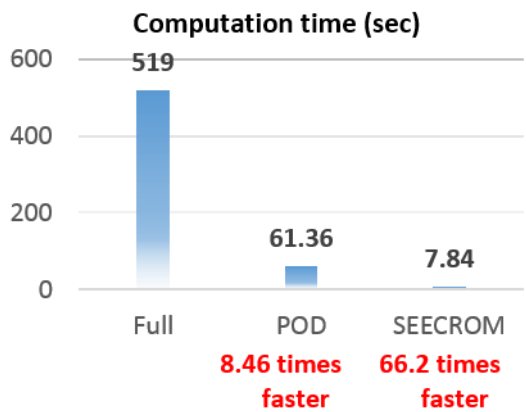

Figure 6.30. Computation time for the four-bar mechanism with parameterization

7. APPLICATON TO OPTIMIZATION PROCESS

7.1. Motivation

The process of the design optimization of finite element structures takes a significant amount of computation time and resources. It needs numerous iterations of system analyses as the values of design parameters are changed in search of the optimal design. The iteration should be repeated until the updated design satisfies a certain condition defined for the optimization problem. If the size of the system is large that the inverse process to obtain the displacement solutions gets inefficient, reduced order methods can be effectively applied. The related researches, which conduct optimizations based on the reduced order model, have been popular in decades.

In the cases when nonlinearities are present in the finite element structures, the optimization process becomes more complex. The system matrices should be reconstructed as the system responses change, which makes the construction process take the half of the computation time of the entire nonlinear analysis. This has been the obstacle to the application of the reduced order modeling to the optimization of nonlinear structures. The optimization process inherits the characteristics of the reduction methods applied for the system analyses. The problem is that most reduction methods for nonlinear structures only reduce the computation time of the solution process of the system, not the construction process of the system matrices.

Parameterizations of reduced order models are also the critical point for the application

of reduction methods to optimization problems. Even if a reduction method efficiently reduces the computation time for nonlinear analyses, without the inclusion of design parameters to the reduced model, the reduced order modeling becomes ineffective in the optimization process. The design parameters are continuously changed until the response of the system meets the design requirements. The system matrices are changed to yield the different responses for the different parameters. Without the parameterization techniques, therefore, the construction of system matrices and the reduced order modeling of these matrices should be repeated as the design parameters change.

In this paper, a new method of parameterized reduced order models is proposed. It is referred to as SEECROM since the reduced order models use stiffness evaluation method based on the element connectivity of finite elements. SEECROM reduces the computation time for the system matrices construction process as well as the time for the solution process. An equivalent model based on SEECROM substitutes the assembly and the integration process of the full system analysis. The input and the output of the equivalent models are the displacements and the corresponding internal forces, respectively. In the stiffness evaluation methods, the internal forces are composed as the sum of the 3rd order polynomial displacements. Each polynomial term is multiplied by the constant coefficients. Theses coefficients are called as 'stiffness coefficients' and they are efficiently obtained with the relation from the finite element connectivity. Then, the reduction technique with Proper Orthogonal Decomposition method is applied to enhance the efficiency of the equivalent model.

SEECROM is especially useful when it comes to the parameterization of nonlinear structures. In the proposed method, the nonlinear internal force model is constructed in

element-wise manner. This simply enables the parameterization. The design parameters can be easily multiplied element by element in the evaluation process of the stiffness coefficients to complete the parameterized reduced order model. With the proposed method, the nonlinear internal forces can be computed effectively without the re-evaluation of these stiffness coefficients since they are constant values which are independent from the displacements or the design parameters. The numerical integration and the assembly process are eliminated as well with the use of the proposed method. Due to the efficiency for the nonlinear analyses and the ability to be parameterized for the design parameters, SEECROM is perfectly fitted for the reduced order modeling of nonlinear structures subjected to the optimization problems.

This section is categorized as follows. First, the conventional process of the optimization of nonlinear structures is presented in Sect. 7.2. The reason for the excessive requirement of computational resources and thus the needs for the reduced order models as well as the parameterization are explained. In Sect. 7.3, the newly developed parameterized reduced order modeling method for nonlinear finite element system, SEECROM, is utilized to the optimization process. The sampling strategy for the multiple design parameters and the issue of the computational efficiency for the large scale problems are also discussed. In the final section, two sample optimization problems are demonstrated. A static structural system with a hyperelastic material and a multibody dynamic system. A thickness design problem of the structure with hyperelastic material is solved under strain constraints and a system of for-bar mechanism based on ANCF elements is subjected a diameter design problem. The formal example is a multi-variables problem with 16 design parameters and the latter example is time-dependent simulation. The sampling strategy is numerically

demonstrated and the computational efficiency is compared in detail.

7.2. Optimization of nonlinear system

A general process of an optimization problem is depicted in the flow chart illustrated in Fig. 7.1. In the search of the optimal values, the design variables are iteratively changed to proceed to the next iteration steps and to find the direction to the optimal state. Whenever the design variables are changed, the system analyses are repeated to get the corresponding system responses which are verified against the design requirements.

As shown in Fig. 7.1, the optimization process consists of the iterative system analyses. One iteration cycle includes the system analysis to get the responses from the system, the validation of the design requirements of the system and the design update. Moreover, to determine the design parameters for the next iteration step, sensitivity analyses are required. The process to find the direction of optimization problems is referred to sensitivity analysis. In the cases when the sensitivity is cannot be obtained analytically, it can be computed from numerical differentiations, which enhances the computational burden. In general, the numerical calculations for sensitivities require the equal number of system analyses to the number of design parameters. Thus the number of system analysis required for one iteration cycle becomes the number of design parameters plus one.

If a structure to be optimized has nonlinear characteristics, an additional iterative process to solve nonlinearities is added in the optimization process to compose two layers of iteration cycles. This is illustrated in Fig. 7.2 where the system analysis itself forms the iteration cycle. In Fig. 7.2, the outer cycle of the iteration is performed with the update of

the design parameters. It is terminated as the desired responses are obtained to meet the design requirements. Within one cycle of the outer iteration, the values of the design parameters are maintained. The inner iterations find the nonlinear system responses from the solutions of the discretized equations, which terminated when the force equilibrium is achieved. Then, with this new equilibrium state, cost and constraint functions are evaluated and the outer cycle resumes.

Therefore, in the optimization process of nonlinear structures, the nonlinear system analysis is performed more than the number of design parameters per design iteration cycle. This is why the reduced order modeling is a tempting technique for the efficiency of the optimization process. Nevertheless, there exist two main obstacles blocking the application of the reduced order models. Firstly, the reduced order models for nonlinear structures should have sufficiently high efficiency. In addition to the reduction of the system matrix size, the construction of the matrices should be performed efficiently. Secondly, the reduced order models should be parameterized by the design parameters. To embrace the change of the design, system matrices should be reconstructed. If the system matrices are parameterized with the design parameters, the construction process can be skipped, which enhance the efficiency of the optimization.

Fig. 7.3 shows the optimization process of nonlinear structures with the reduced order modeling based on POD method. Since it is highly accessible in most cases of reduced order modeling and it represents nonlinear characteristics well, POD method is the most popular in the reduced order modeling concerning nonlinear systems. Check Sect. 4.1 for a more detailed explanation. The process of optimization with POD method is divided into two stages. The offline stage includes all the preparation works required before

proceeding to the optimization process. The reduction modes are computed from the snapshot data obtained in the sampling analyses. The main process of the optimization occurs in the online stage where the iterative system analyses are performed as the design changes. The conventional approach of reduced order models including POD method requires the reconstruction of system matrices as the displacements are updated. Although the discretized equation is solved efficiently with reduced order model, the reconstruction of system matrices cancels the effect.

To skip the process of matrix construction, it should be possible to update the system matrices so that they can take the changes of the input parameters. In the optimization process of nonlinear structures, the input parameters are the displacements and the design parameters. If the reduced order model cannot embrace design parameters, therefore, it should be reconstructed as the design changes, which costs a great deal of computational resources.

For a reduced order model to substitute the nonlinear system analysis, in short, it is important that 1) the model should yield the system response efficiently and 2) accept the design parameters as input variables. Therefore, the efficient method for a parameterized nonlinear reduced modeling is required. This requirement exactly coincides with the descriptions for SEECROM-Parameterization, which was proposed in Sect. 3 to Sect. 5.

7.3. SEECROM-Parameterization for optimization of nonlinear system

7.3.1. Optimization procedure using SEECROM-Parameterization

SEECROM effectively computes the nonlinear internal force and the tangent stiffness to solve an optimization problem for nonlinear systems. Still, there are two main issues to be discussed before the adaptation of the ROM method to the optimization process; 1) SEECROM model should be composed in relation with the design parameters of the optimization problem. 2) A new sampling strategy should be devised for the large number of design parameters. They are discusses in Sect. 7.3.1.1 and Sect. 7.3.1.2, respectively. The complete optimization procedure with SEECROM method is illustrated in Sect. 7.3.1.3.

7.3.1.1. Parameterization by design parameters

SEECROM method constructs an equivalent model to compute nonlinear internal forces from the current displacements. In other words, the input and output parameters for the equivalent model are the displacements and the corresponding internal forces, respectively. The internal force $\tilde{\Gamma}_i(\mathbf{u})$ at the i^{th} degree of freedom can be represented by

$$\tilde{\Gamma}_i(\mathbf{u}) = \tilde{K}_{ijkl}\sum_{n=1}^{AE}\left[u_j u_k u_l\right]_n = \tilde{K}_{ij}\sum_{n=1}^{AE}\left[u_j^c(\mathbf{u})\right]_n \tag{7.1}$$

where $\tilde{K}_{ijkl}$ is the stiffness coefficients and AE indicates the number of adjacent elements.

The addition of the parameterization technique means the addition of the new input parameters which build the corresponding internal forces together. Then, the internal forces, the output parameters of SEECROM model, are changed according to the perturbations of the added input design parameters as well as the update of the

displacements. Since SEECROM model is composed in element-wise manner, the parameterization of SEECROM model is easily achieved by

$$\tilde{\Gamma}_i(\lambda,\mathbf{u}) = \tilde{K}_{ijkl}\sum_{n=1}^{AE}\lambda_n\left[u_j u_k u_l\right]_n = \tilde{K}_{ij}\sum_{n=1}^{AE}\lambda_n\left[u_j^c(\mathbf{u})\right]_n \tag{7.2}$$

The simple modification of Eq. (7.1) leads to the above equation; the design parameters λ_n is multiplied to the original equation for each element. If a design parameter has a linear relation with the internal force such as the thickness of the plane elements, Eq. (7.2) can be directly applied to the parameterization of SEECROM model with the direct substitution of λ_n to the thickness for the n^{th} element.

This process can be modified according to the relation between the design parameters and the corresponding internal forces. For example, if the design parameters is the diameter d_n of a beam element, it is not linearly related to the internal force. In the beam elements, the internal force is obtained as the sum of its bending part and the shear part. These two parts are proportional to the cross-sectional area and the second moment of area, which correspond to d_n^2 and d_n^4, respectively. Thus, the Eq. (7.2) for this specific example can be represented as

$$\tilde{\Gamma}_i(\lambda,\mathbf{u}) = \tilde{K}_{ijkl}\sum_{n=1}^{AE}d_n^2\left[u_j u_k u_l\right]_n + \tilde{K}_{ijkl}\sum_{n=1}^{AE}d_n^4\left[u_j u_k u_l\right]_n \tag{7.3}$$

This can be regarded that the two different input design parameters d_n^2 and d_n^4 are added to the SEECROM model instead of a parameter d_n. This indicates that although the number of design parameter is just one on the surface, the number can be doubled by

the characteristics of the parameter. Whether the design parameters are added linearly or non-linearly, the important thing is that the parameterization of SEECROM can be easily tailored to suit the requirements of the problems.

7.3.1.2. Sampling criteria

The solution sets required to evaluate the stiffness coefficients are collected from the training analyses. In the parameterized modeling, the sets consist of the design parameters, the displacements and the corresponding internal forces. The composition of the solution sets should be compact and sufficient since it determines the accuracy and the efficiency of the SEECROM method. In this section, the criteria to obtain the solution sets will be discussed.

As stated in Sect. 3, the number of required solution sets is determined based on the number of unknown coefficients of displacement combinations. If design parameters are added in the process as shown in Eq. (7.2) and Eq. (7.3), the number of unknown coefficients increases according to the characteristics of the parameters.

The composition of the solution sets comes from the composition of the training analyses. In design problems, the range of the design parameters are given as the design requirements. Then, the training analysis can be repeated under the various compositions of the design parameters. The range of the training analyses as well as the solution sets are determined by the lower and the upper bounds of the design parameters.

The basic rules in the selection of the solution sets are simple. 1) The collected system responses should span the responses may occur in the optimization process. 2) The sampling number should be kept minimum to reduce the computation time for the

training analyses.

However, it is not simple to establish the standards for the sampling analyses. Although ideally, the solution sets should be independent each other, the solution sets of element displacements obtained from training analyses tend to have rank deficiency. Moreover, the full rank sets do not guarantee the accuracy of the equivalent model. Do not forget that the SEEC method is an approximated model based on the polynomial expansion. In other words, it is difficult to obtain a specific number of displacements sets which are independent each other, and it is even not necessary.

In the middle of the identification process of the stiffness coefficients, however, the accuracy of the equivalent model can be checked. The rate of the independent solution sets against the number of unknowns can be used as the indicator γ such as

$$\gamma = \left.\frac{\text{rank of solution sets}}{\text{number of unknowns}}\right|_{element} = \left.\frac{\text{rank of } \lambda\left[u^c(\mathbf{u})\right]}{\text{number of unknowns}}\right|_{element} \tag{7.4}$$

where $\lambda\left[u^c(\mathbf{u})\right]$ is the displacement sets in combination form with design parameters.

Now, based on the indicator γ, it can be determined whether the training analyses should be added more or not. Engineers can design training analyses by the experiences based on the values of the indicator. In the examples in this paper, the equivalent model is constructed with the indicator γ to be larger than 0.5. In the numerical examples in the following section, the relations among the indicator, the model accuracy and the composition of the training analyses are demonstrated.

7.3.1.3. Optimization procedure with SEECROM

The optimization procedure based on POD method in Fig. 7.3 can be modified by

SEECROM method, which is illustrated in Fig. 7.4. The major difference between two figures is the requirement for the system matrix construction in the nonlinear system analyses. With the application of SEECROM method, the construction process can be omitted. The equivalent model based on SEECROM directly takes the changes of the design parameters and the displacements to yield the corresponding internal forces. The downside from the application of SEECROM exists in the offline stage; the identification of the stiffness coefficients takes computational resources. Fortunately, the efficiency loss in the offline stage is easily redeemed in the online stage.

With the strategies of the parameterized ROM for optimization procedures presented above, a sample numerical problem was solved in the following section. A static structure with hyperelastic material is subjected to the design optimization problems. The computation time required for the online and the offline stage is discussed by three different cases of approaches. The system analysis based on SEECROM approach was performed against the reference analyses, which are the full system analysis and the reduced model analysis based on POD method. A design optimization of a multibody dynamic system is also solved for the mass minimization with the diameters of each body as a design parameter. The procedures and the results are demonstrated for the verification of the proposed method.

7.3.2. Numerical examples

Two optimization problems which handle the different nonlinearities are demonstrated in this section. The first example concerns the structural static system with material

nonlinearities. The structure composed with hyperelastic elements is subjected to an optimization problem which has 16 design variables of thickness for 16 sections. The mass of the structure is minimized under strain constraints. The second example concerns the multibody dynamic analysis which requires the time marching analysis. The diameter of each body of the four-bar mechanism is computed from the optimization process with the constraints imposed on the axial stresses.

7.3.2.1. Application to nonlinear structural analysis

The first example is the mass minimization of a nonlinear structure with the hyperelastic material. The square plane with a hole is fixed by one side and loaded by the opposite side. The width of the plane is 0.02 m and the diameter of the hole is 0.004 m. The configuration is shown is Fig. 7.5. The hyperelastic elements are modeled as Neo-Hookean with the shear modulus of μ =1.5 MPa, bulk modulus of κ=1.0 GPa and density of ρ=1,000 kg/m^3. The element has 4 nodes per element and 2 degrees of freedom per node, which makes 8 degrees of freedom per element. The structure is composed of 2,544 elements and 5,360 degrees of freedom. The distributed loads are imposed with the direction of 30˚ as shown in the figure. The magnitude of the static load is 20 N.

Fig. 7.5 also shows the composition of the design parameters. The entire domain is uniformly divided into 16 square regions which can have different thickness as design variables. The each design sections are illustrated with different colors. The mass of $m(\boldsymbol{\lambda})$ is minimized while the constraint enforces a limit on the maximum stain of the structure. The optimization problem is stated as

$$
\begin{aligned}
&\underset{\boldsymbol{\lambda}}{\text{minimize}} \quad m(\boldsymbol{\lambda}) \\
&\text{subject to} \quad |E11| \leq 0.5 \\
&\qquad\qquad\quad |E12| \leq 0.3 \\
&\qquad\qquad\quad 0.001\ \text{m} \leq \lambda_i \leq 0.003\ \text{m}, \qquad i = 1,...,16
\end{aligned}
\tag{7.5}
$$

where $E11$ and $E12$ are the components of Lagrangian strain E.

Test cases for sampling

To solve the optimization problem with SEECROM approach, the equivalent internal force model should be constructed in the offline stage. Since the preparation works in the offline stage take the additional time, the sampling analyses should be performed efficiently while keeping the accuracy of the equivalent model. To this end, sampling strategies should be devised. In Sect. 7.3.1.2, therefore, an indicator γ, which can be calculated by Eq. (7.4), is provided to evaluate the state of the equivalent model.

To observe the relation between the indicator and the accuracy of the equivalent model, 4 cases of training analyses are demonstrated based on the example above. Since the load cases is fixed in the optimization problem, the training analyses are controlled by the composition of the design parameters. The design parameters are selected to have the values in the range of the design requirements. The lower bound λ_L, the upper bound λ_U and the middle value of $\lambda_M = 0.002\ \text{m}$ are used for the demonstration.

In Case A, three full finite nonlinear analyses are performed for sampling. Three different values of thickness ($\lambda_L, \lambda_M, \lambda_U$) are imposed uniformly for each analysis. In Case B, 16 analyses are performed. Each design section is perturbed for each analysis. Based on the lower bound λ_L as default, each design section is perturbed to upper

bound value λ_U. In Case C, the opposite case of the Case B is added to make 32 analyses. The added analyses have the upper bound λ_U as default, and the perturbation is given with the lower bound λ_L. Case D includes 256 analyses upon various combination of design parameters to the Case C. Fig. 7.6 shows the design parameters for each cases in simple drawing.

The indicator γ is calculated for each case in Fig. 7.6. The number of unknowns per element is 164 by the characteristics of the element and the rank of the displacement sets $\lambda\left[u^c(\mathbf{u})\right]$ is computed for each training case. The accuracy of the equivalent model for each case can be evaluated by the comparison of the displacement responses. The design parameters at the optimal state are imposed for the validation. The mean values of response differences between the POD reduction and SEECROM analyses are 0.18 %, 0.025 % and 0.0099 % for Case B, Case C and Case D. In Case A, the SEECROM analysis fails to give solutions.

In practical case, the responses of the equivalent model cannot be computed in the offline stage. Thus the indicator γ is useful, which can be easily computed without a computational burden. In the demonstration of four cases in Fig. 7.6, Case B to Case C have the indicator γ over 0.5. Although the value of indicator increases as the number of training analyses become larger, it should be noted that the computation time also increases by the number of analyses. The Case B is sufficient accuracy and efficiency, in this section, the 16 training analyses of Case B are performed to construct the reduced model.

Test cases for efficiency check

Once the SEECROM model is constructed based on the sampling analyses, the offline stage is completed. Based on the computation time for the offline stage, the validity of the reduced order model for the optimization can be investigated in advance. The time required for the optimization process can be predicted beforehand. Assume that one iteration of optimization cycle consists of the nonlinear analysis at the current design state and the sensitivity analyses. Then, the number of analyses required in an iteration step is equal to the number of design parameters plus one.

To verify the SEECROM approach, the reduced model analysis based on POD method and the full model analysis are conducted as references. If the computation time to solve one set of nonlinear analysis is obtained for each method, the overall time for optimization process can be predicted by the number of iteration step. Case Ⅰ and Case Ⅱ which have different number of elements are tested. They are composed of 5,360 and 21,280 degrees of freedom, respectively. The number of reduced degrees of freedom is 26 for two cases. The computation time is classified in Table 7.1 for each case and each method.

Fig. 7.7 shows the predicted computation time by the iteration number in the optimization process. Due to the offline computation, the full system analysis is favorable in the beginning of the iteration over the analyses based on POD or SEECROM method. In the results shown in Fig. 7.7, the efficiency of SEECROM method beats the full analysis during the first iteration step for both cases. On the contrary, it can be seen that the POD approach gain its efficiency gradually but still takes more time than the full

analysis at the 10^{th} iteration step. It is important to note that the efficiency of SEECROM is maintained as the size of the structural system is multiplied by 4. Moreover, the time for the offline computation can be easily shortened with the parallel computation, which is also shown in Fig. 7.7 with the assumption of 8 workers.

The optimization process is conducted with the optimization toolbox in Matlab. The solver of *fmincon* is used with the algorithm of 'Sequential quadratic programming'. Initially, the design has a mass of m =7.75 × 10^{-4} kg, and the design requirements are satisfied.

The optimization problem is solved with three different approaches. First, the optimization based on the full system analysis is performed for the reference. In addition, the problem is solved with reduced order models; the conventional POD reduction method and the proposed SEECROM method are applied, respectively. For the verification of the effectiveness of the proposed method, the computation time is compared for the three methods as well as the optimized designs and the convergence histories.

The training analyses are conducted for the 16 sets of design parameters. The Case B in Fig. 7.6 is used. While the magnitude of the load is fixed, the 16 compositions of design parameters are imposed for full system analyses. The design parameters, the displacements and the internal forces are saved as the solution set during the iterations.

The structure to be optimized is composed with 2,304 elements and 4,802 degrees of freedom, which is reduced to have 26 degrees of freedom with the reduction rate 0.5 %.

Fig. 7.8 shows the convergence histories of the optimization process. The convergence

is attained after 31~32 iterations. In addition, the evolution of design constraints is depicted in Fig. 7.9. All three approaches have the similar tendencies for the progression in the objectives and the constraints.

The optimized designs are illustrated with Fig. 7.10 and Fig. 7.11. The results from the reduction methods exhibit good agreement with the results from the full analysis. The E11 and E12 strain distributions at the optimal state are also illustrated in Fig. 7.12. The distribution satisfies the design requirement for the allowable strain. In Fig. 7.13, the computation time for the three approaches are compared. The proposed method exhibits significantly faster results than the optimization based on the full system analysis. It is 25.2 times faster than POD based reduction method and 24.6 times faster than the full analysis. POD method is slower than the full system analysis

7.3.2.2. Application to multibody dynamics

The optimization problem concerns the mass minimization of a four-bar mechanism shown in Fig. 7.14. The three flexible links have a constant solid circular cross-section. The material properties including Young's modulus and the density of each link are listed in Table 7.2. The gravity is imposed in the opposite y-direction. The crankshaft is driven by the moment M below

$$M = 180\cos(2.5\pi t) \tag{7.6}$$

The simulation is performed based on ANCF elements presented in Sect. 6. The time marching analysis is conducted with Newmark method with the time step of 0.001 s over the total time of T = 0.2 s.

The design parameters λ_i are the diameters of three flexible links, which are initially

set to 0.075 m. The optimization problem is to find the link diameters which minimize the total mass of the system $m(\boldsymbol{\lambda})$ under axial stress constraints $\sigma_{j,e}(\boldsymbol{\lambda})$ at each time step j for each beam element e, which is stated as

$$\begin{aligned} &\underset{\boldsymbol{\lambda}}{\text{minimize}} \quad m(\boldsymbol{\lambda}) \\ &\text{subject to} \quad \sigma_{j,e} \le 20 \text{ MPa}, \qquad j = 1,...,200, \quad e = 1,...,40 \\ &\qquad\qquad 0.05 \text{ m} \le \lambda_i \le 0.1 \text{ m}, \quad i = 1,...,3 \end{aligned} \tag{7.7}$$

The initial design has a mass of 19.39 kg. The optimization process is conducted with the optimization toobox in Matlab. The solver of *fmincon* is used with the algorithm of 'Sequential quadratic programming'.

The optimization problem is solved with two different approaches. SEECROM method is used against the full order analysis. For the verification of the effectiveness of the proposed method, the computation time is compared as well as the optimized designs and the convergence histories.

In the offline stage to construct the equivalent model, the sampling analyses are trained by the design parameter values. The sampling diameters of 3 sections are subjected with the combinations from the 3 different values (0.05 m / 0.075 m / 0.1 m) which are determined from the lower and upper bounds of the design parameters. Then the number of sampling analyses conducted becomes 3^3, which yield the sufficient number of solution sets to identify the stiffness coefficients. On the other hand, there is an important issue to be considered; the diameter in ANCF elements has the nonlinear relation with the internal forces. It was stated in Sect. 7.3.1.1 where the instructions are given with Eq. (7.3). Thus, the stiffness evaluation should be carried out as instructed in the previous section with the particular care on the design variables.

The cost function and the constraint history are illustrated in Fig. 7.15 and Fig. 7.16. The results from the full system analysis and SEECROM approach was depicted, which shows the similar tendency over the iteration process. The optimized designs are depicted in Fig. 7.17 and Fig. 7.18. It can be seen that the nearly identical designs are obtained from the two approaches. The computation time for the two approaches are compared in Fig. 7.19 and Fig. 7.20, which illustrate the total time of the optimization and the calculation time per iteration, respectively. In both representations, it can be seen that SEECROM is significantly faster than the full analysis.

Table 7.1

Computation time of the test cases for efficiency check (s)

	Case Ⅰ			Case Ⅱ		
	Full	**POD**	**SEECROM**	**Full**	**POD**	**SEECROM**
Offline stage	0	3,281	3,572	0	15,301	16,707
Per nonlinear analysis	163.3	156.4	2.69	832	763.9	10.06

Table 7.2

Material properties of four-bar mechanism

	Crankshaft	**Coupler**	**Follower**
Number of elements	10	20	10
length (m)	0.2	0.9	0.52
Density (kg/m^3)	2,709	2,709	2,709
E (GPa)	73	73	73

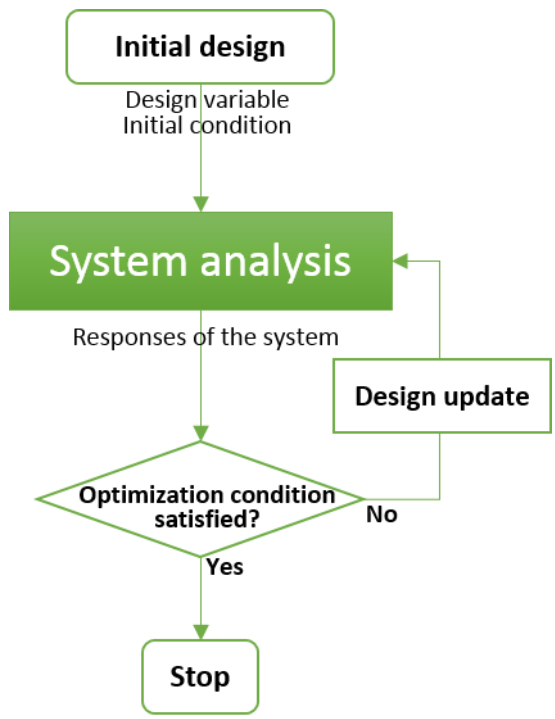

Figure 7.1. General process of optimization problem

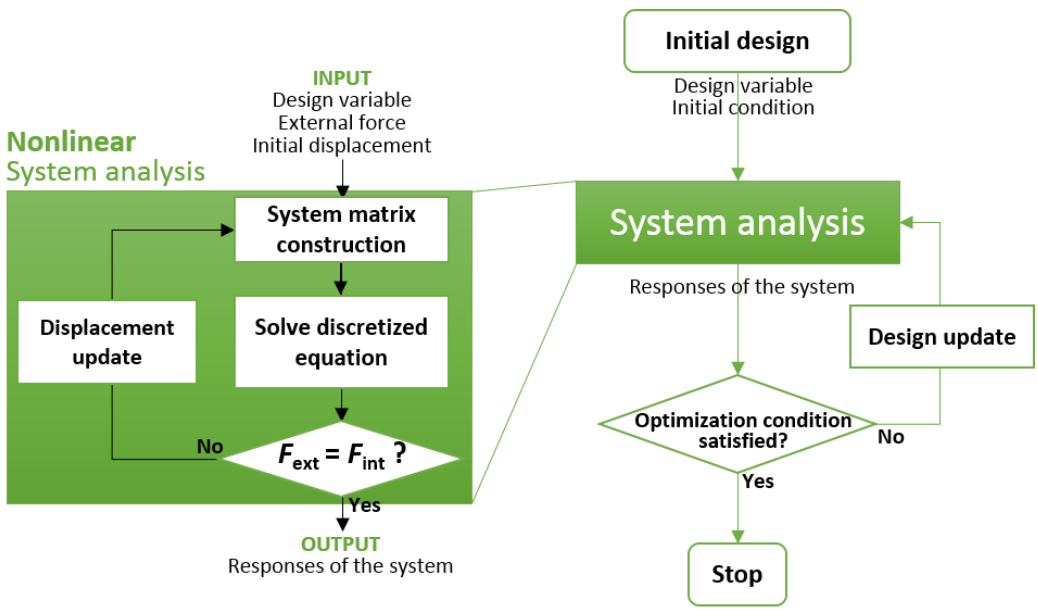

Figure 7.2. General process of optimization problem with nonlinear system

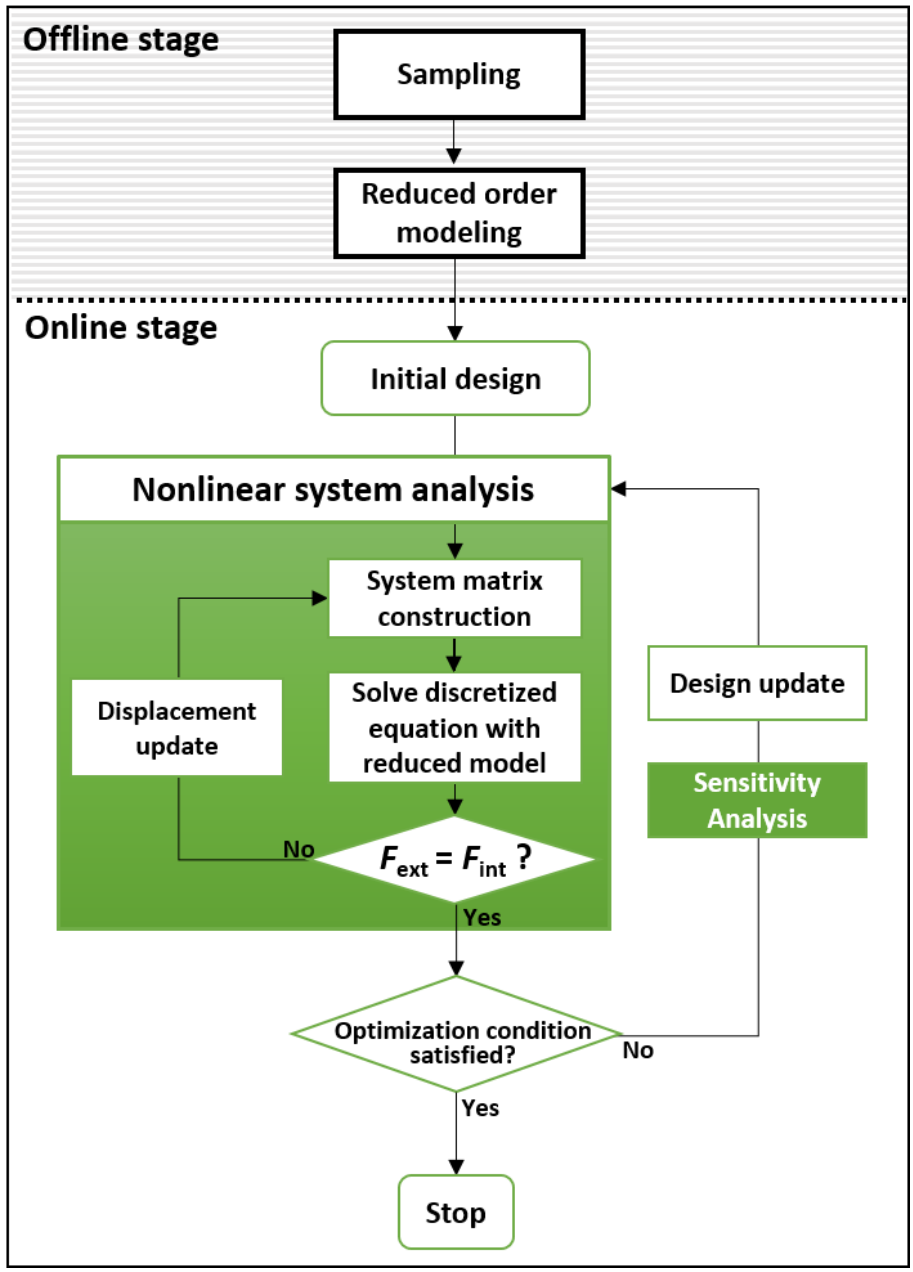

Figure 7.3. Process of optimization problem for nonlinear structure with reduced order modeling based on POD method

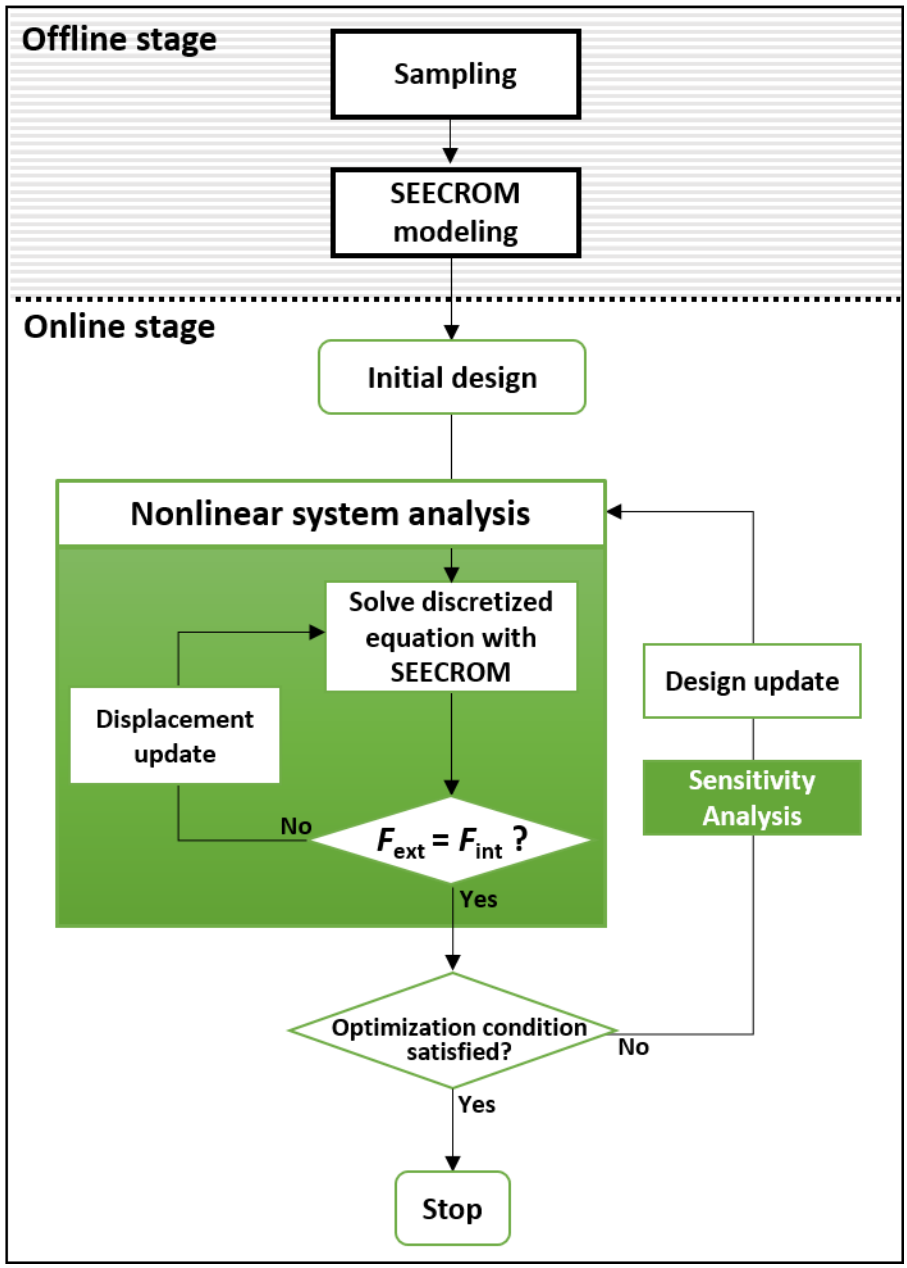

Figure 7.4. Process of optimization problem for nonlinear structure with SEECROM method

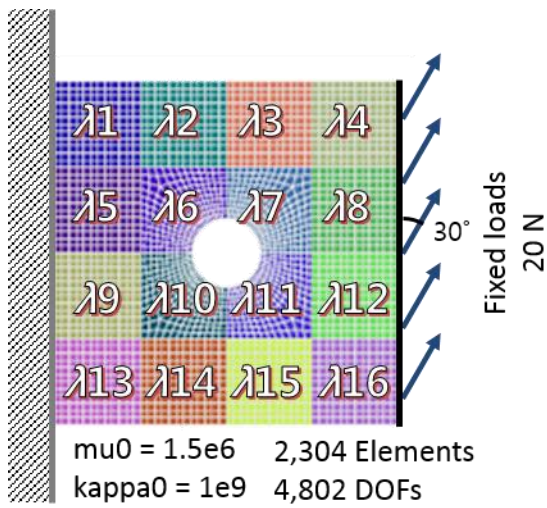

Figure 7.5. Nonlinear structure subjected to the optimization problem

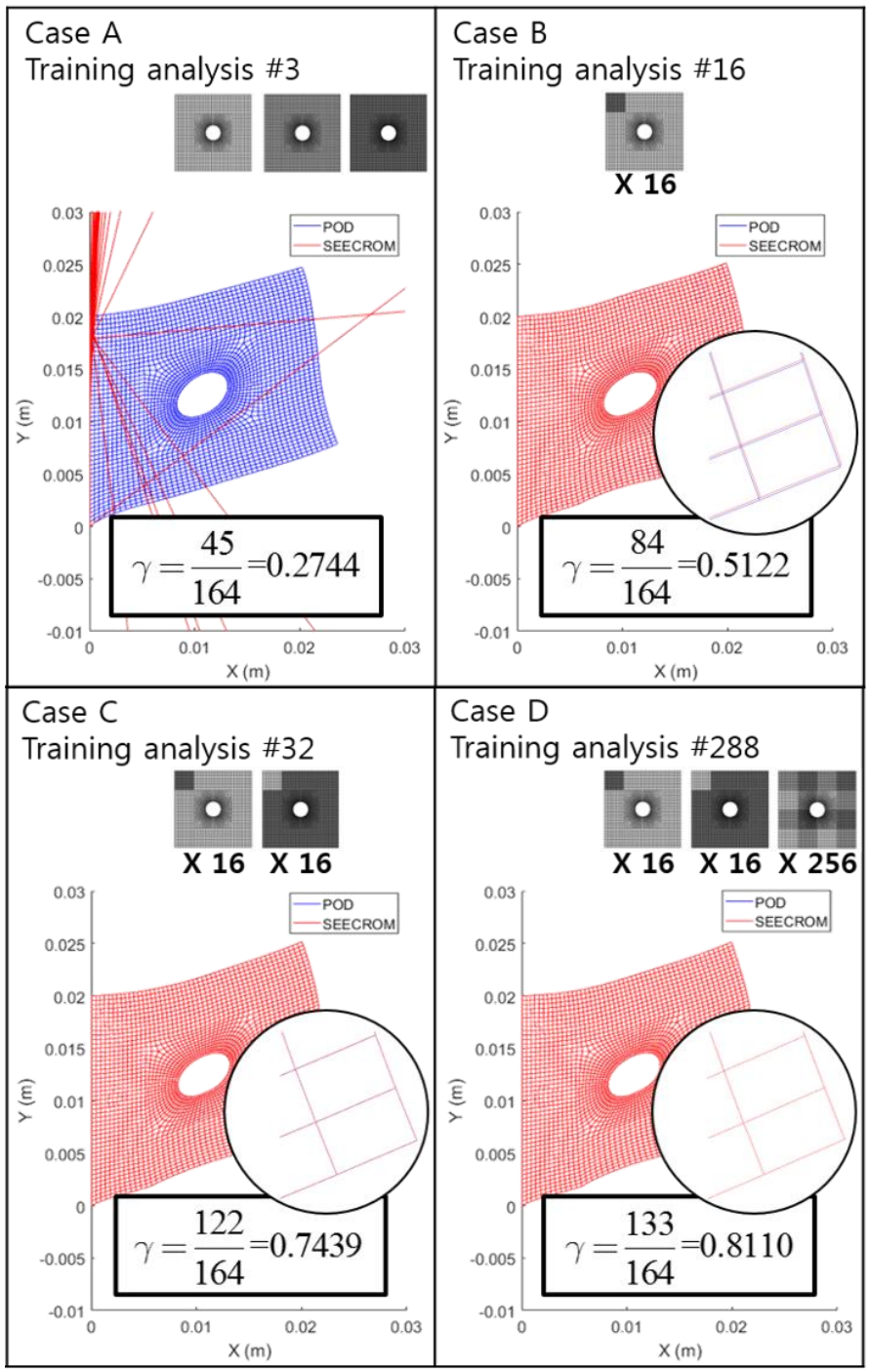

Figure 7.6. Test cases for sampling

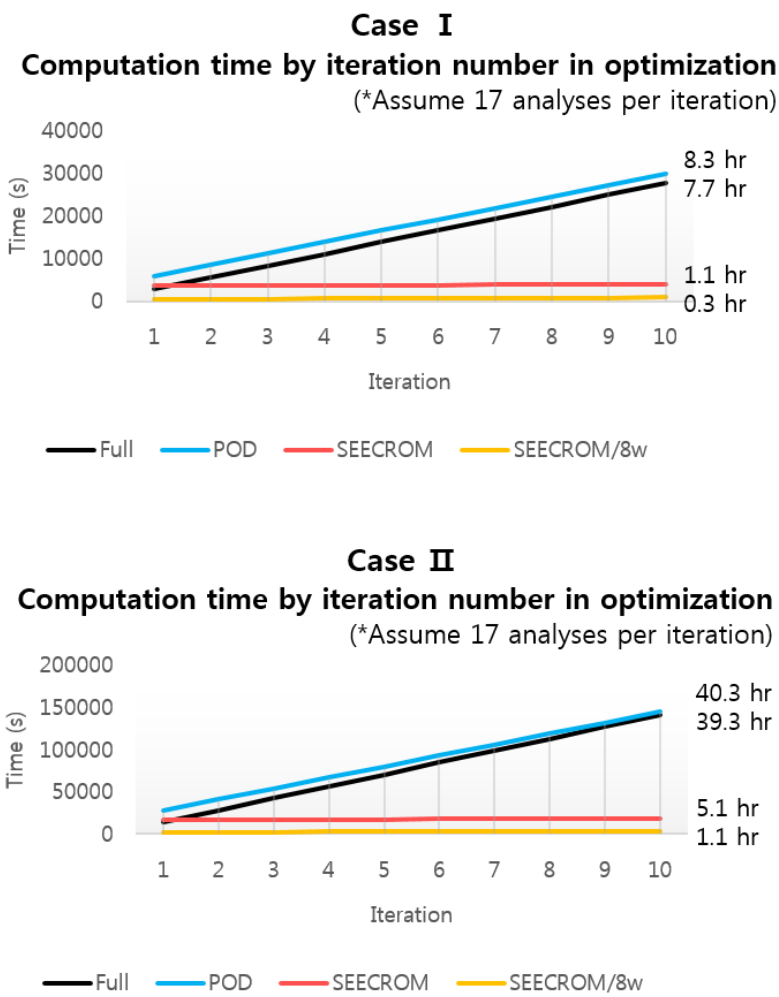

Figure 7.7. Test cases for efficiency check: prediction of computation time

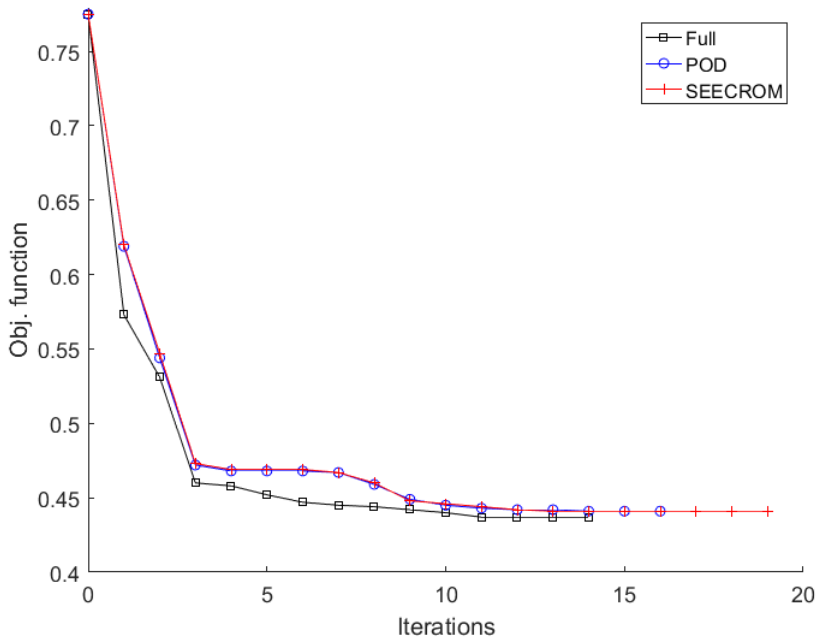

Figure 7.8. Cost function history from the optimization problem of material nonlinear analysis

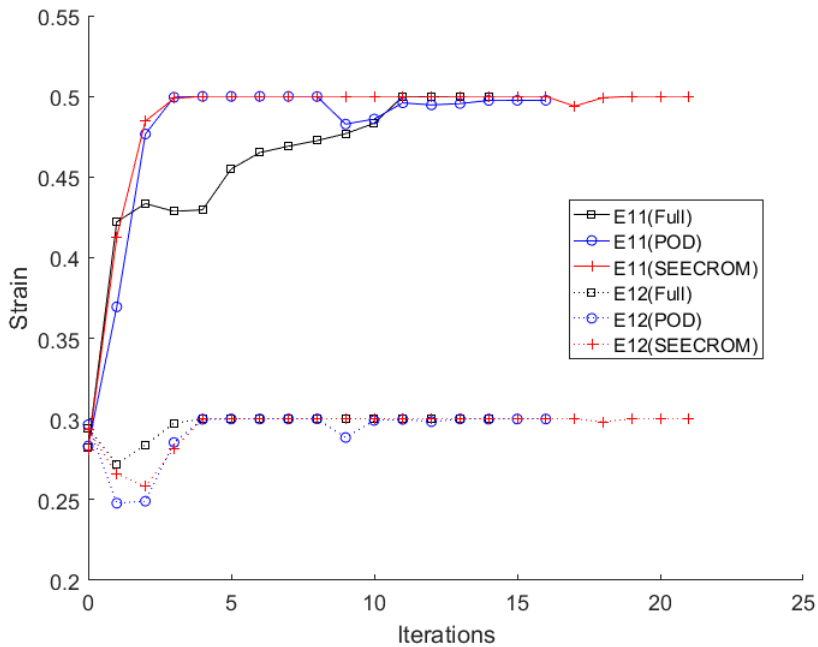

Figure 7.9. Constraints history from the optimization problem of material nonlinear analysis

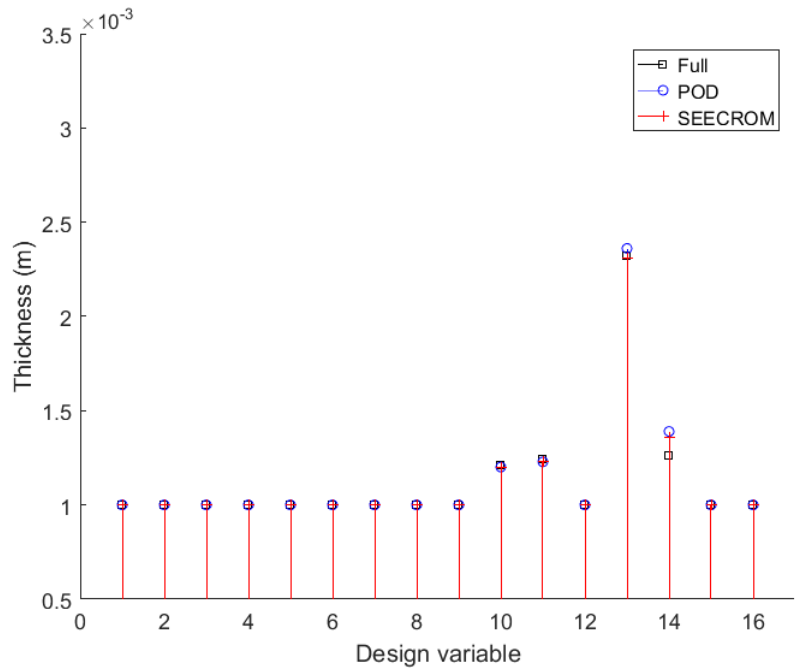

Figure 7.10. Design parameters at the optimal state from the optimization problem of material nonlinear analysis

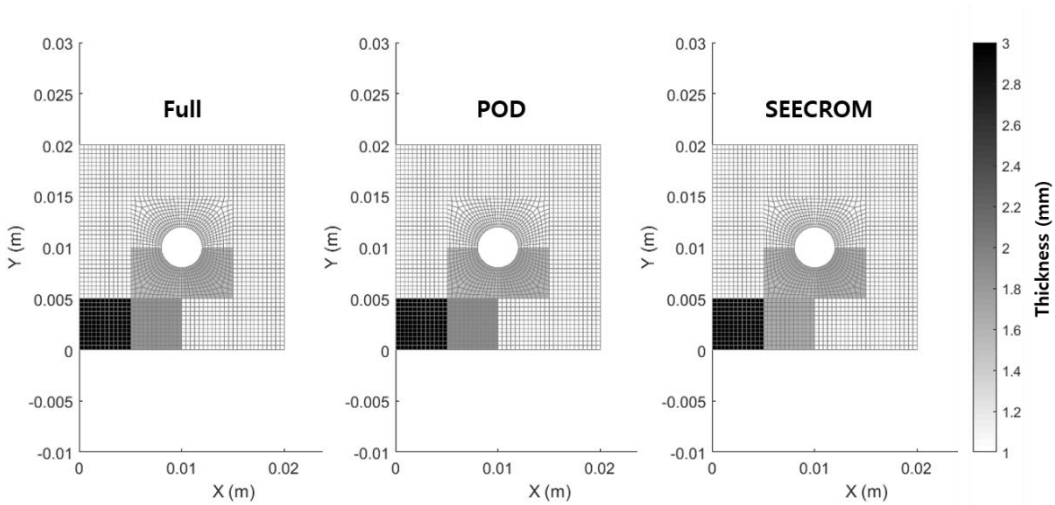

Figure 7.11. Optimal designs from the optimization problem of material nonlinear analysis

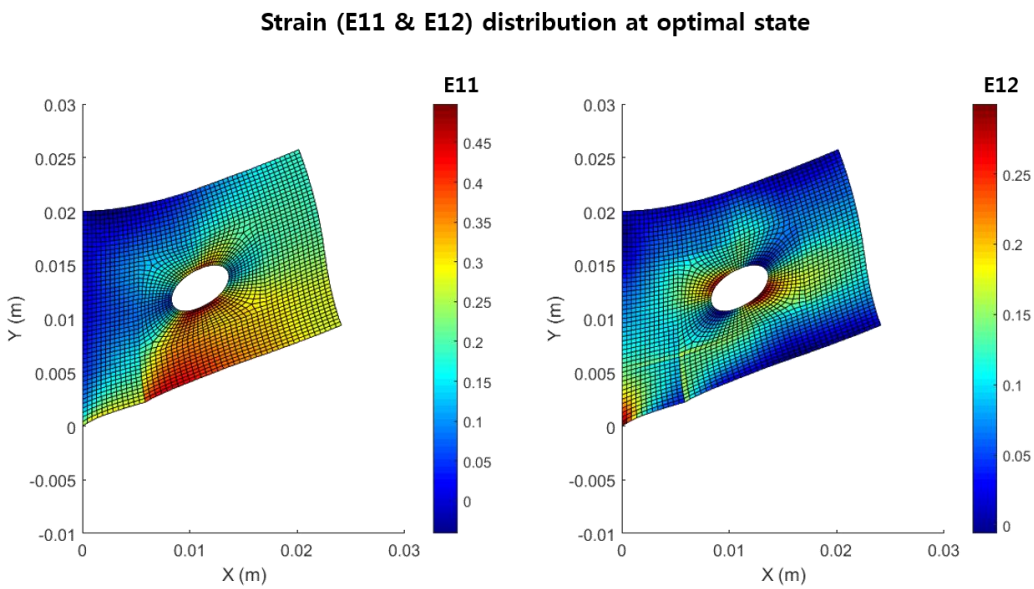

Figure 7.12. Strain distribution at the optimal state from the optimization problem of material nonlinear analysis

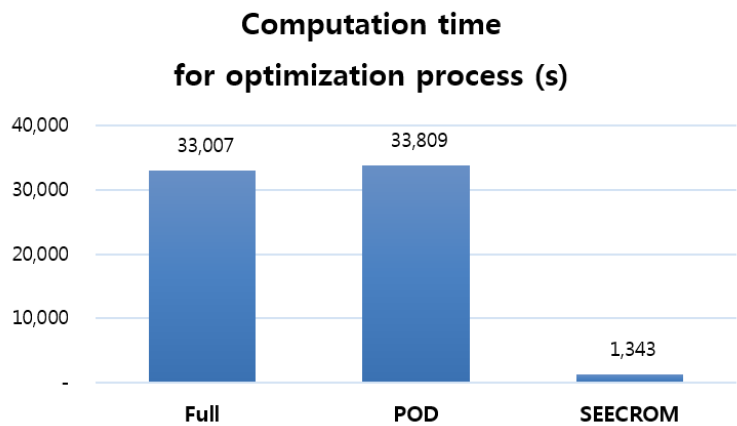

Figure 7.13. Computation time for the optimization problem of material nonlinear analysis

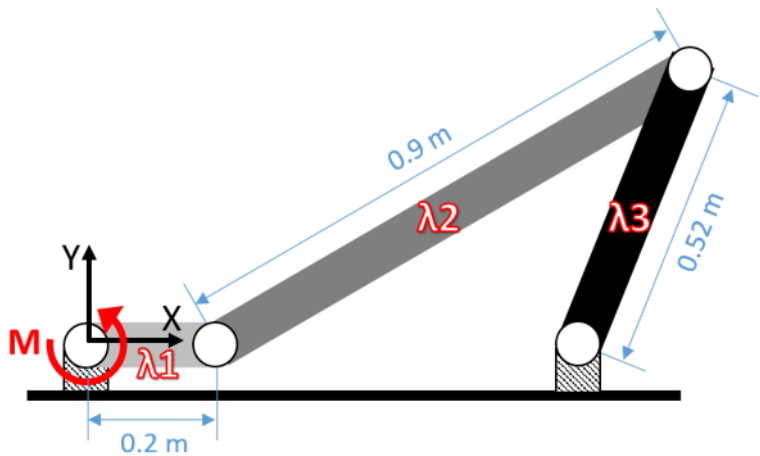

Figure 7.14. Four-bar mechanism subjected to the optimization problem

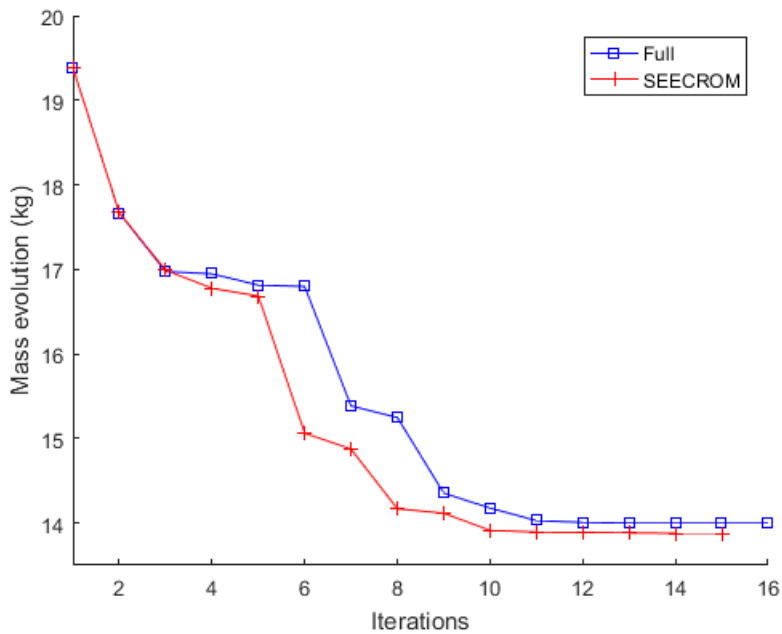

Figure 7.15. Cost function history from the optimization problem of multibody dynamics

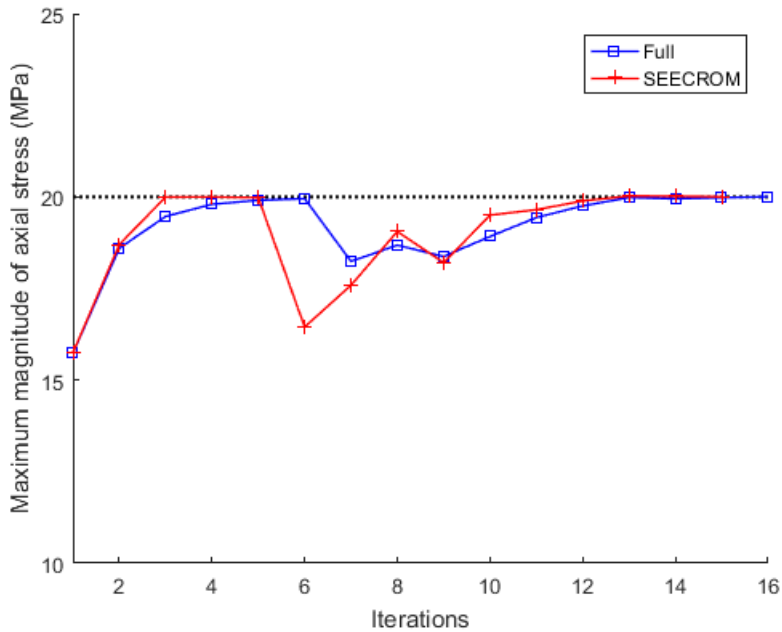

Figure 7.16. Constraints history from the optimization problem of multibody dynamics

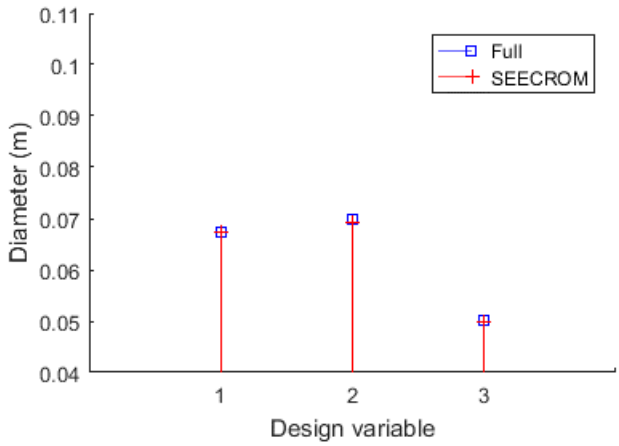

Figure 7.17. Design parameters at the optimal state from the optimization problem of multibody dynamics

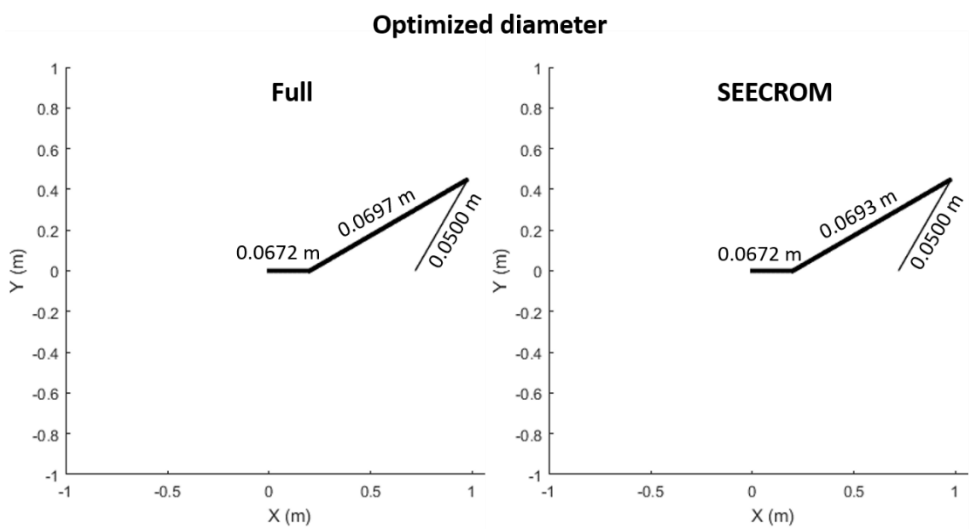

Figure 7.18. Optimal designs from the optimization problem of multibody dynamics

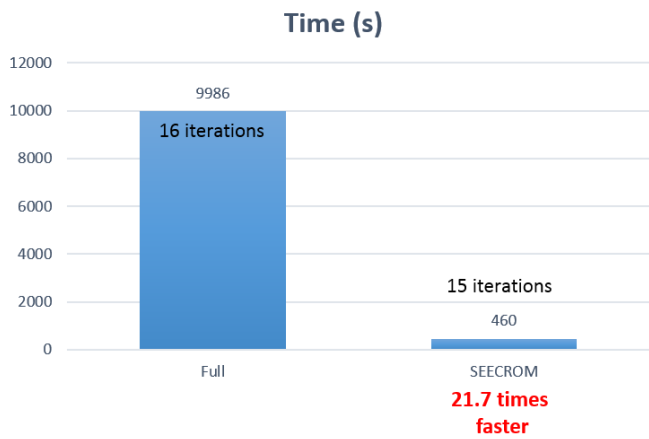

Figure 7.19. Computation time for the optimization problem of multibody dynamics

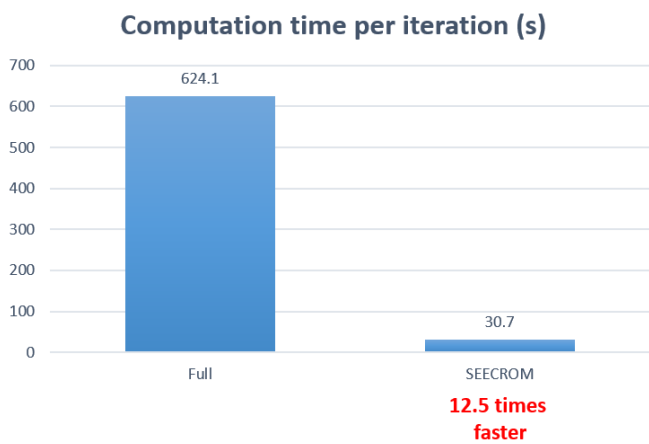

Figure 7.20. Computation time per iteration for the optimization problem of multibody dynamics

8. CONCLUSIONS

This research was conducted to present a new nonlinear model reduction method that has both sufficient efficiency and accuracy to be applied to structural dynamic analyses or design optimization problems. To this end, the stiffness evaluation method, which is one of the nonlinear model reduction approaches, was modified to enlarge its potential applications. First, a new stiffness evaluation method that has less dependency on the size of the problem was proposed for applications to large-scale problems. In addition, a parameterization technique was adapted to the proposed method for applications to design problems.

To be specific, the proposed method, referred to as SEECROM, was developed to enhance the conventional stiffness evaluation methods. First, the element connectivity of the finite elements was used to reduce the number of unknown stiffness coefficients. SEECROM relies on the characteristics of the finite element itself rather than on the complexity or the size of the problem. The application sequence of ROM was reversed to guarantee both accuracy and efficiency. The parameterization of SEECROM was also developed directly based on the characteristics from the element connectivity. The design parameters were simply added to the input parameters of the SEECROM model by using the element-wise nature of the proposed algorithm.

SEECROM and its parameterization technique were directly applied to the reduced-order modeling of flexible multibody dynamics. Various numerical examples with ANCF beam elements successfully demonstrated the efficiency and accuracy of the proposed

method. In future investigations, plate and solid elements based on ANCF will be implemented with the SEECROM method. Applications can be expanded to numerical examples with more constraints, including contact problems. Overall, SEECROM gives more possibilities to ANCF methods, which could contribute to the study of multibody dynamics for highly flexible structures.

The extension of the SEECROM-Parameterization to the optimization problems was also achieved. Since the nonlinear reduced order modeling has recently became an active research field, its application to optimization problems is in the beginning stage. Although the proposed method was successfully solved the problem concerning structural nonlinearities as well as multibody dynamics, further extensions are required. In future investigations, large-scale optimization problems will be solved for various applications. The applications can be expanded to multi-physics problems, and this can be accelerated with the aid of commercial programs.

REFERENCES

[1] Muravyov, A. A., & Rizzi, S. A. (2003). Determination of nonlinear stiffness with application to random vibration of geometrically nonlinear structures. Computers and Structures, 81, 1513–1523.

[2] Mignolet, M. P., Przekop, A., Rizzi, S. a., & Spottswood, S. M. (2013). A review of indirect/non-intrusive reduced order modeling of nonlinear geometric structures. Journal of Sound and Vibration, 332(10), 2437–2460.

[3] Hollkamp, J. J., Gordon, R. W., & Spottswood, S. M. (2005). Nonlinear modal models for sonic fatigue response prediction: A comparison of methods. Journal of Sound and Vibration, 284(3-5), 1145–1163.

[4] Radu, A. G., Yang, B., Kim, K., & Mignolet, M.P. (2004). Prediction of the dynamic response and fatigue life of panels subjected to thermo-acoustic loading. Proceedings of the 45th Structures, Structural Dynamics, and Materials Conference, 19-22.

[5] Mignolet, M. P., & Soize, C. (2008). Stochastic reduced order models for uncertain geometrically nonlinear dynamical systems. Computer Methods in Applied Mechanics and Engineering, 197, 3951–3963.

[6] Capiez-Lernout, E., Soize, C., & Mignolet, M. P. (2012). Computational stochastic statics of an uncertain curved structure with geometrical nonlinearity in three-dimensional elasticity. Computational Mechanics, 49, 87–97.

[7] Capiez-Lernout, E., Soize, C., & Mignolet, M. P. (2014). Post-buckling nonlinear static and dynamical analyses of uncertain cylindrical shells and experimental validation. Computer Methods in Applied Mechanics and Engineering, 271, 210–230.

[8] Perez, R., Wang, X. Q., & Mignolet, M. P. (2014). Nonintrusive structural dynamic reduced order modeling for large deformations: Enhancements for complex structures. Journal of Computational and Nonlinear Dynamics, 9(July 2014), 031008.

[9] Adrian, F., Tran, L. D., Matthies, H. G., & Ohayon, R. (2015). An integrated method for the transient solution of reduced order models of geometrically nonlinear structures. Computational Mechanics, 327–344.

[10] NAG Fortran Library Manual–Mark 24, (2012). The Numerical Algorithms Group Limited.

[11] Golub, G. H., & Van Loan, C. F. (1996) Matrix Computations (3rd Edition). Johns Hopkins University Press, Baltimore.

[12] Kim, S., Ryu, J., & Cho, M. (2011). Numerically generated tangent stiffness matrices using the complex variable derivative method for nonlinear structural analysis. Computer Methods in Applied Mechanics and Engineering, 200(1-4), 403–413.

[13] Sirovich, L. (1987). Turbulence and the dynamics of coherent structures. I - Coherent structures. II - Symmetries and transformations. III - Dynamics and scaling. Quarterly of Applied Mathematics (ISSN 0033-569X), 45(July), 561.

[14] Breuer, K. S. (1991). The use of the Karhunen- Loève procedure for the calculation of linear eigenfunctions. Journal of Computational Physics, 96(2), 277–296.

[15] Liang, Y. C., Lee, H. P., Lim, S. P., Lin, W. Z., Lee, K. H., & Wu, C. G. (2002). Proper orthogonal decomposition and its applications—Part I: Theory. Journal of Sound and Vibration, 252(3), 527–544.

[16] Lee, J., (2015), Proper orthogonal decomposition-based parametric reduced order models for structural analysis and design optimization. Ph.D. Dissertation, Seoul National University.

[17] Escalona, J. L., Hussien, H. A., Shabana, A. A., (1998), Application of the Absolute Nodal Co-Ordinate Formulation To Multibody System Dynamics. J. Sound Vib. 214, 833–851.

[18] Yakoub, R. Y., Shabana, A. A., (1999), Use of Cholesky coordinates and the absolute nodal coordinate formulation in the computer simulation of flexible multibody systems. Nonlinear Dyn. 20, 267–282.

[19] Berzeri, M., Shabana, A. A., (2000), Development of Simple Models for the Elastic Forces in the Absolute Nodal Co-Ordinate Formulation. J. Sound Vib. 235(4), 539–565.

[20] Shabana, A. A., (2013), Dynamics of multibody systems. Cambridge University Press.

[21] Gerstmayr, J., Ambrósio, J. A. C., (2008), Component mode synthesis with constant mass and stiffness matrices applied to flexible multibody systems. Int. J. Numer. Meth. Engng. 73, 1518–1546.

[22] Kobayashi, N., Wago, T., Sugawara, Y., (2011), Reduction of system matrices of planar beam in ANCF by component mode synthesis method. Multibody Syst. Dyn. 26(3), 265–281.

[23] Sun, D., Chen, G., Sun, R., (2014), Model reduction of a multibody system including a very flexible beam element. J. Mech. Sci. Technol. 28(8), 2963–2969.

APPENDIX A

VALIDITY OF 3rd DEGREE POLYNOMIAL APPROXIMATION

Using the first Piola-Kirchhoff stress P_{ji}, the total Lagrangian form of internal nodal forces at node I are integrated over the initial configuration , which is given by

$$f_{iI}^{\text{int}} = \int_{\Omega_0} \frac{\partial N_I}{\partial X_j} P_{ji} d\Omega_0 \tag{A1}$$

where N_I is the shape function and X_j is the initial position.

In this equation, it should be noted that only the stress term is dependent on the displacements. Therefore, the compositions of the first Piola-Kirchhoff stress determine the approximation order of the polynomial description in the stiffness evaluation methods.

For the simplest nonlinear material model, a St. Venant-Kirchhoff material that exhibits large deformations can be considered. The first Piola-Kirchhoff stress tensor of the material is defined as

$$\mathbf{P}(\mathbf{F}) = \mathbf{F}[2\mu\mathbf{E} + \lambda \text{tr}(\mathbf{E})\mathbf{I}] \tag{A2}$$

$$\text{where Green strain tensor is } \mathbf{E} = \frac{1}{2}(\mathbf{F}^T\mathbf{F} - \mathbf{I}) \tag{A3}$$

From the above equations, it can be seen that the stress is a 3rd degree polynomial function of the deformation gradient tensor $\mathbf{F}$. Moreover, by the definition of $\mathbf{F}$ in Eq. (A4) and the interpretation of the displacements with nodal quantities in Eq. (A5), it can be derived that the nodal force is discretized as cubic polynomials of nodal deformations.

$$F_{ij} = \frac{\partial x_i}{\partial X_j} = \frac{\partial (X+u)_i}{\partial X_j} = \delta_{ij} + \frac{\partial u_i}{\partial X_j} \tag{A4}$$

where x_i is the current position and u_i indicates the deformation.

$$u_i = \sum_{I=1}^{n_e} u_{iI} N_I \tag{A5}$$

where u_{iI} is the nodal displacement and n_e is the number of nodes of the element. Hence the use of a 3rd order polynomial from the components of the nodal displacements is adequate for the representation of the internal nodal force of the nonlinear model given above.

Alternatively, the updated Lagrangian form using the Cauchy stress σ_{ji} gives

$$f_{iI}^{\text{int}} = \int_{\Omega} \frac{\partial N_I}{\partial x_j} \sigma_{ji} d\Omega \tag{A6}$$

where Ω indicates the integration over the current configuration.

$$\sigma_{ji} = J^{-1} F_{jk} P_{ki} \quad \text{where} \quad J = \det(\mathbf{F}) \tag{A7}$$

As described below, by the relation between the first Piola-Kirchhoff stress and the Cauchy stress in Eq. (A7), Eq. (A6) is easily transformed into (A1).

$$f_{iI}^{\text{int}} = \int_{\Omega} \frac{\partial N_I}{\partial x_j} \sigma_{ji} d\Omega = \int_{\Omega_0} \frac{\partial N_I}{\partial X_k} \frac{\partial X_k}{\partial x_j} J^{-1} F_{jm} P_{mi} J d\Omega_0 = \int_{\Omega_0} \frac{\partial N_I}{\partial X_j} P_{ji} d\Omega_0 \tag{A8}$$

This implies that the stiffness evaluation method can be applied regardless of the type of the formulations since the method only uses nodal deformations u_{iI} and the

corresponding internal forces f_{iI}^{int}. They are invariant to the stresses or the reference coordinates used in the computation process.

If a material takes a more complex form than a St. Venant-Kirchhoff model, the applicability of the stiffness evaluation method can be verified as follows. First, in the total Lagrangian approach shown in Eq. (A1), where the relation between the first Piola-Kirchhoff stress and the deformation gradient is the sole factor, the order of the polynomial of u_{iI} used to express the stress $\mathbf{P}$ should be identified. If the relation cannot be expressed in analytical form, the exact results and the approximate results from the 3rd order polynomial representation can be compared. Likewise, in the updated Lagrangian formulation in Eq. (A6), this can be achieved by the transformation into the total Lagrangian form.

However, there are some cases when the updated form is preferred. For example, if the stress is computed by update algorithms, including the hypoelastic material in which the stress is provided in the rate form, the analyses are generally based on the updated Lagrangian formulation. In these cases, one can examine the Cauchy stress representation by the nodal deformation u_{iI} as follows. In Eq. (A9), the inverse of the matrix is decomposed into its determinant and the adjugate. Using this expression, the internal force in the updated form is represented as Eq. (A10) in which only the term $A_{kj}\sigma_{ji}$ is dependent on the nodal displacements u_{iI}.

$$\mathbf{F}^{-1} = \det(\mathbf{F})^{-1}\text{adj}(\mathbf{F}) = J^{-1}\mathbf{A} \qquad \text{where} \quad \mathbf{A} = \text{adj}(\mathbf{F}) = \text{adj}\left(\frac{\partial \mathbf{x}}{\partial \mathbf{X}}\right) \qquad \text{(A9)}$$

$$f_{iI}^{\text{int}} = \int_{\Omega} \frac{\partial N_I}{\partial x_j} \sigma_{ji} d\Omega = \int_{\Omega_0} \frac{\partial N_I}{\partial X_k} F_{kj}^{-1} \sigma_{ji} J d\Omega_0 = \int_{\Omega_0} \frac{\partial N_I}{\partial X_k} A_{kj} \sigma_{ji} d\Omega_0 \qquad \text{(A10)}$$

Then, the sufficiency of the 3rd order polynomial of u_{iI} for $A_{kj}\sigma_{ji}$ can be evaluated from the values of the stresses obtained in the sampling stage.

In this work, a Neo-Hookean material, which is one of the isotropic constitutive models, was used for the demonstration of the proposed approach. The Piola-Kirchhoff stress of an isotropic constitutive model and the Neo-Hookean elasticity are defined in Eq. (A11) and Eq. (A12), respectively.

$$\mathbf{P}(\mathbf{F}) = \frac{\partial \Psi}{\partial I_1} \cdot 2\mathbf{F} + \frac{\partial \Psi}{\partial I_2} \cdot 4\mathbf{F}\mathbf{F}^T\mathbf{F} + \frac{\partial \Psi}{\partial I_3} \cdot 2I_3\mathbf{F}^{-T} \qquad \text{(A11)}$$

where Ψ is the strain energy and I_1, I_2, and I_3 are the invariants of the deformation gradient $\mathbf{F}$.

$$\Psi(I_1, I_3) = \frac{\mu}{2}\{I_1 - \log(I_3) - 3\} + \frac{\lambda}{8}\{\log(I_3)\}^2 \qquad \text{(A12)}$$

Then, the Neo-Hookean stress is computed as

$$\mathbf{P}(\mathbf{F}) = \mu\mathbf{F} - \mu\mathbf{F}^{-T} + \frac{\lambda \log(I_3)}{2} \cdot \mathbf{F}^{-T} \qquad \text{(A13)}$$

$$\text{where } I_3 = \det(\mathbf{F}) \qquad \text{(A14)}$$

To verify the applicability of the stiffness evaluation methods to a Neo-Hookean material, it should be checked in advance in the sampling stage that whether a 3rd degree polynomial of $\mathbf{F}$ can approximate the stress $\mathbf{P}$ with sufficient accuracy, which is shown as follows.

First, by the definition of $\mathbf{F}$ in Eq. (A4), $\mathbf{F}^{-T}$ and $\log(\det(\mathbf{F}))$ can be

approximated with Neumann series and Tayler series, respectively. See Eq. (A15) and Eq. (A16)

$$\mathbf{F}^{-T} \approx \mathbf{I} - \mathbf{H}^T + (\mathbf{H}^T)^2 - (\mathbf{H}^T)^3 + \cdots \tag{A15}$$

$$\log(\det(\mathbf{F})) \approx -\mathrm{tr}(-\mathbf{H}) - \frac{1}{2}\mathrm{tr}((-\mathbf{H})^2) - \frac{1}{2}\mathrm{tr}((-\mathbf{H})^3) - \cdots \tag{A16}$$

where $\mathbf{H}$ is given by

$$\mathbf{F} = \mathbf{I} + \mathbf{H}, \quad H_{ij} = \frac{\partial u_i}{\partial X_j} = \frac{\partial N_I}{\partial X_j} u_{iI} \tag{A17}$$

Then, the exact stress and the result from the 3rd order approximation of can be compared to assess the availability of the stiffness evaluation methods. For instance, in the sampling analyses of the example in Sect. 5.2.1., the maximum percentage error of the stress was computed as 4.74%. The values of the strain when the maximum error occurs were ε_{xx} =0.064, ε_{xy} =-0.499, ε_{yy} =0.374. The approximation in the example was considered sufficient since the maximum error is under 5% at the point of deformation with near 50% strain, which was proved by the high accuracy of the complete SEECROM model.

From the sampling data in the offline stage, as shown in the case above, one can predict the validity of the given method and modify the target problems or the finite element model to raise the accuracy of representative model. Since the error increases with the magnitude of the strain, it is recommended that the strain as well as the stress approximation error should be checked before the application of the stiffness evaluation methods.

국문요약

기하 비선형 및 재료 비선형 거동을 고려한 구조 해석에서 최종 변형을 도출하기 위해서는, 내력 벡터와 강성 행렬을 반복적으로 도출하며 변형을 갱신해 나아가는 과정을 거쳐야 한다. 이는 비선형성을 고려한 정적 및 동적 해석에 있어서 계산 시간이 급증하는 까닭이다. 따라서 효과적인 해석을 위하여 다양한 축소 모델 기법들이 제안되어 왔지만 그 효율성이 높지 않다. 보통의 축소 기법은 각각 시스템 행렬의 크기를 줄이고, 줄어든 크기의 시스템 행렬을 통해 효율적으로 응답을 도출할 수 있도록 한다. 즉, 축소 기법을 적용하기 위해서는 시스템 행렬을 미리 구축해야 하는 것이다. 비선형 해석의 경우 변형에 따라 시스템 행렬의 구축을 반복해야 하며, 이에 소요되는 시간이 상당하다. 그러나 기존의 축소 기법은 시스템 응답 도출과 관련된 효율성만 높이며, 행렬 구축에 소요되는 시간은 그대로 남는다.

등가 강성 행렬 기법(Stiffness Evaluation)을 활용하면 비선형 시스템 행렬 구축의 효율성을 높일 수 있다. 해당 기법은 비선형 시스템의 내력 벡터를 다항함수를 활용한 등가 모델로 나타낸다. 일단 해당 다항함수의 계수들을 도출해 놓으면, 변형의 갱신을 즉각적으로 고려하여 내력 벡터와 강성 행렬을 계산할 수 있으므로 행렬 구축에 소요되는 시간을 크게 줄일 수 있다. 문제는 등가 모델 구축에 소요되는 시간이 시스템 크기의 3승에 비례하여 늘어나기 때문에, 효율적이지 않다는 것이다.

본 연구에서는 유한 요소의 연결성을 고려하여 개선한 새로운 등가 강성

행렬 기법(SEEC; Stiffness Evaluation based on Element Connectivity)을 제안한다. 유한 요소의 연결성을 이용하면, 다항함수의 구성 및 해당 계수들의 도출을 국부적 및 병렬적으로 진행할 수 있다. 적합직교분해법(POD; Proper Orthogonal Decomposition)을 활용한 축소 모델 또한 연동되어 효율성을 높인다. 등가 강성 행렬 기법의 계수들을 요소 연결성을 고려하여 효과적으로 산출한 뒤, 축소 기법을 연동하면 정확도 및 효율성을 동시에 확보할 수 있다. 이 제안 기법을 SEECROM으로 칭한다. SEECROM은 각 유한 요소의 특성을 활용하여 국부적으로 구성된다는 특성을 갖기 때문에, 파라메트릭 기법의 적용이 용이한 장점도 갖는다. 제안 기법의 효율 및 정확성은 기하 비선형성을 가지는 쉘 구조물의 동적 해석과 초탄성 재료를 가지는 비선형 구조의 정적/동적 해석에 적용하여 검증하였다.

제안 기법은 유연 다물체 동역학에도 적용할 수 있다. 보통의 유연 다물체 동역학은 상대 절점 좌표계를 활용하여 해석하며, 그 경우 시스템 행렬의 비선형성이 강성 행렬이 아닌 질량 행렬에 나타난다. 관성력과 관련하여 추가되는 행렬도 고려하여야 하기 때문에, 동적 구조 해석을 기반으로 개발된 축소 기법을 유연 다물체 동역학 문제에 그대로 활용하기에는 어려움이 있다. 절대 절점 좌표계를 기반으로 하는 ANCF(Absolute Nodal Coordinate Formulation) 기법의 경우, 유한 요소 기법을 적용한 지배 방정식이 비선형 동적 구조 해석 모델과 유사한 형식을 갖는다. 따라서 ANCF 기법을 활용하면 구조 해석을 기반으로 개발된 SEECROM을 유연 다물체 동역학에 적용할 수 있다. 제안 기법과 파라메트릭 기법을 4절 기구를 포함한 주요한 유연 다물체 동역학

예제들에 적용하고 그 효율성과 정확성을 검증할 수 있었다.

파라메트릭 기법이 적용된 SEECROM은 비선형 시스템 구조의 최적 설계 문제에도 적용이 용이하다. 현재 비선형 시스템의 축소 기법에 대한 연구가 진행 중인 단계라, 이를 최적 설계 문제에 적용하는 연구는 아직 활발하지 않은 분야이다. SEECROM은 다양한 종류의 비선형 시스템을 효율적으로 축소하며, 파라메트릭 기법의 적용 또한 유용하기에 앞으로 다양한 최적 설계 문제를 효과적으로 다룰 수 있을 것이라 예상된다. 본 연구에서는 비선형 재료 거동을 갖는 구조 시스템과 4절 기구의 유연 다물체 동역학 시스템의 구조 설계 문제를 예제로 들어 제안 기법의 효과를 검증하였다.

제안 기법은 요소 및 절점을 기반으로 수행되는 다양한 비선형 문제에 적용이 가능할 것이다. 비선형성을 가지는 대형 시스템, 다물리 연성 시스템, 상용 프로그램을 활용한 효율적인 해석 및 설계로의 확장이 기대된다.

주요어: 파라메트릭 축소 모델, 기하 비선형 해석, 재료 비선형 해석, 등가 강성 행렬 기법, 유연 다물체 동역학, 구조 최적 설계

학번: 2010-20662